Project SOAR: Sensing Oxygen Autonomously in Real-time

A Major Qualifying Project

by
Erin Dixson
Emma MacIntyre
Alex Markoski
Tyler McNeill

Date:
26th of April, 2018

Report Submitted to:

Kristen Billiar, Ph.D., Project Advisor
Worcester Polytechnic Institute
Philip Keegan, Ph.D., Industry Advisor
Jonathan Coppeta, Ph.D., Industry Advisor
Charles Stark Draper Laboratories

TABLE OF CONTENTS

LIST OF FIGURES

LIST OF TABLES

AUTHORSHIP

All group members contributed equally to writing and editing all components of this report. These team members include: Erin Dixson, Emma MacIntyre, Alex Markoski, and Tyler McNeill.

ACKNOWLEDGEMENTS

We would like to extend our thanks to the following people and departments for helping us during the course of this project:

- WPI and Draper Laboratories
- Professor Kristen Billiar, Ph.D.
- Jonathan Coppeta, Ph.D. and Philip Keegan, Ph.D.
- Lisa Wall and Elyse Favreau
- Torsten Mayr, Ph.D.
- Matthew Gleason
- Andrew Teixeira, Ph.D.
- Biomedical Engineering Department
- Chemical Engineering Department

ABSTRACT

In the beginning of the drug approval process, thousands of compounds are tested for effectiveness; this is extremely costly and time intensive for companies. Animal models are often used in the beginning of the process to test the efficacy of these compounds. However, animal models do not match human physiology, making them inaccurate predictors of how the compound will perform later on in the drug approval process. Based on this, there is a need for an intervention early on in the process to reduce time and cost and increase predictive power. Organ-on-a-chip technology is a promising answer to these problems since these devices have the ability to host organ and tissue types that are more predictive of human physiology. Additionally, these devices can easily test compounds in bulk. To make these systems as robust as possible, it is advantageous to incorporate sensing capabilities into the device. The capability to sense oxygen is valuable, being that these readings are directly correlated to cellular metabolic activity.

Project SOAR collaborated with Draper, a research and development organization based in Cambridge, MA, to integrate real-time oxygen sensing capabilities into Draper's organ-on-a-chip device. The goal of this project was to identify and determine a means of incorporating an oxygen quenchable sensor format into the existing device. This format must be able to sustain the conditions of normal device use including thermal cycling, sterilization, and exposure to cell culture media for prolonged periods of time. By working with various possible formats and iterating on the best incorporation method, the team was able to create a design able to fulfill all of Draper's required specifications. The final format was comprised of a nanoparticle indicator solution that was processed under 1000 lbs of force (450 psi of pressure) at 120 degrees Celsius

for a period of 15 minutes using a Carver press. By incorporating the nanoparticle format in such a way, the team greatly improved the pre-existing standard employed at Draper.

Compared to Draper's previous format, the nanoparticles proved to be more versatile, showing the ability to have signal intensities that can be fine-tuned to the desired signal strength. To verify the capacity to easily utilize this format in Draper's final device, the team performed a wide array of validation testing on this sensor format, as well as the other formats of interest. Qualitative optical clarity testing proved that the nanoparticles would be a better format to incorporate into the final device compared to the foil and dye formats, both of which significantly impeded optical clarity during standard microscopy examination. The concentration of nanoparticle solution was not sufficient to achieve an optimal signal intensity above the 50 mV threshold specified by PyroSciene following the soak test; however, this can be remedied easily to allow this format to withstand the current parameters of final device use. The nanoparticle format also showed overall successes following the thermal, sterilization, and duration tests. Overall, the successes during validation testing further proved that the nanoparticles, when processed using the Carver press, are the best sensor format to incorporate within Draper's final device.

CHAPTER 1: INTRODUCTION

Successful development of a single drug typically takes 10 to 12 years and roughly 2.5 billion dollars [1]. Within this drug development process, nearly 90% of drugs that pass animal studies will fail in human clinical trials [2]. This creates a need for a better way to simulate how a drug will react, improving upon the animal models that are currently used. To accommodate this need, organ-on-a-chip devices employing microfluidic principles have emerged in recent years. The principles of microfluidics involve the manipulation of small amounts of fluids using micrometer-scale channels [3]. Through microfluidics, pharmacology researchers are better able to mimic *in vivo* conditions and it is possible to inexpensively produce multiple replicates of drug tests while minimizing volumes of consumables. The market for organ-on-a-chip devices is expected to grow by 69.4% in the next 10 years to a total market of 6.13 billion dollars by 2025 [4].

To accurately simulate *in vivo* conditions, organ-on-a-chip technology must have analyte sensing capabilities to monitor cell viability [5]. There are a variety of analytes that can be monitored including oxygen, carbon dioxide, glucose, and pH. Of these, oxygen analytes are the most successfully implemented parameter in microfluidics, as they show the capacity to quantify the behavior and viability of cell types as well as drug effectiveness [6], [7]. Oxygen levels can be measured via mechanical, optical, or electrochemical means; however, optical oxygen sensing is the most ideal in cellular environments because it does not contact cell media and does not consume the analyte.

Draper, a not-for-profit research and development company, is in the process of developing a 96-well organ-on-a-chip platform with multifunctional capabilities including the

sensing of dissolved oxygen. Current methods for oxygen sensing used at Draper are labor intensive, low-throughput, and not compatible with microscopy. Their current system uses the Piccolo$_2$ oxygen sensor as an optical platform, which operates using red flash technology and a sensing foil. The term optical platform refers to the source of the excitation flash and where the associated emission is received. Both of these components have been developed by PyroScience to acquire an oxygen percentage reading without submerging the Piccolo$_2$'s fiber optic cable in the cell media [8]. This system requires that the single fiber optic be manually moved between each of the 96 wells of the microfluidic device. Further, the PyroScience foil that is currently in use is opaque, making cellular imaging below the foil impossible.

The goal of this project was to create an accurate high-throughput oxygen sensing system that maintains optical clarity for cellular imaging. The oxygen sensing system consisted of two major components, the optical platform and the sensing format. The optical platform is semi-automated or high-throughput in terms of providing a continuous dissolved oxygen percentage feedback to a computer program. One major goal of this device over previous methods is the capability to run without user interaction after setup, thereby eliminating the necessity for researchers to be present during testing. The oxygen sensing format is optically clear, biocompatible, able to withstand a cellular environment for up to 14 days in culture, compatible with the optical platform, and able to survive the fabrication process of the microfluidic device. An appropriate format able to be quenched by oxygen was identified and a method of incorporating this format into the current device was implemented. As a final design, this format is optically clear, robust in that it can withstand normal device use, and able to produce accurate readings indicative of the oxygen percentage in the organ-on-a-chip device. Overall, this project set out to improve Draper's current sensing system to more accurately represent *in vivo*

conditions by monitoring oxygen in cellular environments while maintaining optical access of the cells being studied via the use of custom fabricated and implemented oxygen sensing format.

CHAPTER 2: BACKGROUND

The environment in which a cell exists can influence over various cellular characteristics, such as proliferation and differentiation. Such environmental variability can come in the form of temperature fluctuations, salinity, or oxygen levels. To ensure that cellular studies are representative of *in vivo* characteristics, researchers must be able to accurately monitor and mimic the different factors of a natural cellular environment.

2.1 Microfluidics

To advance efforts in biomedical research, microfluidic systems are being used to create smaller scale multi-functional platforms that replace current macroscale assays [9]. This technology forms the basis for organ-on-a-chip devices, which are used to advance progress in clinical research and drug development efforts. Starting with processes of the 1950s aimed at generating integrated circuits rapidly and inexpensively, researchers have continuously strived towards creating high-speed, energy-efficient electronic systems at small-scales [10]. Combining these circuit studies with analytical chemistry techniques, particularly capillary electrophoresis as well as gas-phase and high-pressure liquid chromatography, scientists began to develop and rapidly expand a field known as microfluidics [11], [12]. Microfluidic devices manipulate small amounts of fluids, ranging from the attoliter to the microliter scale, using micron-scale channels. By applying fluid characteristics to small-scale devices, microfluidic technologies allow for precise control of concentrations of molecules in space and time [12]. Microfluidic technology has seen a significant expansion in recent years, with subsequent application in fields like chemical analysis and medical diagnostics.

Typically, microfluidic devices are utilized in bioanalytical and medical studies because their physical size provides advantages over normal lab-based devices [13]. Most of the societal need associated with organ-on-a-chip technology arises from the prospects of using these devices in both investigational research and in product development. For example, within the current drug development process, new medications have a success rate of approximately 8% of going from preclinical toxicology to market approval [14]. Microfluidics allows pharmacology researchers to mimic *in vivo* conditions inexpensively on the microscale, which allows for multiple replicates and less waste.

Current organ-on-a-chip devices have shown the capability of mimicking the microarchitecture of organs. An example of this is from the Wyss Institute for Biologically Inspired Engineering at Harvard University, which has been able to simulate the functions of organs such as the lung, intestine, and kidney using organ-on-a-chip devices [15]. From this research, the Wyss Institute launched a startup company entitled Emulate, Inc., which aims to commercialize this technology in hopes of bettering standards of industrial development in the pharmaceutical industry and personalized medicine. In a recent study performed by the Wyss Institute, researchers were able to perform a toxicity study on primary human kidney proximal tubular epithelial cells [16]. Such work proves that microfluidic devices have the potential to recreate *in vivo*-like conditions that could serve as a tool for evaluating a wide array of physiological phenomena. Additional companies, such as Nortis Bio, are working to incorporate microfluidic devices into the existing biotechnology market as means of growing cells into three-dimensional human tissues. Nortis uses a microfluidic chip with a custom perfusion platform to simulate human tissue microenvironments for vascular and organ-on-a-chip studies [17].

2.2 Microfluidic Oxygen Sensing

To aid in the successful use of microfluidic devices for clinical and medical research, there must be constant monitoring of the system state to ensure a standardized and regulated environment. Based on this need, research has shown that oxygen-sensing capabilities within microfluidic cell culture environments shows the capacity to quantify the behavior and viability of cell types as well as drug effectiveness [18]. Oxygen is a parameter of interest in cell culture, fermentation, and biocatalyst monitoring. Compared to pH, carbon dioxide, and glucose, oxygen is the most successfully implemented detection analyte in microfluidic applications. This is due to its ability to monitor cell metabolism via its simple sensing principle [6]. There are various sensing methods able to determine dissolved oxygen percentage including optical detection methods, Winkler titration, mechanical or pressure-based methods, and electrochemical methods [19].

Winkler titration is a titrimetric method of oxygen sensing which is commonly used in larger-scale dissolved oxygen monitoring, such as environmental applications. There are various types of Winkler titrations. The Azide-Winkler method is a commonly accepted, precise standard for dissolved oxygen sensing but has limitations that eliminate its feasibility for use in microfluidic environments [20]. Winkler titration cannot be modified for continuous oxygen sensing and samples must be taken from the device and contaminated with titrants [19]. This process is time consuming and it would not be ideal to integrate into a micro-sized system [20].

Electrochemical methods are more applicable to smaller volumes, like those characteristic of microfluidic devices, than the Winkler titration method. Figure 1A demonstrates the operating principle of the Clark electrode method. These systems consist of a silver anode and a platinum cathode, where oxygen is reduced. This generates a steady state current that can

be correlated to the percentage of dissolved oxygen in the solution [21]. Clark-electrode type

sensors have been incorporated into microfluidic devices as illustrated in Figure 1B. This device

consists of a miniaturized Clark-type electrode embedded below the microfluidic device. When

potential is applied to the system, oxygen is reduced on the cathode and the change in current can

be correlated to the dissolved oxygen percentage [22]. Clark electrode based systems are widely

used but are not desirable for cellular based microfluidic systems because the electrode

consumes oxygen and other gases can interfere with the sensing system [19].
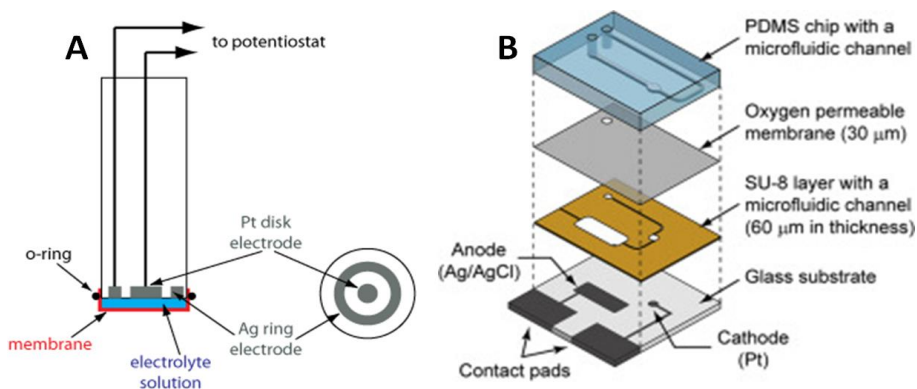
Figure 1: A: Graphic indicating the components of a Clark electrode for sensing dissolved oxygen percentage. This image has been reproduced under the Creative Commons Attribution-Noncommercial-ShareAlike 4.0 International License [23]. B: Miniaturized Clark-type electrode in a microfluidic application © Elsevier. Reproduced with Permission, Courtesy of Elsevier. See Appendix J: Copyright Approval [22].

Pressure-based mechanical methods are not widely applied in oxygen sensing due to their

invasive nature. Colorimetric oxygen sensing methods can also be used to detect dissolved

oxygen levels but are not directly applicable to microfluidic devices. Indicators like indigo

carmine and rhodazine D can be used in this method, but the indicators must be permanently

added to the sample. This means that small volumes would need to be removed from the

microfluidic device or the sample would be completely ruined. After adding the indicator, a

measurement must be made in a short window of time [20]. Based on the drawbacks of these

methods, optical techniques have gained popularity and are the preferred method for microfluidic applications. This is because these principles do not consume oxygen, are completely reversible, maintain good precision and accuracy, operate non-invasively, can be easily miniaturized, and have a variety of sensor format options [19].

2.3 Optical Oxygen Sensing

The major principle behind optical oxygen sensing is luminescence quenching. Luminescence quenching is a reversible process that entails quenching of an excited medium. This medium can take a variety of forms like dyes or luminophores and excited energy is transferred to oxygen, rather than being emitted as light [24]. This results in an inverse relationship between the amount of dissolved oxygen and the emitted light. Figure 2 illustrates the luminescence quenching principle utilized in many optical based oxygen sensors. An excitation pulse of a known wavelength is supplied to the sensing medium and then a signal with a different wavelength is emitted from the sample proportional to the oxygen percentage present in the environment of interest. As illustrated in Figure 2, an important characteristic of this sensing principle is a Stokes shift between the emission wavelength and the excitation wavelength. In a general sense, it is ideal to maximize the Stokes shift to increase sensor accuracy and make it easier for the sensing component to distinguish emission light from background light [25].

Stokes Shift (nm) = Emission wavelength − Excitation wavelength
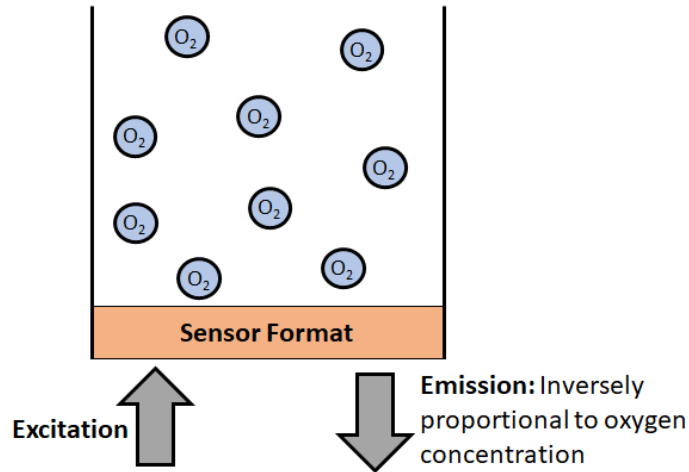
Figure 2: Illustration of the luminescence quenching principle used in many optical oxygen sensors. The sensor is able to measure the emission wavelength which can be correlated to the oxygen concentration present in solution. The difference in excitation and emission wavelength is referred to as the Stokes shift, with higher Stokes shifts having better sensor performance [25].

Using luminescence quenching, oxygen can be detected via lifetime or intensity based measurements. Lifetime mechanisms can detect luminescence through either the frequency or the time domain in a reversible reaction with quenching molecules. In the time domain method, excitation pulses can be passed to the sample and emission intensity data is acquired at specified time points. Frequency domain based methods involve detecting phase differences. Both methods allow for the recording of the decay in signal after excitation, which is directly correlated to the amount of quencher molecule attached to the sensing format [24].

Overall, intensity based methods are simpler than lifetime based methods; however, they fall short in their susceptibility to leaching and photobleaching. Intensity-based sensing principles are typically improved by applying ratiometric sensing principles. This refers to when there is an oxygen sensitive medium and an oxygen insensitive medium. Both dyes will be excited by the same source and the ratio of emission intensities is calculated to determine oxygen

percentage. Overall, lifetime-based sensing principles are preferable to intensity-based methods due to superior contrast and elimination of confounding background noise [24].

When focusing on the reduction of fluorescence intensity, two different types of quenching processes are most often cited, collisional quenching and static quenching. Collisional quenching occurs when contact between an excited fluorophore and a molecule result in non-radiative transitions to the ground state. Static quenching occurs when a fluorophore and a molecule form a complex that is non-fluorescent. There are many different equations that can be used to quantify fluorescence lifetime through quenching processes, such as the Stern-Volmer equation [26]. The Stern-Volmer equation relates observed emission intensities in the presence of quencher molecules to fluorescence lifetime. The Stern-Volmer equation is as follows:

$$\frac{I_0}{I_Q} = 1 + \tau_f k_q [Q]$$

In this equation, I_0 represents the rate of fluorescence when there is no quencher molecule present, I_Q represents the rate of fluorescence in the presence of a quencher, k_q is the Stern-Volmer constant, τ_f is the lifetime of the emissive excited state of the chemical species of interest, and $[Q]$ is the concentration of the quencher [27].

Furthermore, sensor formats, specifically some form of a reference indicator, must be considered when focusing on optical means of sensing oxygen. Some of the current formats utilized in research include luminescent dyes and nanoparticle-based systems [28]. One way to incorporate luminescent dyes is printing them directly onto a platform in which oxygen levels are of interest. Likewise, nanoparticles can be suspended within fluid systems where oxygen levels are being studied. Nanoparticle indicators can be delivered to these systems by either being encapsulated within polymer probes or being suspended directly in the fluid system. However,

when the nanoparticles are suspended directly in the fluid, there is a potential for phototoxicity.

Additional sensor format possibilities include thin-film sensors attached to external substrates,

optical fiber sensors, and water-soluble macromolecule probes [24].

2.4 Oxygen Quenchable Chemical Compounds

Various chemistries have been identified in literature as able to be quenched in the

presence of molecular oxygen. This quenching process is a reversible process and does not result

in consumption of the oxygen analyte. There is a wide range of optical luminescent indicators,

which can be categorized as shown in Table 1 below.

Table 1: Outline of the pros and cons of various indicators used for oxygen-based measurements

Indicator	Pros	Cons
Polycyclic Aromatic Hydrocarbons	● Long excitation lifetimes and good pressure sensitivity	● Non ideal excitation range: 300 nm and 390 nm
Polypyridyl Complexes	● Wide range of absorption and emission wavelengths ● Some of the most common oxygen indicators on the market	● Short lifetime ● Brightness ● Subject to thermal quenching ● Low accuracy in low oxygen ● Cytotoxic effects over repeated excitation ● Inefficient in their percent oxygen resolution ● Difficult to suspend in PDMS
Metalloporphyrins	● Strong phosphorescence and good molar absorption coefficients	● N/A
Cyclometalated Complexes	● Large stoke shifts ● Photostability ● High luminescence quantum yields	● Short decay times ● Poor absorbance in the visible light region

The polycyclic aromatic hydrocarbons, PAH, are indicators that are characterized by long excited lifetimes and good pressure sensitivity. Some limitations of PAH-based sensors are centered around their lack of solubility in polymeric matrices and having a very small Stokes shift, which is defined as the apex of the absorption and emission spectra [29]. The excitation range of PAH indicators is between 300 and 390 nanometers which is not ideal due to background fluorescence that can interfere with readings at such small Stokes shifts. Due to these downsides, these indicators are rarely chosen over some of the following options [30].

The second group of indicators are transition metal based polypyridyl indicators. Typical transition metals incorporated into these indicators include ruthenium and osmium. Depending on the exact composition, this group of indicators has a wide range of absorption and emission wavelengths. For instance, a Stokes shift of just under 400 nanometers is seen in the platinum based polypyridyl indicator, $Pt(ddp)(CN)_2$. Most of these indicators, especially Ru(II)-based indicators, are excited through blue light. A disadvantage of these complexes is their characteristic short lifetime, brightness, their ability to be subject to thermal quenching, low accuracy in low oxygen settings, and cytotoxic effects over repeated excitation making these possibly hazardous for long term cellular testing. Additionally, while these are some of the most common oxygen indicators on the market, they are inefficient in their percent oxygen resolution and are difficult to suspend in polydimethylsiloxane (PDMS) and other oxygen permeable polymers. Overall, this makes using these indicators very difficult for large scale testing and prototyping.

Metalloporphyrins are very commonly used as optical oxygen sensors, specifically due to their large Stokes shifts, strong phosphorescence, and good molar absorption coefficients. The indicators in this class incorporate both Pt(II) and Pd(II) porphyrins. A major advantage of these

indicators is their ability to be excited by red light with an emission in the NIR range allowing for distinguished input and output signals indicated by a large Stokes shift. Indicators with these capabilities are often preferred due to good performance in scattering media and reading low oxygen levels while also having the ability to incorporate cheaper sensing components, than blue light excitable indicators.

Cyclometallated complexes are also used for optical oxygen sensing. Advantages of this class of indicators include large Stokes shifts, photostability, and high luminescence quantum yields. Negatives of these indicators are centered around poor absorbance in the visible light region as well as short decay times. There are also various other classes of oxygen quenchable indicators with differing central atoms. Important factors that must be considered when selecting an oxygen quenchable indicator include toxicity to the environment of interest and the fabrication of the indicator [30].

2.5 Examples of Current Optical Oxygen Sensors

Current optical oxygen sensors used in industry and research include the Agilent Seahorse, the PyroScience Piccolo$_2$ and FirestingO$_2$, the PreSens Duo1, and the PreSens SDR SensorDish.

2.5.1 Agilent Seahorse

The Seahorse is an incubation system that invasively measures dissolved oxygen and pH in cell culture media in a 96-well plate, as seen in Figure 3 and Figure 4 [31], [32]. This device gives accurate readings efficiently in real-time. However, it is large and there is a possibly of disturbing the cells in the media.
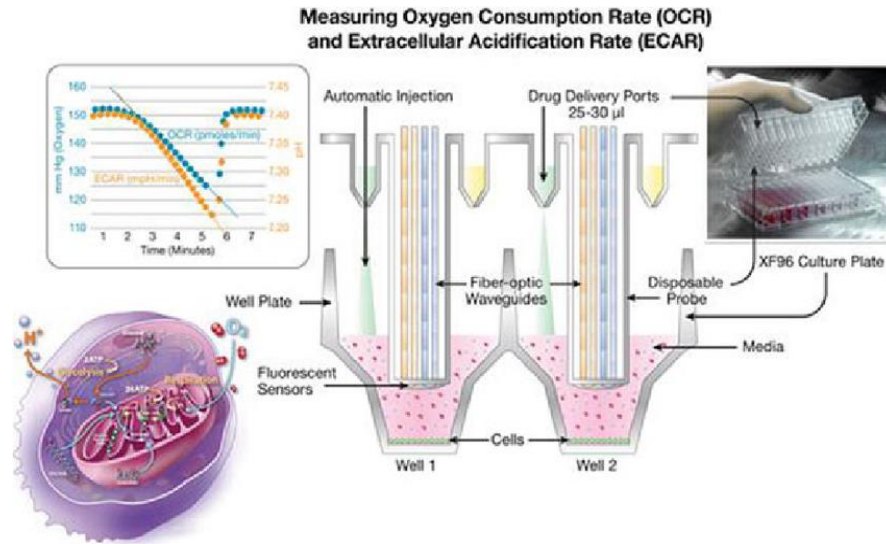
Figure 3: This diagram illustrates the operating principles behind Aligent's Seahorse XF Analyzer. This device is able to monitor dissolved oxygen and pH, but the sensors are in direct contact with the cellular environment. This image has been reproduced under the terms of the Creative Commons Attribution License [31].

Figure 4: The Seahorse XFe96 Analyzer used to measure oxygen consumption rate and extracellular acidification rate in cellular samples in a 96-well format. This device is compact and able to fit on a laboratory benchtop [32]. © Agilent Technologies, Inc. Reproduced with Permission, Courtesy of Agilent Technologies, Inc. See Appendix J: Copyright Approval.

2.5.2 PyroScience Piccolo$_2$ and FirestingO$_2$

The Piccolo$_2$ and FirestingO$_2$ are both made by PyroScience and utilize red flash technology to determine the oxygen percentage non-invasively and in real-time using a sensor format. There is no oxygen consumption due to the optical format, but the device is hard to work with and requires extensive manual labor to move from channel to channel in a 96-well device. The Piccolo$_2$ can be seen in Figure 5 and has a fiber optic cable that is inserted into the device and produces a red flash on a sensor format to obtain oxygen percentage readings [33]. The Piccolo$_2$ solely measures oxygen percentage, which is greatly affected by temperature variations requiring the system to be used in a temperature controlled environment. On the other hand, the FirestingO$_2$ has the capability of incorporating four oxygen sensors and a temperature sensor. Figure 6 illustrates the FirestingO$_2$ with the leftmost port being a temperature port and the remaining four ports allowing for attachment of a fiber optic cable for oxygen sensing [34].

Figure 5: Piccolo$_2$ device for measurement of oxygen concentration in solution. One end of the device serves as a USB connection, while the other end allows for attachment of a fiber optic cable to transmit excitation light and receive emitted light from the sample. All data gathered during use of this device is collected and processed through a custom program created by PyroScience [35]. © PyroScience GmbH. Reproduced with Permission, Courtesy of PyroScience GmbH. See Appendix J: Copyright Approval.

Figure 6: FirestingO$_2$ device for measurement of oxygen concentration in solution with built in temperature control. This device is essentially four Piccolo$_2$ devices in one with the addition of a temperature probe to reduce errors due to temperature sensitivity [34]. © PyroScience GmbH. Reproduced with Permission, Courtesy of PyroScience GmbH. See Appendix J: Copyright Approval.

2.5.3 PreSens Duo1

The Duo1, pictured in Figure 7, is similar to the Piccolo$_2$ and FirestingO$_2$, but uses blue flash technology. It non-invasively monitors oxygen in real time using a sensor format without any oxygen consumption. However, the sensor is too large to read the small wells in a 96-well plate accurately. The Duo1 also has an incorporated camera that records the oxygen levels and displays them to the user in a visual color-coded map [35].

Figure 7: Duo1 device and sensing format for determining oxygen concentration in solution. This device operates using blue flash technology [35]. © PreSens Precision Sensing. Reproduced with Permission, Courtesy of PreSens Precision Sensing. See Appendix J: Copyright Approval.

2.5.4 PreSens SDR SensorDish

The PreSens SDR Sensor Dish is a high-throughput detection device with the capability to sense both pH and oxygen in a non-invasive manner. As illustrated in Figure 8B, the device is a plate that has 24 different integrated pH and oxygen sensors [36]. When using this device, well plates with a sensor spot in the bottom of each well must be used. The well plate is placed on the sensor dish such that the sensor spots are directly over the sensors as illustrated in Figure 8A [36]. To obtain accurate analyte readings, this device must be operated in a dark area such as an incubator. Additionally, this system can work in parallel with its duplicates, seen in Figure 8C, in turn reducing the number of output cables to one instead of having one for each system. One drawback of this device is that the sensor dish is only made for custom twenty-four or six well plates and requires the purchase of PreSens's custom well plate.
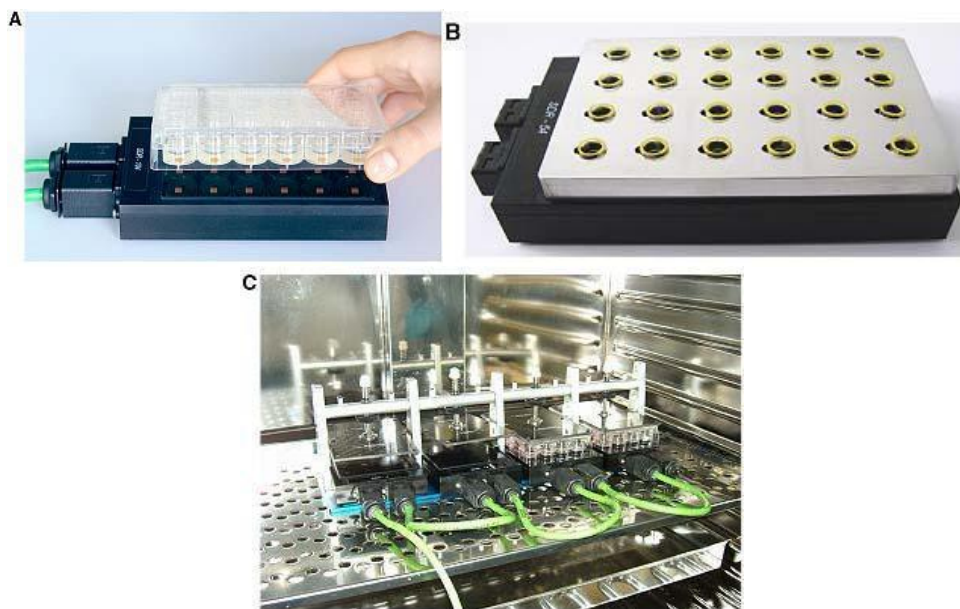
Figure 8: SensorDish device capable of simultaneously reading oxygen concentration in real-time in a custom 24-well plate. The plate to be tested sits on top of the excitation source; this device can also be operated in an incubator as illustrated in picture C above [36]. © John Wiley and Sons. Reproduced with Permission, Courtesy of John Wiley and Sons. See Appendix J: Copyright Approval.

2.6 Current System at Draper

Organ-on-a-chip technology has been a central focus of Draper's biomedical research department over the past 15 years. The device Draper is currently testing started as a single channel structure and evolved to a device with one column of eight separate channels. Now, Draper is working on a device consisting of 96 separate channels. Each step in this iterative process has consisted of validation and testing to ensure that the fabrication process, device materials, biocompatibility, channel structure, and bonding method support the device as it advances towards its final goal: mass development for drug testing.

The 96-well design has the same dimensions of common 96-well plate formats found in most laboratories as dictated by ANSI standards. This form makes the device more marketable to the general research community while providing 96 replicates for maximum drug studies. While Draper's device follows the format of a 96-well plate, it is not an addition to pre-existing 96-well devices; instead, it acts as its own system. Additionally, instead of wells, each of these 96 sections is occupied by a microfluidic construct that allows for the containment and culture of human or animal organ cells. Each channel is composed of a top and bottom segment separated by a semipermeable membrane and has two inlets and two outlets. The final version of this 96 well plate design consists of 384 separate reservoirs on the top of the device to separate the inlets and outlets. This top component integrates with a pumping system supplying the bottom channel with a supply of new media. A full depiction of the current device can be seen in Figure 9.
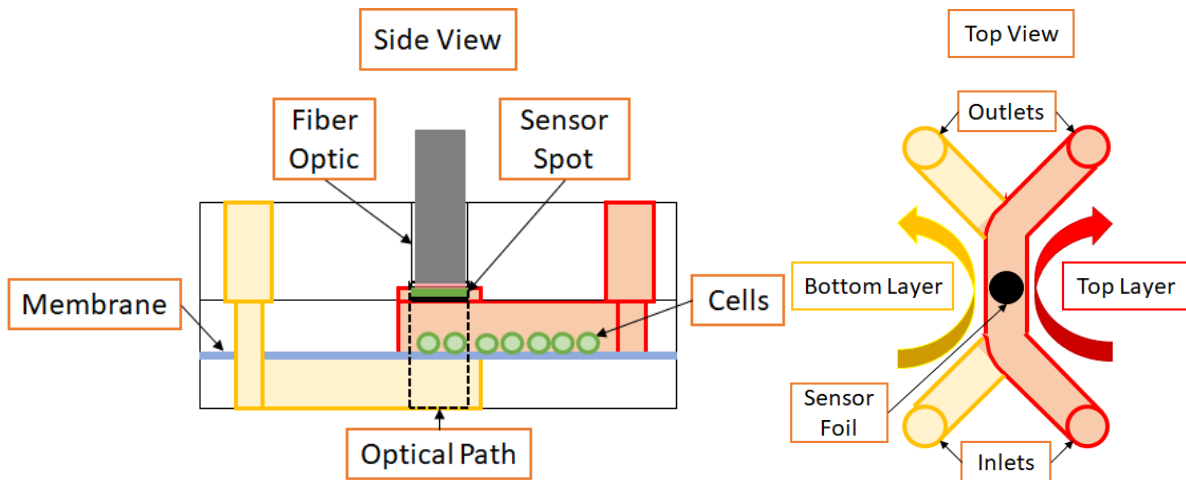
Figure 9: A graphic depicting a side view and top view of Draper's current microfluidic device. The device consists of two channels separated by a semipermeable membrane that allows for the diffusion of oxygen and nutrients between the channels. Cells are seeded in the top channel of the device via an inlet port. Oxygen concentration is currently sensed in this system through use of the Piccolo$_2$ sensor and a corresponding sensor foil as illustrated in the image above. The sensor foil inhibits the optical path in the area below the foil, as illustrated by the dotted region in the figure above.

The purpose of the semi-permeable membrane between the channels is to allow cells to be seeded in one of the chambers through the inlet port while permitting the bottom channel to be perfused continuously with fresh media. This bilayer format allows for the ability to co-culture epithelial and endothelial cells. The semi-permeable membrane prevents flow from dislodging the cells after seeding, while allowing the proper nutrients and oxygen to pass through to help maintain cell viability. Previous attempts to integrate oxygen sensing into this device utilized the removable fiber optic cable from PyroScience's Piccolo$_2$. The top layer has a specific cut out for the fiber optic to get as close as possible to an oxygen sensitive foil material, represented by the green and black rectangle in the top channel. A thin transparent film of cyclic olefin copolymer, otherwise referred to as COC, between the fiber optic and foil ensures that the channel is still a closed system, while limiting the amount of COC that separates the two. Currently the foil is 50 µm in height, which requires an extra step in the fabrication process to create a recess to place the foil into the channel without it obscuring flow. A downside of this

system is that it requires the single Piccolo$_2$ to be manually moved between each of the 96 wells of the microfluidic device.

Overall, Draper is interested in the development of an oxygen sensing system that can be added to their final product for multiple reasons. Since the final product's purpose is to enable drug testing using human organ cells, it is imperative to monitor cell viability before, during, and after testing. Oxygen sensors have proven to be an effective medium to achieve this task in real time. Moreover, Draper has previously explored the possibilities of monitoring both pH and glucose levels in their organ-on-a-chip device and the addition of an oxygen sensor will improve the functionality and marketability of their final product. Another inherent benefit of integrating an oxygen sensor is the ability to monitor oxygen in the environment where the device is being tested. Many incubators, when operating at hyperoxic levels, pump in oxygen to maintain specific environmental levels at preset rates, which can be expensive. Alternatively, an oxygen sensor can be used to ensure new media is only added when oxygen percentage is too low. In some cases the desired oxygen level may be different from what the incubator is set at, leading to the overuse of oxygen or compromised data from inaccurate oxygen levels. In addition, recording oxygen levels in these environments allows for metabolic profiling capabilities, particularly when pH is monitored in conjunction.

CHAPTER 3: METHODOLOGY

3.1 Initial Client Statement

Our team worked with Draper to aid in the design and implementation of a system for real-time oxygen measurements within organ-on-a-chip systems. The existing system is a high-throughput, microfluidic tissue culture platform capable of generating and sustaining physiologically relevant multicellular culture environments. Ideally, the results of this project should allow oxygen levels to be easily measured in Draper's platform without impeding the current capabilities of the device. Furthermore, this system must be validated through detailed procedures involving both solutions of known oxygen percentages.

3.2 Objectives

The team determined the design objectives seen in Figure 10 based on the client's needs and the information from background research. The final design should be biocompatible, optically clear, accurate, stable and adaptable, acquire data over extended periods, acquire data in an automated fashion, compatible with the current device fabrication process, and able to integrate within the current system in a high-throughput manner.
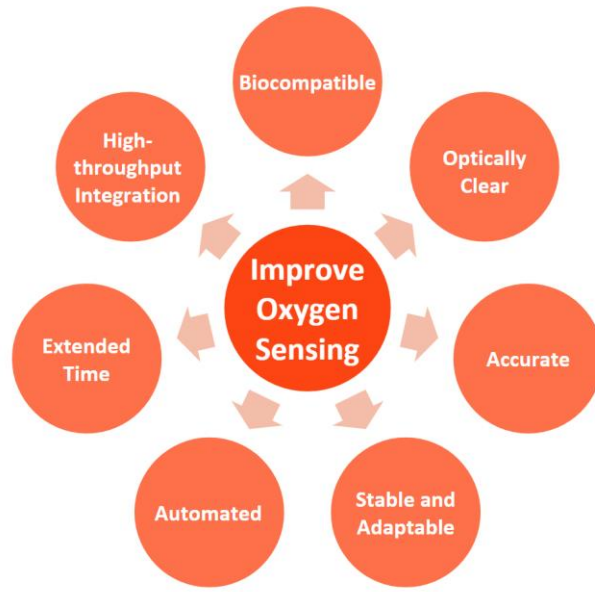
Figure 10: Design objectives. Within the central circle, the overarching goal of the project is shown. Each surrounding circle represents an objective of the solution that is ideal to assure project success.

3.2.1 Biocompatible and Bioinert

The team's addition to the current system should not affect cellular viability during normal device operation. Additionally, the oxygen indicator and incorporation method utilized within this system should not affect cellular function or phenotype throughout the testing process. To prove that cellular viability, function, and phenotype are not impeded or altered during the entire span of device utilization, all systems must be tested and compared to baseline data collected using the system currently employed by Draper. This comparison will allow the biocompatibility of the device to be evaluated.

3.2.2 Optical Clarity

The sensor format that the team pursues should allow for cells in the 96-well plate to be imaged by microscopy. Therefore, the sensor format that is selected and its associated incorporation method must be optically clear or out of the optical path, which is defined as the

channel in which tissue and cellular cultures are seeded. As defined by the clients, optical clarity can be determined through visual analysis. This means that the optical clarity of the system is sufficient if the cellular structures tested within the device can be identified and imaged.

3.2.3 Accuracy

The final device must provide accurate oxygen percentage data. Based on the PyroScience Piccolo$_2$ currently used at Draper, this is defined as a signal intensity greater than 50 mV [33]. Prior to each study, the Piccolo$_2$ must be calibrated using known oxygen standards to account for any drift in accuracy. The method of calibration depends on the sensor format being used; for example, the system has separate calibration codes specific to the sensor format that must be inputted into the PyroScience data acquisition software. Most importantly, the indicator cannot consume any oxygen because this could impede cell growth and would not reflect correct oxygen levels of the media.

3.2.4 Adaptable and Stable

The selected indicator should be adaptable, as it is meant to be used for drug research, which requires varying conditions in accordance with the type of test. For example, the sensor format must be able to work under multiple sampling rates, meaning that it must have a sufficient response time to match testing conditions. Additionally, the format should be able to withstand the environment produced during device testing and employment. This means the indicator must be able to work in standard cell culture environments with a range of parameters such as pH and salinity. Furthermore, the sensor format must be able to withstand temperature fluctuations to accommodate possible testing conditions used in drug development.

3.2.5 Extended Time

The sensor format that is selected must be able to undergo constant use for periods of up to 14 days. This means that there should not be variability in data readings at the points of primary and final testing.

3.2.6 Automated Acquisition

The indicator should be located within the channel to allow for high-precision signal acquisition. The location of the sensor format must ensure that optical sources of excitation and emission readings are able to reach the sensor without any user input. For example, the final device should not require the user to move the sensor across the channel to obtain oxygen percentage readings at desired points.

3.2.7 High-Throughput Integration

The sensor format should be able to be incorporated into the existing platform in a high-throughput manner. For example, the end user can integrate the sensor format using a multi-channel pipette or a robotic liquid handler. Similarly, the sensor format can be incorporated into the final system during the manufacturing of the plate.

3.2.8 Pairwise Comparison

The team ranked the objectives described above using a pairwise comparison chart, as seen in Table 2. A pairwise comparison chart determines the importance of design objectives by listing the objectives across the first row and down the first column of a table. Then the objective in the column is compared against the objective in the top row. A '1' in the table indicates that the objective in the column is more important than the one in the row, a '0.5' means that the two

objectives are of equal importance, and a '0' means that the objective in the column is less important than the one in the row. The total in the final column is the sum across the table, which indicates the weight of each objective. The project sponsor and team found the order of importance, ranging from most important to least important to be biocompatible and bioinert, accuracy, adaptable and stable, automated acquisition, extended time, high-throughput integration, and optical clarity. Since cells are used during device use, the clients determined that the biocompatibility of the indicator must take precedence over other objectives. This project is primarily concerned with the ability to measure accurate oxygen levels within microfluidic devices, which results in this objective being ranked second. Although optical clarity optical clarity was ranked as a '0' for the total score, it does not mean that it was not considered when the team evaluated each sensor format. This ranking means that optical clarity of the sensor format is not imperative for the system to function on a base level. For comparison, if the format was not biocompatible and toxic to cells the organ-on-a-chip device would not be functional; however, even if optical clarity was impeded the device could still be used.

Table 2: A pairwise comparison chart using the team's design objectives. Each objective is ranked comparatively to the other objectives. This allows the team to derive which objective is considered the most important with respect to the final outcome.

	Biocompatible and Bioinert	Optical Clarity	Accuracy	Adaptable and Stable	Extended Time	Automated Acquisition	High-Throughput Integration	Total
Biocompatible and Bioinert		1	1	1	1	1	1	6
Accuracy	0		1	1	1	1	1	5
Adaptable and Stable	0	0		1	1	1	1	4
Automated Acquisition	0	0	0		1	1	1	3
Extended Time	0	0	0	0		1	1	2
High-Throughput Integration	0	0	0	0	0		1	1
Optical Clarity	0	0	0	0	0	0		0

3.3 Design Constraints and Specifications

Based on input from Draper and background research, the team determined design constraints of patterning, functionality, robustness, morphology and imaging, biocompatibility, and project budget and timeline. Design constraints refer to parameters that must be met for the system to be functional. Each constraint is paired with associated quantitative specifications as illustrated in Table 3.

Table 3: Design constraints (left) and specifications (right). Each constraint is considered essential for project success. The specifications further quantify the constraints of the project to better define the requirements that characterize the constraints as being met or unmet.

Constraints	Specifications
Patterning	• 300µm - 800µm diameter • 100µm tolerance in position and size
Functionality	• Adhesion to COC substrate • <10µm thickness of sensor format • Optical signal strength (50 mV) at 1mm standoff distance
Robustness	• 7 - 14 days in 5% CO_2 and 37°C cell culture media • Withstand 120°C for 1 hour • Withstand EtO sterilization • Total force of 18,000 lbs for 15 minutes • Total force of 3,700 lbs for 40 minutes
Morphology/Imaging	• Able to obtain clear images through sensor format
Biocompatibility	• Sensor format must be biocompatible

3.3.1 Patterning

For the sensor format to be compatible with the channel size used in Draper's device, the diameter of the sensor format must be between 300 μm and 800 μm. Additionally, the means of patterning the sensor format onto the device must have a 100 μm tolerance in terms of both format positioning and size of the drops due to the channel size of the current device.

3.3.2 Functionality

In terms of functionality, the sensor format must be able to adhere to the COC substrate such that it does not wash off when subjected to the various flow conditions used during device operation. The sensor format must also yield an adequate signal intensity reading from the optical platform when the excitation source is placed a maximum of 1 mm away from the sensor format. Signal intensity refers to an output of the current optical platform, which relates to the accuracy of the readings. Higher signal intensities correspond to more accurate data and lower signal intensities mean that the output data is less likely to be representative of true parameters. The current optical platform cites that a signal intensity greater than 50 mV is required for sufficient data acquisition [33]. Additionally, the sensor format height should not exceed 10 μm since this would interfere with device operation by obstructing flow.

3.3.3 Robustness

Robustness refers to the ability of the sensor format to maintain integrity after being exposed to various parameters common during device operation. The sensor format must be able to withstand typical cell culture conditions of an incubated environment. This means the device must be able to operate within specified temperature and humidity ranges characteristic of common incubation units. The format should maintain functionality after 7 to 14 days submerged

in cell culture media in a 5% CO_2 and 37°C environment. Based on current device fabrication parameters used at Draper, the sensor format must be able to withstand exposure to a temperature of 120°C for one hour, a total force of 18,000 pounds for 15 minutes, a force of 3,700 pounds for 40 minutes, and EtO sterilization parameters.

3.3.4 Morphology and Imaging

To monitor cells in the final device during testing, the sensor format must be able to be imaged through. When imaging through the sensor format, the true cell morphology must not be altered or obstructed by the sensor format in any way.

3.3.5 Biocompatibility

The sensor format must not interfere with any features of the cellular environment including cell viability, cell functions, and phenotype.

3.3.6 Project Budget and Timeline

The project must be completed by May of 2018. The final device should be identified and prototyped for a cost of no more than $2,000 spent during the development process. A prototyping cost breakdown is detailed in Section 3.7.1 Financial Approach.

3.4 Sensor Format Functions and Functional Blocks

After developing the objectives and design constraints, the necessary functions of the device were established as illustrated in Figure 11.

Integrate into current organ-on-a-chip platform in a high-throughout manner	Provide accurate oxygen readings when used with Draper's optics platform
Functions	
Quench oxygen in response to visible light excitation	Have a lifetime of at least 14 days
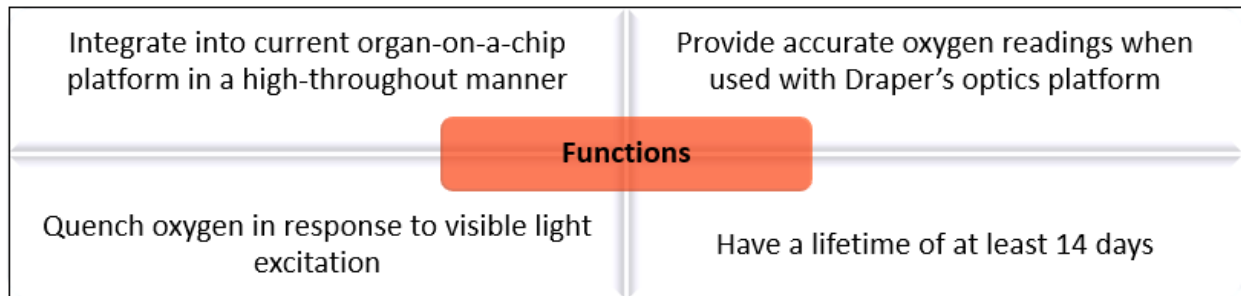
Figure 11: Functions necessary to create an improved oxygen sensing system. These functions must be accomplished by any of the selected sensor designs and their associated formats. By accomplishing all of the functions, the oxygen sensing system is assured to work within the existing microfluidic device.

The sensor format that is created must be able to integrate into the current organ-on-a-chip system in a high-throughput manner. The chosen sensor format must also be able to quench oxygen in response to visible light excitation and provide accurate readings with the optics platform at Draper. This platform will allow for the wavelength of the excitation light to be modified depending on the properties of the sensor format that is being used. However, this sensor format must have the correct chemistry to be able to quench oxygen in response to a specific excitation frequency. The sensor format also must have a high enough Stokes shift for the emission light to be differentiated by the optics platform. Lastly, the format must function for a two week time period and not degrade in exposure to cell media or visible light excitation.

3.5 Design Standards

Standards specific to microfluidic platforms have begun to emerge as these devices are becoming increasingly prevalent in industry, as seen in Figure 12.
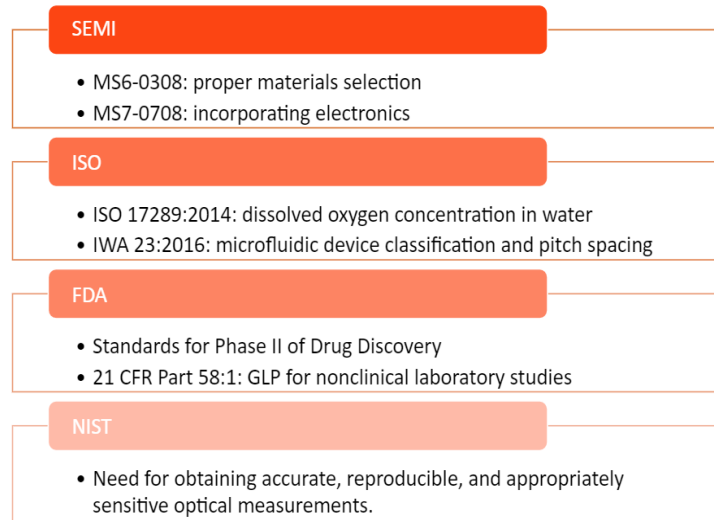
Figure 12: This figure displays the standards that the final device must follow. The device must abide by these standards, established by a variety of organizations, during the fabrication process. This process includes incorporation of the oxygen sensing system.

The National Institute of Standards and Technology, NIST, has various categories of standards that must be considered during the design of microfluidic devices. Specifically of interest to this project, the NIST recognizes the importance of obtaining accurate, reproducible, and appropriately sensitive optical measurements [37]. Few standards have been adopted by the microfluidics industry and individuals have identified a need for comprehensive standards to be adhered to throughout the field [38]. The Semiconductor Equipment and Material International, SEMI, organization has a standards program and have specifically created two major standards for microfluidics. MS6-0308 is a standard created by SEMI that outlines proper material selection for devices and design parameters that should be considered when creating a device. This standard is directly applicable to design of microfluidic devices and will be useful in selecting appropriate sensor format materials to add to the device. Secondly, MS7-0708 is applicable to this project as it has guidelines for how electronics should properly interface with

microfluidic devices, which should be considered because of integration of an optics platform with the device [39].

The International Organization for Standardization, ISO, also has two standards that are applicable to this project in terms of using an optical sensor and classifying microfluidic devices. ISO 17289:2014 outlines guidelines for determining dissolved oxygen content in water. Since our system determined dissolved oxygen content in cell media, this is not directly applicable but content in this standard will serve as a valuable reference [40]. Secondly, IWA 23:2016 contains guidelines for pitch spacing and microfluidic device classification. Although this is more applicable to the existing device than the sensing mechanism, it will be important to understand this standard to ensure the system does not violate any guidelines for proper classification [41].

The device created in this project is meant to be incorporated in a general microfluidic testing platform that can be used for drug discovery. Given this application, the device is not able to be classified as a medical device and would not be subjected to FDA standards in regards to medical devices. However, the FDA does have standards that outline the drug development process that must be considered during design if the device is intended to be used for drug discovery. The FDA splits the drug development process into five different stages with step two dealing with preclinical research and being the most applicable to organ-on-a-chip devices. This phase requires that researchers use good laboratory practices, also known as GLP, when testing drugs both *in vivo* and *in vitro*. The FDA regulations in regards to GLP that should be followed can be found in 21 CFR Part 58.1: Good Laboratory Practice for Nonclinical Laboratory Studies [42]. These standards must be known during the design process to prevent any complications in compliance when the product is complete.

3.6 Revised Client Statement

As stated in the original client statement, one of the major goals of this project is to improve the current method for acquiring oxygen percentage data from Draper's 96-well organ-on-a-chip device. This statement is broad to prevent any restrictions on the process of ideation, in turn allowing for exploration into a variety of solutions. Since the initial statement, the project has gained more dimensions and structure based off research and early design ideas.

According to the revised client statement, the scope of this project is to improve the current standard of oxygen sensing in Draper's organ-on-a-chip devices. The client wanted the team to identify possible indicators compatible with an optical platform and determine a means of incorporating this indicator into the existing device. The indicator must not compromise the usability of the current device.

3.7 Management Approach

To achieve all of the tasks outlined within the scope of this project, multiple organizational strategies were developed and are described in the following sections.

3.7.1 Financial Approach

Ultimately, this project should result in a completed oxygen sensing system by May of 2018. The entirety of this project must be completed within the given $4,000 budget. This budget has been subdivided such that 50% of all funds are allocated towards device research and development while 50% is allocated to travel costs, as per client request. As seen in the following pie graphs, displayed in Figure 13A, the design budget was subdivided into three main phases: the research phase, the prototyping phase, and the final design phase. These phases were allocated 5%, 15%, and 80% of the design budget, respectively. The final design budget was

then further divided to include budgeting towards the indicator format, means of incorporating the indicator within the microfluidic device, and additional hardware utilized throughout the production process; this division can be seen in Figure 13B. The majority of money is allocated to indicator format purchases since many luminescence quenching dyes and nanoparticles cost greater than $100 for only a gram of material. For example, the PyroScience nanoparticles cost upwards of $292.00 for 10 mg of raw nanoparticles, where eight 3 cm^2 pieces of foil material from PyroScience cost $280. Secondly, the indicator incorporation budget is also substantial due to the cost of adhesives such as PDMS or other biocompatible epoxies.
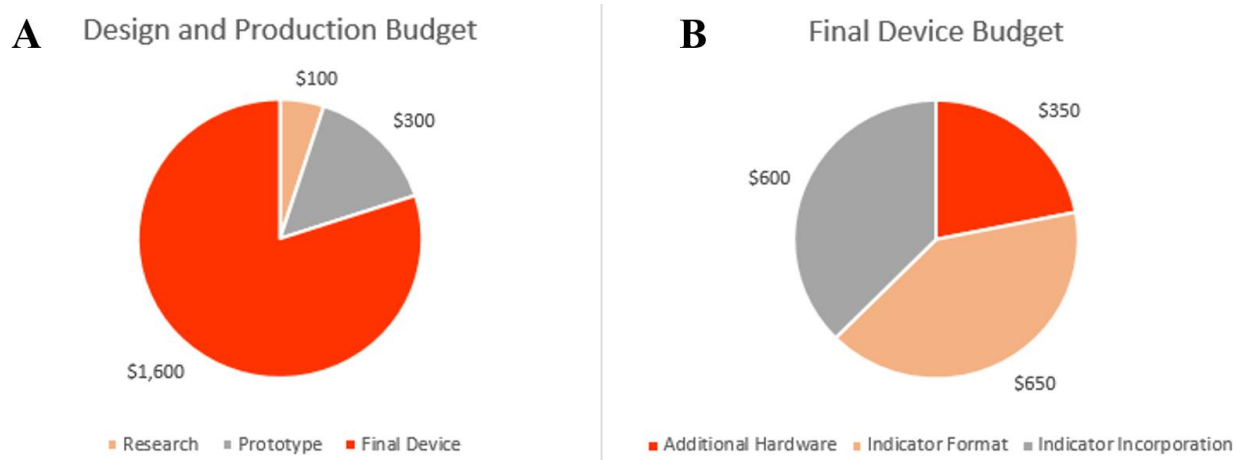
Figure 13: A: The estimated budget for the total scope of the project. This includes the three main phases of the project: the research phase, the prototyping phase, and the fabrication phase. B: The estimated budget for final device design, fabrication, and testing. The final device budget includes separate components for determining the sensor format and for determining the means of incorporating the selected format within the final device.

3.7.2 Work Breakdown

To reach this end goal, the entirety of this project has been divided into three main phases classified by their staggered completion goals throughout the 2017-2018 academic year. Initially, during phase one of this project, user requirements will be solidified. These requirements will then be analyzed to determine their total contribution to the client-defined requirements and

subsequent conceptual designs will be generated. In phase two of this project, proof of concept prototypes will be created to demonstrate the varying levels of design feasibility. The third phase of this project includes the construction and validation of a final system in accordance with methods and techniques mentioned in the client statement. To ensure the project is completed in a timely manner, each phase of the project has been subdivided into required tasks, which are included on the Gantt chart in Appendix A: Gantt Chart. To further classify the subdivisions of work that are detailed within the provided Gantt chart, the team generated a work breakdown chart shown in Appendix B: Work Breakdown Chart to ensure thorough understanding of the project scope.

CHAPTER 4: DESIGN PROCESS

4.1 Conceptual Designs

After determining the priority of the objectives, design constraints, and functions, conceptual designs were brainstormed. Two major project components were identified that are required for a fully functional system as illustrated in Figure 14. These components include the optical platform and the sensor format. In terms of the sensor format, the team considered both the fabrication method and how the format will be implemented into Draper's existing device. The optical platform refers to the means of providing visible light excitation to a sensor format in the organ-on-a-chip device in a high-throughput manner that does not require user input. Secondly, the format of the oxygen quenchable sensing material was evaluated. After deciding on a sensor format, the team considered how to fabricate the sensor format into something that could be implemented into the existing device. Lastly, the procedure for implementing the sensor format into the device was determined.
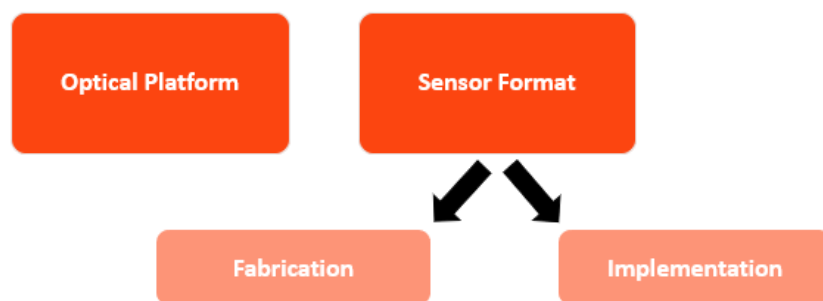
Figure 14: A breakdown chart of the project components and subcomponents. The sensor format, being the major component of interest to this team, is further broken down to fabrication and implementation components to better exemplify the different aspects that must be considered for project success.

Six different conceptual ideas were identified for the optical platform as illustrated in Figure 15.
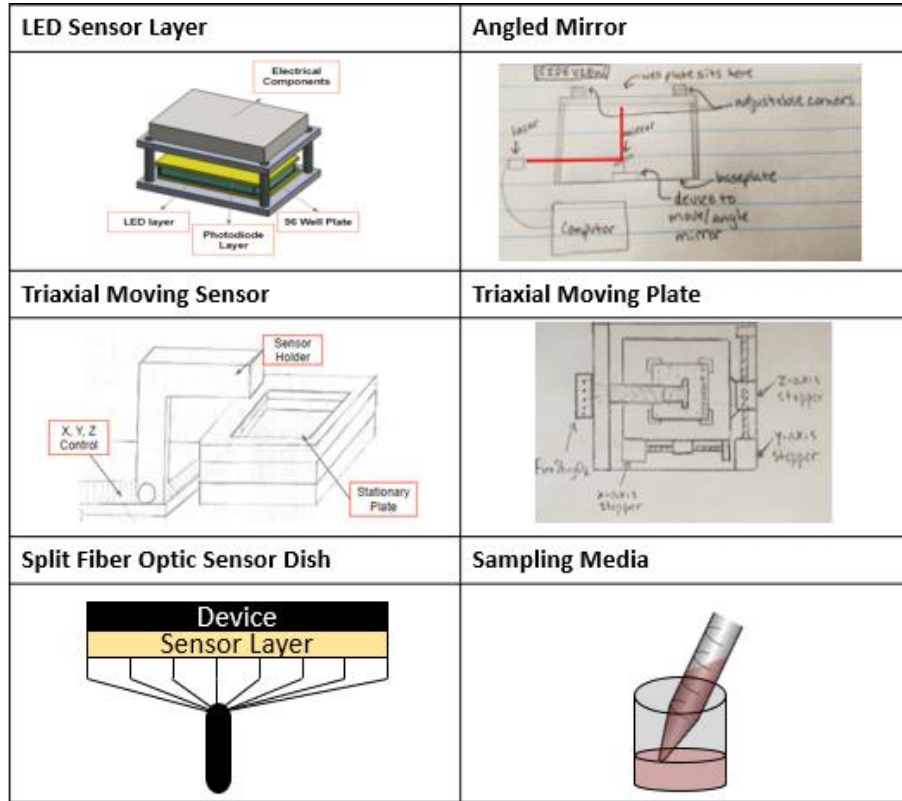
Figure 15: Conceptual designs for the optical platform. These different optical platforms operate under the same principle of sensing oxygen through optical technology. In the top left, an array of LEDs would provide excitation and emission readings to each of the 96 channels simultaneously. In the top right, an angled mirror would direct the excitation and emission signals to each of the channels in the device, moving the optical pathway to each channel. The two middle designs involve triaxial movement; the one on the left moves the sensor while the idea shown on the right moves the plate. The bottom left involves multiple fiber optic cables attached to a single sensor; each cable accesses one of the channels within the device. The bottom right corner depicts a method of sampling the media and taking oxygen readings of the sample using a standard oxygen measurement device.

The first concept was an array of 96 LEDs and photodiodes that would be matched to the excitation wavelength of the chosen sensor format. This method would completely replace the Piccolo$_2$ and could result in decreased accuracy. Secondly, a device in which a light source is shined on a mirror that could be angled to each well to excite the dye was created. The next two

conceptual designs incorporate the existing PyroScience sensor, but in a high-throughput

manner. In one iteration, a fiber optic holder, able to be moved in the x, y, and z-axes, using

three different stepper motors would move the cable to get a reading from each channel. In a

similar sense, the optical platform could be held stationary and the organ-on-a-chip device could

be moved in a triaxial manner to align each well for taking a reading. The next concept uses a

split fiber optic cable such that there is one fiber for each channel in the device. This would be

incorporated into a optical platform that the organ-on-a-chip device can sit on top of while

simultaneously acquiring readings from all channels. Lastly, the team identified that media could

be sampled from each channel and tested using Raman spectrometry. However, this method is

not feasible as it contaminates the cellular environment and is more time consuming than the

current method used by Draper. Based on these preliminary concepts, Draper decided to move

forward with creating an array of 96 LED sensors, as illustrated in Figure 16 while the team

focused on the associated format and the corresponding fabrication and implementation methods.
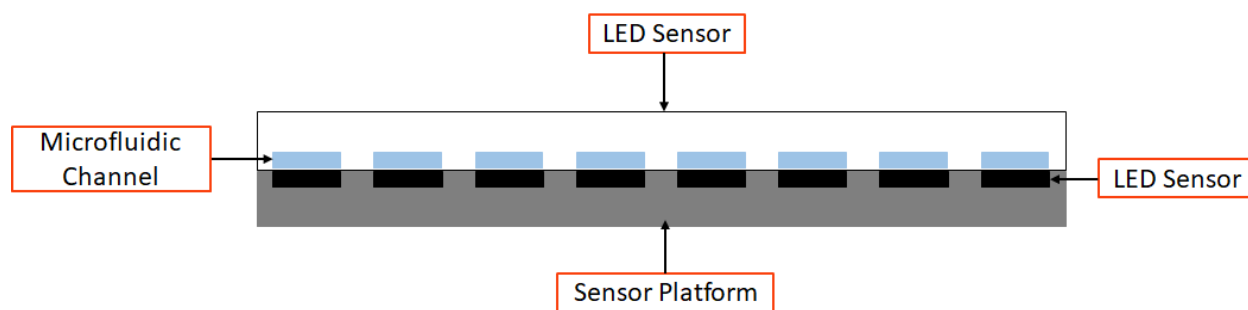
Figure 16: One-row cross section of the optical platform designed by Draper. This device consists of a 96 LED sensors able to excite a sensor format in each microfluidic channel to obtain real-time oxygen concentration measurements in each channel.

Three sensor formats for incorporating the oxygen quenchable dye were identified based

on their compatibility with the current system as illustrated in Figure 17. The first possibility

uses a raw dye solution, which can either be purchased from a vendor or synthesized in a lab.

Alternatively, the same chemical that is in the dye is commercially available through vendors,

like PyroScience, in different forms including foils and nanoparticles. The foils come in small

sheets in which different shapes can be punched out and incorporated into the existing device. In

contrast, the nanoparticles can be suspended in solution and put into a matrix or directly injected

into the culture media. All of the sensor formats pursued operate using the principle of

fluorescence quenching in the lifetime domain.
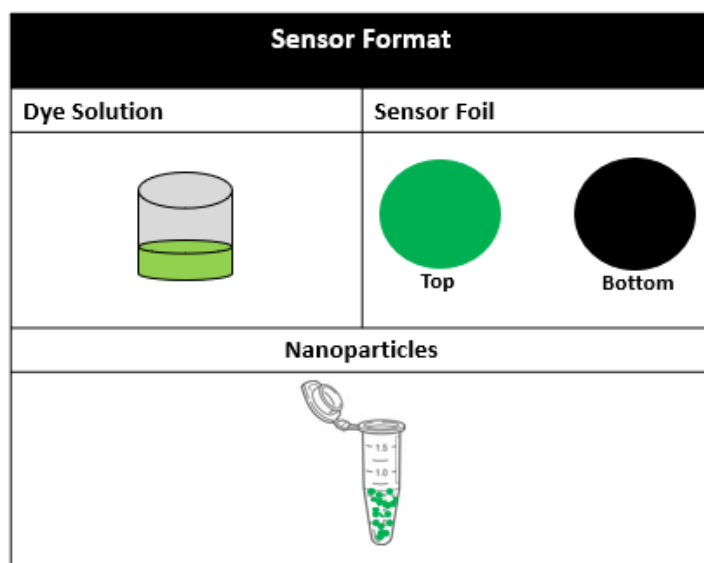
Figure 17: A diagram of three possible sensing formats that incorporate the oxygen quenchable dye. The top left shows a dye-based solution that incorporates the oxygen-sensitive chemical. This same chemical is used in the sensing foil, shown in the top right, and the nanoparticle-based indicator, shown in the bottom.

After determining the possible sensor formats, fabrication methods were brainstormed, as

seen in Table 4. One option would be that the nanoparticles could be suspended in a solution like

DI water or a detergent. Additionally, the sensor format could be placed in a matrix like PDMS

through various means. One example would be a PDMS stamp with nanoparticles acting as the

ink. Furthermore, the nanoparticles could be mixed with PDMS prior to polymerization.

Table 4: Table of the different fabrication methods explored during this project. Each fabrication method is displayed in the left column. The different sensor formats to which these methods are applicable are shown in the right column.

Fabrication	
Suspended Solution	• Nanoparticles in cell media • Nanoparticles in detergent (SDS, Triton x 100, CTAB)
Dried on Surface	• Dried nanoparticle suspended solution
PDMS Stamp	• Nanoparticles dried on glass slide, PDMS cured on top
Mixed in PDMS	• Nanoparticles mixed in PDMS prior to polymerization • Dye encapsulation in PDMS

After considering the excitation methods, the team considered sensor formats, fabrication methods, and concepts for implementing the format into the existing device, as seen in Table 5. The first concept explored used PDMS to adhere the fabricated sensor format into each channel. Alternatively, another adhesive like epoxy could be used in a similar fashion. However, it was uncertain if epoxy will react with the chemical dye and render it unreliable. Additionally, if the sensor format is fabricated in a solution it could be injected into the inlet port of each channel. The sensor format could also be patterned onto the COC prior to bonding and dried onto the surface as a film. The final possibility involved depositing a uniform layer of the indicator on the COC and processing the sample using a Carver press. A Carver press simultaneously heats and applies pressure to a material that is placed between its platens. The team hypothesized that heating the material just under the glass transition temperature would cause the sensor format to be pressed into the COC due to softening at elevated temperatures.

Table 5: Table of the different format implementation methods explored during this project. In the left column, a general name that represents each of the implementation methods is displayed; in the right column, these methods are explained in further detail.

Implementation	
PDMS	• Bond sensor format to device with PDMS
Epoxy	• Bond sensor format to device with epoxy
Injection	• Inject dye or nanoparticle solution into each channel
Dried	• Dry patterned dye or nanoparticle solution into each well of the device
Heat Press	• Even distribution of nanoparticles on COC surface • Put surface in between a clamp and heat below glass transition temperature

4.2 Alternative Designs and Feasibility Testing

The team then identified alternative designs to pursue in terms of implementing sensor formats and their fabrication. The alternative designs selected are illustrated in Figure 18 and will be elaborated on in this section.
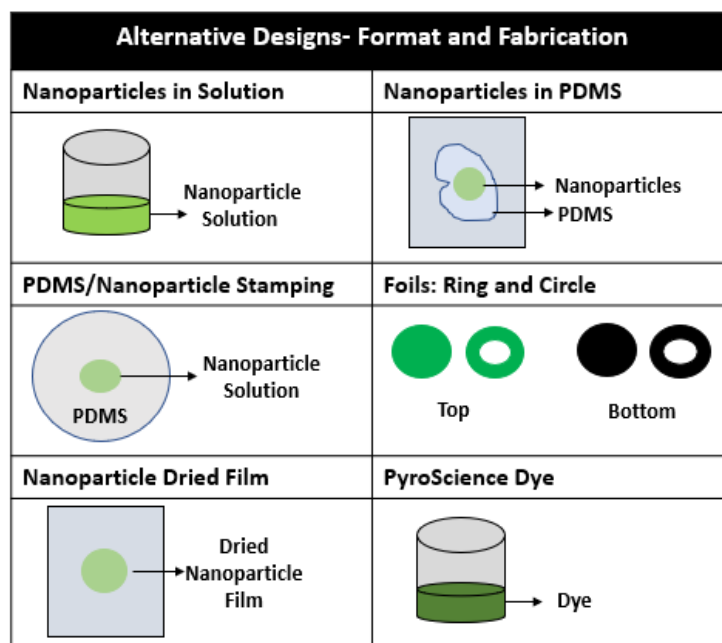
Figure 18: Alternative designs to pursue in terms of implementing sensor formats and their fabrication. Each of the blocks in this figure represent a combination of the different format and fabrication methods. The implementation component of this project is not included in this diagram.

4.2.1 Foil Testing

Testing was performed with the foil material that is used in the current system at Draper, to determine if altering foil geometry was a feasible solution to the optical clarity objective. A solid circle and a ring of foil material were bonded to a polystyrene well plate using PDMS, as illustrated in Figure 19. To gauge the optical clarity of these of formats, they were each imaged at 4X magnification as illustrated in Figure 20. Despite having better clarity, due to the open center, the ring was concluded to not provide sufficient optical clarity.

Figure 19: Preliminary foil testing with solid foil and ring foil, foils were bonded to polystyrene well plate using PDMS. The foils were cut using standard biopsy punches and then set in the PDMS. The PDMS was allowed to cure for 48 hours at room temperature.
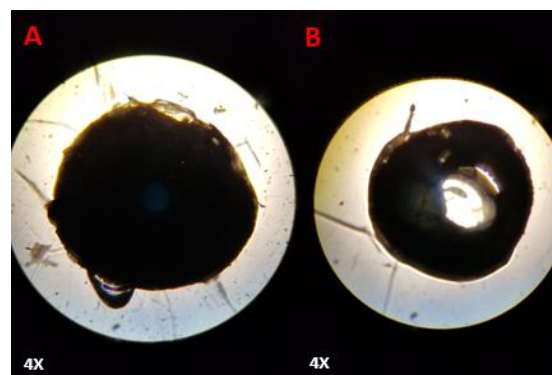
Figure 20: Optical impedance of a 1 mm diameter foil under 4X magnification. The black spots indicate the location of the foil within the well. This representatively shows the significant optical impedance of the microfluidic channel generated through the use of the foils.

In addition to optical clarity tests, the signal intensity measured with each foil geometry was recorded as illustrated in Table 6. These tests concluded that the ring foil would not provide sufficient signal intensity unless the Piccolo$_2$ was moved to the border of the foil. This would not improve upon Draper's current system and therefore was not considered for further evaluation. Further testing could be run to determine the minimum foil size necessary to obtain adequate signal intensity; however, this would mean that there would still be a portion of the channel that is not optically clear which does not meet the project objectives.

Table 6: Piccolo$_2$ signal intensities corresponding to a solid foil, the center of a foil ring, and the edge of a foil ring. The fiber optic cable of the Piccolo$_2$ was held flush to a polystyrene well plate, corresponding to a distance of 1.8 mm away from the foil.

Foil Geometry	Signal Intensity (mV)
Solid foil	89.09
Center of ring of foil	39.44
Edge of foil ring	81.99

4.2.2 PyroScience Dye

The team also pursued using a dye-based form of the indicator solution, which was the raw form of the nanoparticles. The dye comes in both hydrophilic and hydrophobic forms; fabrication instructions of both forms of this dye can be found in Appendix C: Dye. Appendix C highlights the effects of the chemicals, which are used in the creation of the two dye forms, on COC. This serves as means of validating the compatibility of these chemicals in reference to the final device. To explore the concentration of the indicator in the dye, the team analyzed droplets of the hydrophilic dye suspension via microscopy, shown in Figure 21. Initial visual inspection

indicated that the dye is highly concentrated; despite this, initial testing using the Piccolo$_2$ system resulted in a signal intensity in the 128 mV range, which was much lower than expected.
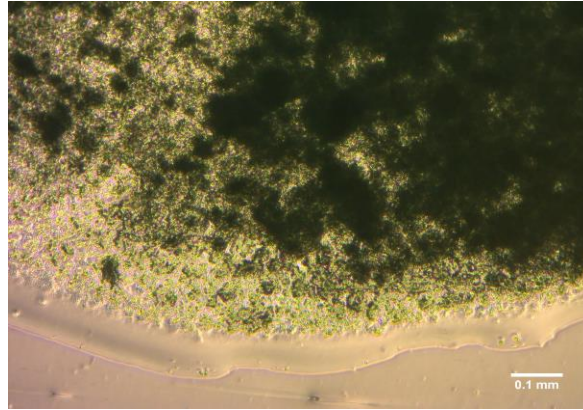
Figure 21: Droplet of the hydrophilic dye suspension under 10X magnification. As shown, the dye is extremely concentrated and, thus, causes significant impedance of the optical pathway of the device.

As shown in the above figure, the hydrophilic dye suspension resulted in an opaque layer across the surface of the COC. To determine the topography of the dye layer, the team imaged the center of the droplet under a laser confocal microscope at 20X magnification, the results of which are displayed in Figure 22 below. As shown, there was significant variation in the height across the surface of the COC after the dye dries. This was most likely because the hydrophilic form of the dye exists as a suspension rather than a homogeneous solution and contains particles of significant size that affect the overall surface topography.
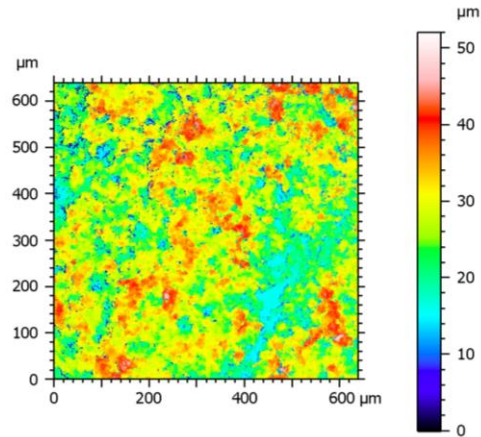
Figure 22: Laser confocal analysis at 20X magnification of a hydrophilic dye solution droplet dried on a piece of COC. This figure shows the rough surface topography of the dye when placed on COC and shows the prominent height of the dye solution. Being that the dye solution is nearly 50 microns in height, there would be flow impedance within the microfluidic channel.

4.2.3 Nanoparticles

To determine the best method for incorporating nanoparticles into Draper's device, the team explored various preparation methods using nanoparticles. The team first looked at suspending nanoparticles in solution, then nanoparticles mixed in PDMS, PDMS stamping of nanoparticles, and a dried film of nanoparticles.

4.2.3.1 Nanoparticles in Solution

The team performed additional testing with nanoparticles mixed with a 21% oxygen DI water solution. 2 mL of nanoparticle stock solution at a concentration of 5 mg/mL was created by adding 2 mL of deionized water to the dry stock of nanoparticles. Team members created dilutions from 5 mg/mL to 0.5 mg/mL, decreasing in 0.5 mg/mL increments, with two replicates for each concentration. A concentration of 0.1 mg/mL was also prepared since this is the minimum concentration recommended by PyroScience. The setup for the dilution well plate can be seen in Figure 23. Throughout this testing, all data was analyzed using a MATLAB program the team developed which can be found in Appendix D: MATLAB Code for Piccolo$_2$ Data

Analysis. This testing illustrated the immense difficulties with creating a homogeneous

distribution of nanoparticles on the bottom of a hydrophilic surface. Not only did the

nanoparticles noticeably settle in less than two minutes, but also they visibly clumped to the

center of the well. Additionally, higher concentrations of nanoparticles showed a greater signal

intensity compared to lower nanoparticle concentrations. Detailed testing data can be seen in

Appendix E: Dilution Testing of Nanoparticles.
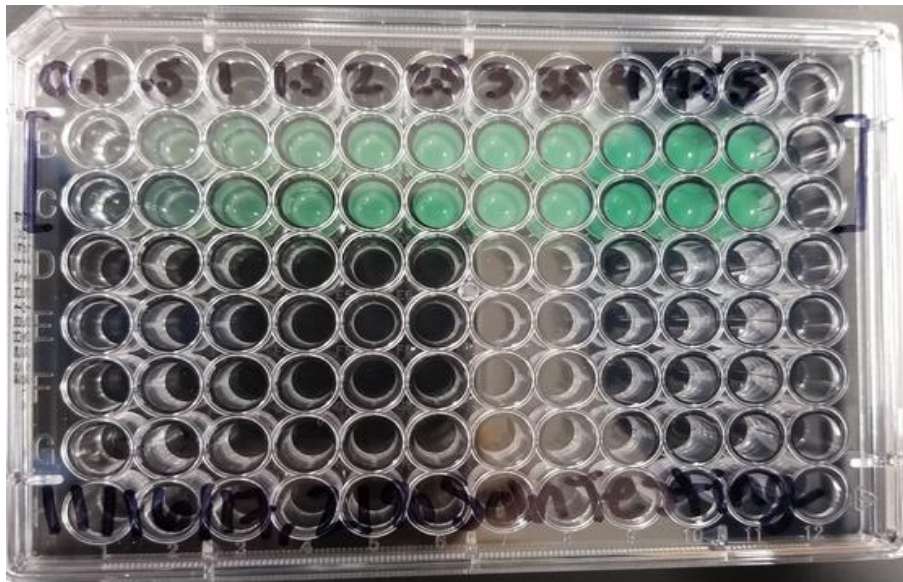
Figure 23: Nanoparticle dilution testing setup with two replicates for each concentration. Moving across the different columns of this well plate from left to right, the concentration of the nanoparticle solution increases. The initial concentration is 0.1 mg/mL, followed by a concentration of 0.5 mg/mL. All subsequent concentrations span between 0.5 mg/mL and 5 mg/mL in increments of 0.5 mg/mL.

4.2.3.2 Nanoparticles in PDMS

The next method of interest involved the use of polydimethylsiloxane, referred to as

PDMS, which is a biocompatible polymer created through the combination of a two-part silicone

based organic polymer. The specific type of PDMS used for testing was Sylgard 184, which has

a fast curing rate of 45 minutes at a low temperature of 75°C, making it extremely easy to

prototype with and rapidly produce. PDMS was utilized in various ways for alternative design

testing with both the PyroScience nanoparticles and foils. The first study that was performed was a PDMS peel method in which 3 µL drops of nanoparticle solution at concentrations between 2.5 mg/mL and 5 mg/mL in 0.5 mg/mL increments, were dropped onto a glass slide. The droplet was then allowed to dry at room temperature. After drying, uncured PDMS was dropped on top of each dried film of nanoparticles as illustrated in Figure 24. The glass slides were then put into an oven at 70°C for 50 minutes to allow the PDMS to cure. A large amount of residual nanoparticle solution was left on the glass slides after peeling off the PDMS, resulting in low nanoparticle concentrations on the PDMS and signal intensities below the 50 mV threshold. Due to the insufficient signal intensities from this method, the nanoparticles were mixed with PDMS to prevent the nanoparticles from sticking to the glass slide, thus creating a higher nanoparticle concentration. However, this resulted in the nanoparticles being encased in the PDMS, which gave inaccurate oxygen readings. The complete data from these tests can be found in Appendix F: Nanoparticles in PDMS.

Figure 24: Testing setup for PDMS stamp with nanoparticles testing. Nanoparticle solution was dropped on the slide and then PDMS was cured over the dried drop.

4.2.3.3 PDMS Stamping

To determine means of effectively transferring the oxygen indicator solution to the device, PDMS stamping was explored as a possible option. In reference to this project, PDMS stamping involves exposing a raised pattern on pieces of PDMS to the indicator solution and

placing the exposed stamp onto a piece of COC. In theory, the indicator will transfer from the

PDMS onto the COC, thereby distributing the solution across the surface in that pattern.

Two methods were explored as means of exposing the PDMS to the indicator solution.

The first method involved placing a PDMS stamp in a bath of nanoparticle solution and allowing

the stamp to sit in the solution for a set period of time as seen on the left in Figure 25. The

second method involved placing the nanoparticle solution directly onto the top of the PDMS

stamp for a set amount of time as seen on the right in Figure 25. The PDMS stamp was exposed

to the nanoparticle solution for 5 minutes and then transferred to a piece of COC patterned side

down. Despite being able to transfer a visible pattern, the PDMS stamp proved ineffective at

transferring the required amounts of nanoparticles for accurate intensity readings as illustrated in

Figure 26.
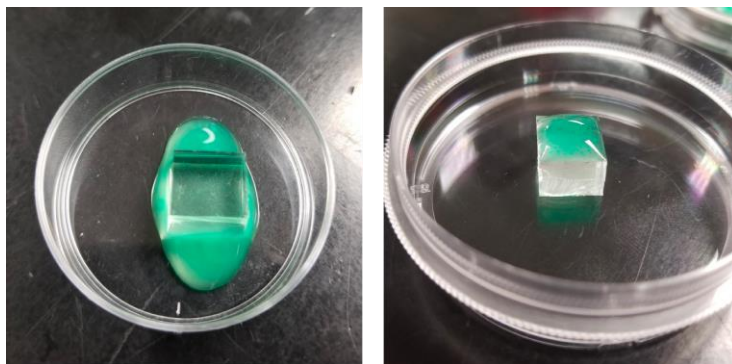
Figure 25: PDMS stamp soaking in a bath of nanoparticle solution (left) and a PDMS stamp with nanoparticle solution placed on the top, patterned face (right). These two methods were used to coat the PDMS stamp with the nanoparticle solution prior to placement on the COC surface.
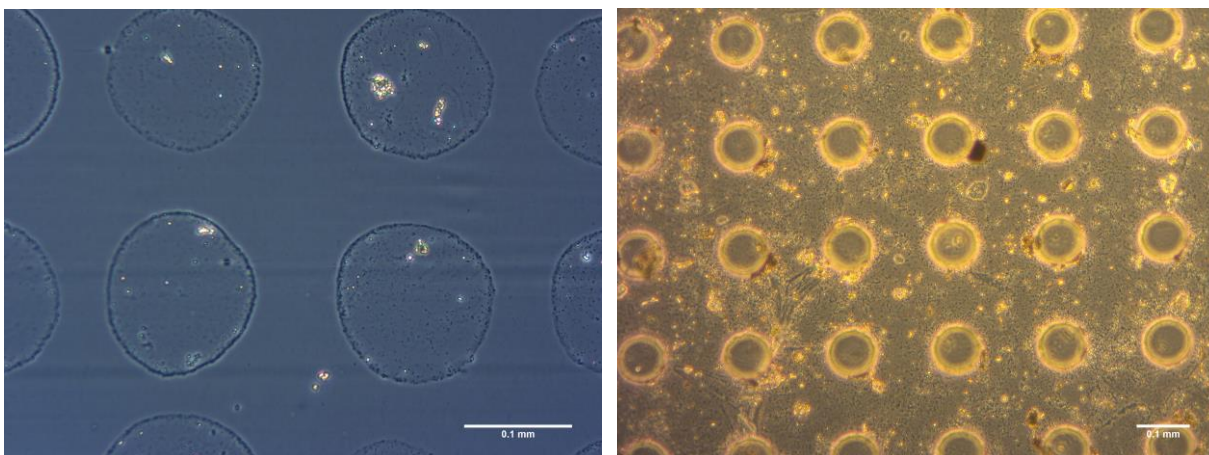
Figure 26: Nanoparticles patterned onto a piece of COC at 20X (left) and residual nanoparticles on the PDMS stamp at 10X (right). There is a much more obvious prevalence of the nanoparticles on the surface of the PDMS stamp as opposed to the surface of the COC.

4.2.3.4 Dried Film

The team dropped the nanoparticle solution onto pieces of COC. This resulted in a clumpy and dense droplet of nanoparticles due to the hydrophobicity of the COC, as seen in Figure 27 below. This clumping caused a significant impedance of optical clarity.
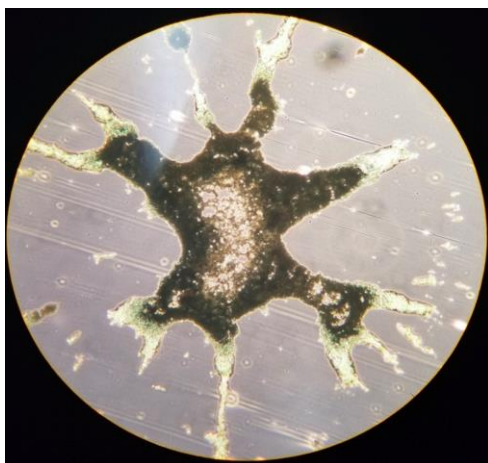
Figure 27: Dried droplet of nanoparticle solution onto the COC at 10X. This image shows the clumping that can occur in accordance with the static nature of the nanoparticles and hydrophobicity of the COC.

In an attempt to obtain a more even distribution of nanoparticles, the team explored salts

and detergents as means of modifying the surface tension of the solution. This testing resulted in

a more even distribution of the nanoparticles. However, these options were not pursued because

the detergent would modify the cellular environment and the salt left apparent crystals that

impeded optical clarity. Further results of this testing can be seen in Appendix G: Nanoparticle

Dried Film.

To avoid this clumping without altering the chemistry of the indicator dye, the team

altered the surface chemistry of the piece of COC by plasma treatment. Prior to plasma

treatment, the contact angle of the nanoparticle solution on COC was measured to be 66° versus

a contact angle close to zero after plasma treatment, these results are qualitatively shown in

Figure 28.
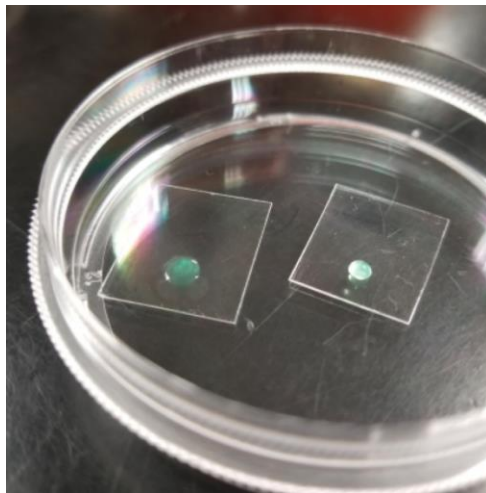
Figure 28: Nanoparticle solution on the surface of plasma-treated COC (left) and on untreated COC (right). As shown, there is a much more significant distribution of the nanoparticle solution on the surface of the oxygen plasma treated COC.

4.2.3.5 Narrowing the Nanoparticle Preparation Method

After experimenting with the four different preparation methods of the nanoparticles, the team determined that the best option to pursue was the dried film on a plasma treated COC surface. This method yielded a sufficient distribution of particles and adequate signal intensity. Mixing the nanoparticles in aqueous solution was determined to not be a feasible option due to the need for contaminating device media. Mixing the nanoparticles with PDMS also had a low signal intensity and any oxygen readings would be inaccurate due to complete encapsulation of the nanoparticles in PDMS. PDMS stamping was determined to be ineffective due to lack of sufficient transfer and a corresponding low signal intensity.

4.3 Format Implementation Testing

Based on the dye having a height higher than the required specifications and the nanoparticle dried film not completely adhering to the COC, the team looked to using heat and pressure to flatten and adhere the formats to the COC. This led the group to use a Carver press to embed the particles into the surface of the COC by heating it to just below the glass transition temperature. Figure 29 below displays the setup used for the Carver press method.
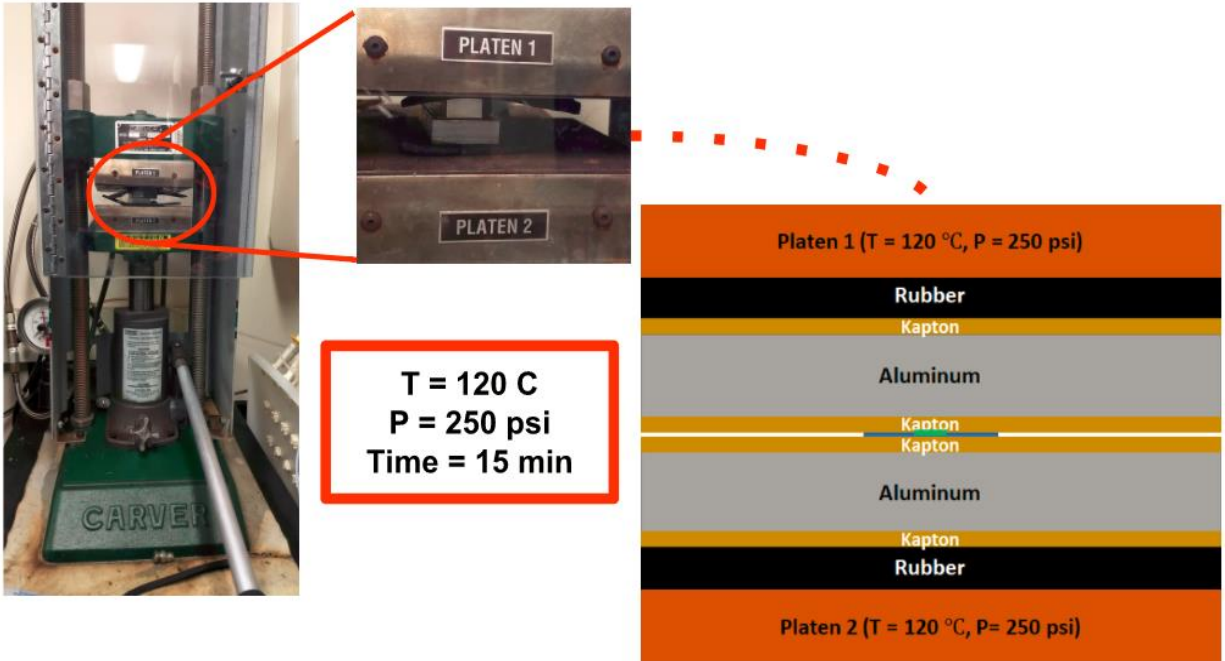
Figure 29: Carver press setup. As shown, the Carver press involves the use of two heated platens designed to apply set amounts of temperature and pressure over a pre-specified time interval. The COC and sensor format is placed between layers of Kapton, aluminum, and rubber. The rubber primarily act as a compliance layer and fosters heat transfer to the COC.

The initial Carver press settings were 120°C at 250 psi for 15 minutes. This initial testing was performed on three samples of COC with dried nanoparticles. This testing had some surprising results as it appeared that the core of the nanoparticles were made of a polymer with a transition temperature at or below that of the COC which caused the particles to flatten and spread as the polymer melted. In accordance with this spreading, the team noted that the pressed samples showed significant improvements in optical clarity as illustrated in Figure 30.
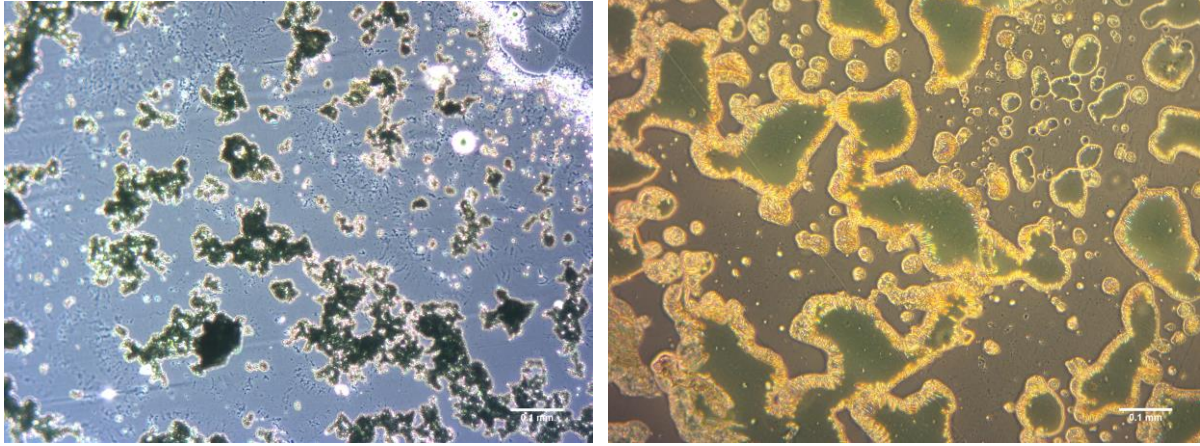
Figure 30: Nanoparticles before Carver press processing (left) and nanoparticles after initial Carver press processing (right) at 10X. As shown, the particles are much more distributed across the surface of the COC due to the pressure and temperature of the Carver press. Additionally, following processing with the Carver press, the nanoparticle mixture allows for much less optical impedance, as shown by the lighter color of the nanoparticles, which indicate that more light is able to pass through.

The team also processed a PyroScience dye droplet sample using the Carver press at 250 psi of pressure at 120°C for 15 minutes. This test was performed to determine if the dye would act similarly to the nanoparticles by creating an optically clear layer as well as reducing the height of the drop. Images taken prior to and following this pressing can be seen in Figure 31. As shown, there was a much more uniform layer across the surface where the droplet was, though there was still significant amounts of opacity that affected the overall optical clarity of the indicator causing it to be rejected for future analysis.
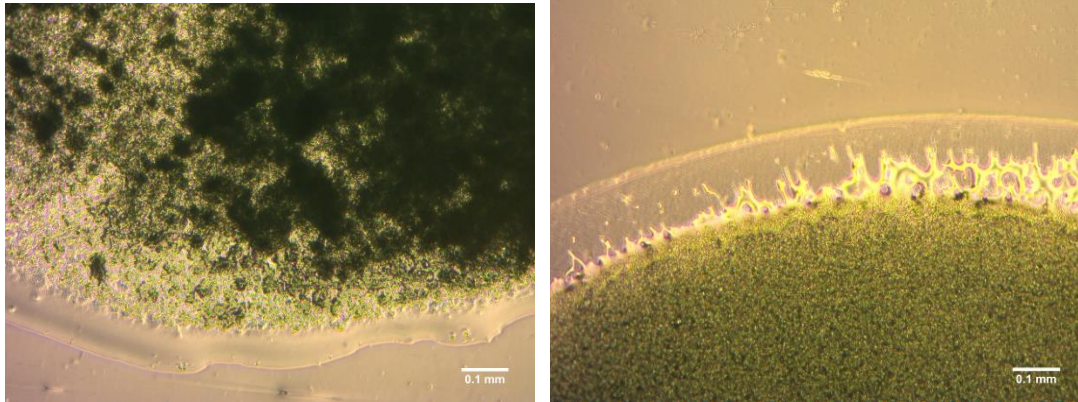
Figure 31: Dried hydrophilic dye droplet on COC prior to Carver press processing at 10X (left) and the dried hydrophilic dye droplet on COC after using the Carver press at 10X (right). Similar results to that of the nanoparticles following processing with the Carver press were seen, being that the dye is much more evenly distributed than prior to the Carver press processing.

4.4 Durability Testing

Each of the samples of COC were put through durability testing after being processed in the Carver press to determine if the formats were sufficiently adhered to the COC. This testing included a light wash, a heavy wash, and two scratch tests. Before all testing, a marker was placed on the pressed area and an image was taken using the confocal microscope to ensure that the same area was being imaged each time. The light wash consisted of a continuous light spray of DI water for five seconds onto the dried drop of nanoparticles. During the heavy wash, the team vigorously rinsed the piece of COC for five seconds. After the wash test, a scratch test was performed using a plastic pipette tip, which was dragged across the surface of the pressed area. A second scratch test was performed using a metal point, which was also dragged across the surface of the pressed area. After each round of testing, an image was taken for comparison with the original to see if anything was removed from the surface. For almost all, this testing had no effect on the pressed sample.

A tape test was also performed on some of the samples to see if the particles could be removed. A premium lab grade labeling tape was used and the group saw that some of the

nanoparticles had been lifted off with the tape, as seen below in Figure 32. The team concluded

that this test removes a portion of the nanoparticles. However, this effect was not concerning,

because the results were not representative of how the particles would be used in the final device.

When in use, the nanoparticles would not experience normal tensile forces that are generated

when removing the tape.
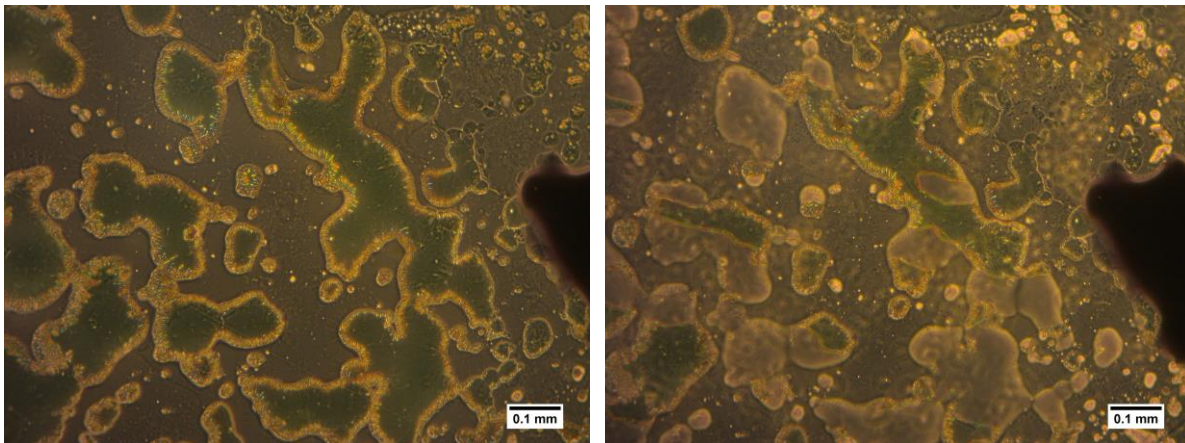
Figure 32: Before (left) and after (right) tape testing at 10X. Significant amounts of the nanoparticles were removed following the tape testing. However, these tests are deemed to not be representative of the conditions under which the device will operate.

Both the nanoparticles and dye saw more desirable characteristics after processing with

the Carver press and based on initial durability tests, were sufficiently adhered to the COC.

Based on these results, this method was chosen as the final mean of sensor format

implementation for this project.

CHAPTER 5: DESIGN VERIFICATION

After determining that the Carver press method was the best for implementing the oxygen indicator, a series of validation tests were designed and run on the foil, nanoparticle, and dye formats to determine the final design. These tests aligned with the constraints of the project and included an optical clarity test, a soak test, a thermal test, a sterilization test, and an oxygen duration test using the PyroScience Piccolo$_2$.

5.1 Optical Clarity Testing

The team used histological slides of a section of human skin tissue to test optical clarity using the method illustrated in Figure 33.
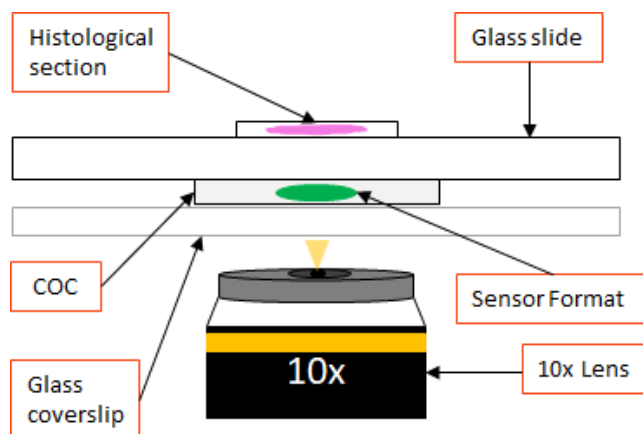
Figure 33: Test method for evaluating the optical clarity of each sensor format. The sample of COC with the sensor format patterned on it was placed on top of a glass coverslip, which was then placed on the microscope stage. The histological section adhered to a glass slide was placed directly on top of the sensor format sample.

Figure 34 shows half-overlaid comparisons between each of the sensing formats on top of and underneath the histological slide. The foil material on top of the slide allowed for very little of the tissue sample to be seen, while on the bottom, none could be seen. The pressed dye

allowed the tissue sample to be seen when on top, but not on the bottom. On the other hand, the tissue sample could be seen through the pressed nanoparticles on top and on the bottom of the slide. Imaging through the bottom represented the worst-case scenario because the microscope would have to look through the sensor format to focus on the biological sample.
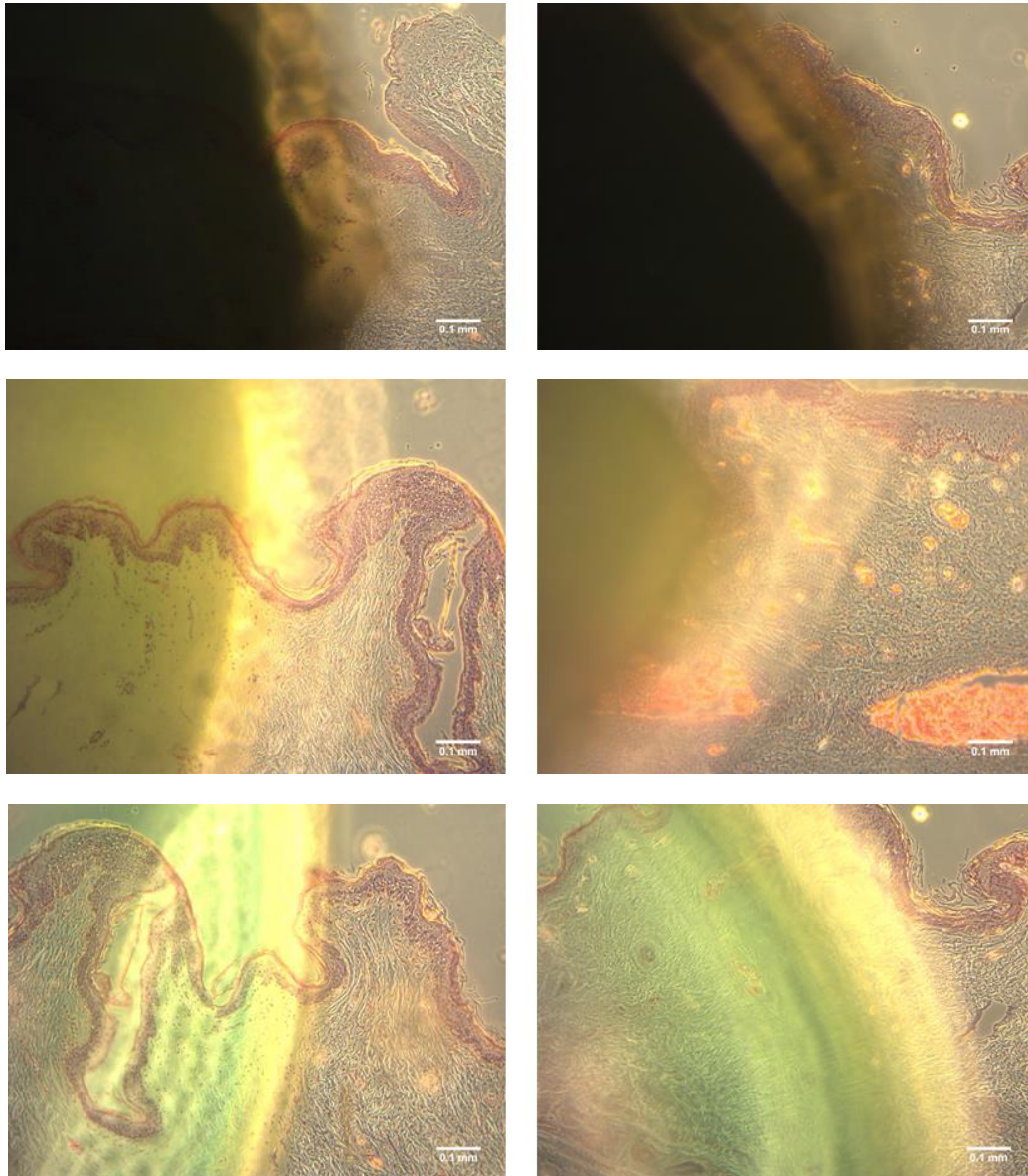
Figure 34: Foil material on top of histological slide (top left), foil material under histological slide (top right), pressed dye on top of histological slide (middle left), pressed dye under histological slide (middle right), pressed nanoparticles on top of histological slide (bottom left), and pressed nanoparticles under histological slide (bottom right) all at 10X.

5.2 Verification of Durability Testing

For the soak test, thermal test, and sterilization test, the team used the PyroScience Piccolo$_2$ to test the integrity of the sensor by comparing intensity readings before and after the test. To do this, the sample was placed in a 12 well polystyrene cell culture plate and the Piccolo$_2$ was held flush to the bottom of the plate, as seen in Figure 35. The thickness of the polystyrene plate, meaning the distance between the fiber optic and the sensor format, was 1.8 mm. The Piccolo$_2$ was allowed to stabilize and then the signal intensity was recorded for each point of interest.
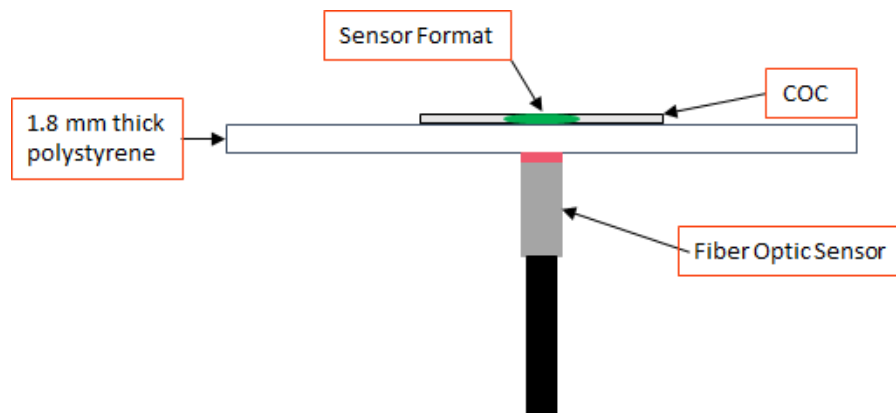
Figure 35: Piccolo$_2$ test method for validating the integrity of the sensor format after soak, thermal, and sterilization testing. The Piccolo$_2$ sensor was held flush to the bottom of a 12 well cell culture plate and the signal intensity was recorded.

5.3 Soak Testing

One form of validation that the group tested the samples with was a soak test, designed based off recommendations from ASTM standard C1247-14. In preparation for this, a 3 mm foil circle was placed in a drop of PDMS on a cut piece of COC, a 3uL drop of 40 mg/mL nanoparticle solution was placed onto COC and pressed, and a 3uL drop of hydrophilic dye was placed onto COC and pressed. Signal intensity data and images were gathered for all samples.

Each of these samples were then placed in contact with 2 mL of standard cell culture media in a well of a 12 well cell culture plate, as seen in Figure 36 below. The media is comprised of 10% fetal bovine serum (FBS), 1% Penicillin Streptomycin, 1% GlutaMAX supplement, and 88% Dulbecco's Modified Eagle Medium (DMEM). These samples and media were put in an incubator at 37°C. After 14 days, each sample was tested for signal intensity and imaged on the inverted microscope.
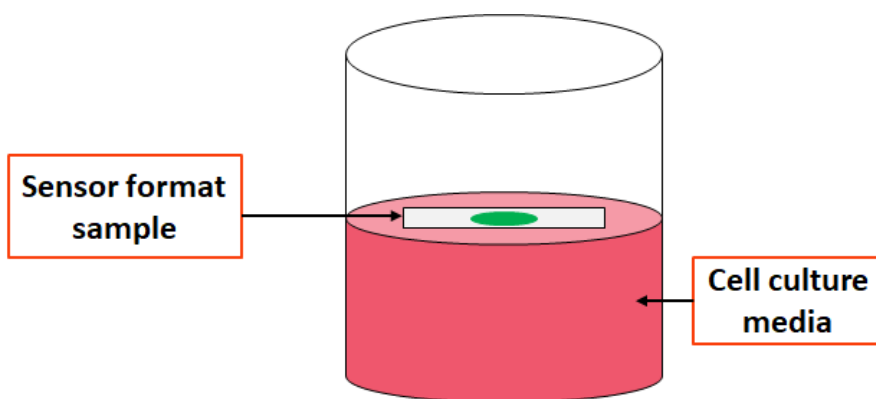
Figure 36: Diagram of the sensor format sample in 2 mL of cell media in one well of a 12 well cell culture plate.

The data displayed in Table 7 showed that the signal intensity for the hydrophilic dye sample increased after 14 days, the nanoparticles decreased to an inadequate signal intensity, and the foils decreased but stayed above 50mV. The decrease in signal intensity below the 50 mV threshold for the nanoparticles was due to a low concentration of the prepared nanoparticle solution. However, this could be easily remedied by using a higher concentration of nanoparticles meaning that all sensor formats have the ability to withstand 14 days in cell culture media.

Table 7: Signal intensity readings before and after the soak test.

Sensor Format	Intensity Reading Prior (mV)	Intensity Reading Post (mV)
Dye	72	103
Nanoparticles	56	30
Foil	64	55

5.4 Thermal Testing

Another validation test that the group performed was a thermal test, which was designed in accordance with ASTM D7895/D7895M-14. This was done to ensure that the signal intensity of the samples would not be affected during Draper's fabrication process of the organ-on-a-chip device. In preparation for this test, a foil circle was placed in a drop of PDMS on a cut piece of COC, a 3uL drop of 40mg/mL nanoparticle solution was placed onto COC and pressed, and a 3uL drop of hydrophilic dye was placed onto COC and pressed. Signal intensity data was collected and images were taken on an inverted microscope for each sample prior to the thermal test. The samples were then placed in an oven at 120°C for one hour, as seen in Figure 37 below, and signal intensity data and images were collected after the test.
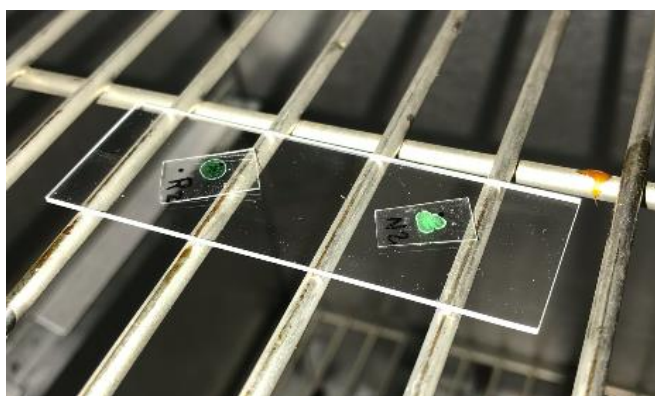
Figure 37: Nanoparticle and dye resting on a glass slide in the oven during the thermal test.

Table 8 shows that all of the samples maintained a sufficient signal intensity after thermal testing.

Table 8: Signal intensity readings before and after the thermal test.

Sensor Format	Intensity Reading Prior (mV)	Intensity Reading Post (mV)
Dye	111	106
Nanoparticles	100	105
Foil	76	68

5.5 Sterilization Testing

Being that the final microfluidic device is subjected to ethylene oxide (EtO) sterilization, the sensor format must be able to provide accurate readings following this processing, as seen in Figure 38. All samples were subjected to EtO sterilization for a period of 12 hours. The samples were then left on the bench top for a period of 24 hours to degas. This testing was designed based off recommendations from ISO 11135:2014.
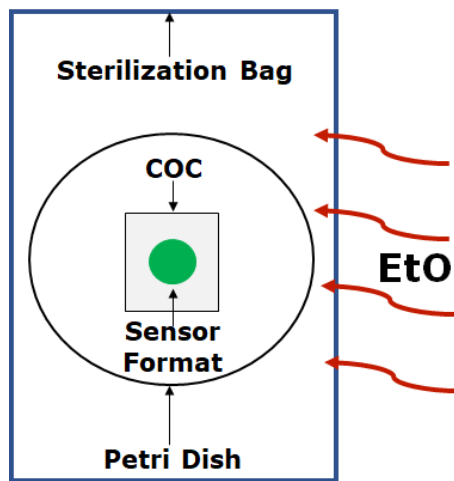
Figure 38: Diagram of ethylene oxide sterilization.

As shown in Table 9, there was not significant variability in the signal intensity readings prior to and following EtO sterilization.

Table 9: Signal intensity readings before and after the ethylene oxide sterilization.

Sensor Format	Intensity Reading Prior (mV)	Intensity Reading Post (mV)
Dye	75	63
Nanoparticles	84	69
Foil	72	61

5.6 Duration Testing

To assess the stability of each format's oxygen percentage readings, duration testing was conducted. This test consisted of performing a two-point calibration for each format in an incubator at 37°C using a solution of 21% oxygen DI water for a 21% point and a solution of 30 g/L sodium sulfite for a 0% point. Post calibration, each format was submerged in a 21% oxygen DI water solution and read using the Piccolo$_2$ inside an incubator for the span of an hour. The PyroScience software took samples every second at a fixed intensity. Both the oxygen percentage and signal intensity were monitored and recorded in real time. The signal intensity for all three samples was above the 50 mV threshold and the Piccolo$_2$ was held at a distance 1mm away from the sensor format.

The results of the Piccolo$_2$ duration testing for each sensor format are illustrated in Figure 39. Both the foil and the nanoparticle samples appeared to reach stable oxygen percentage levels by the end of data collection. On the other hand, the dye sample continued to display a downward trend even at the tail end of the 4,000 seconds of data collection.
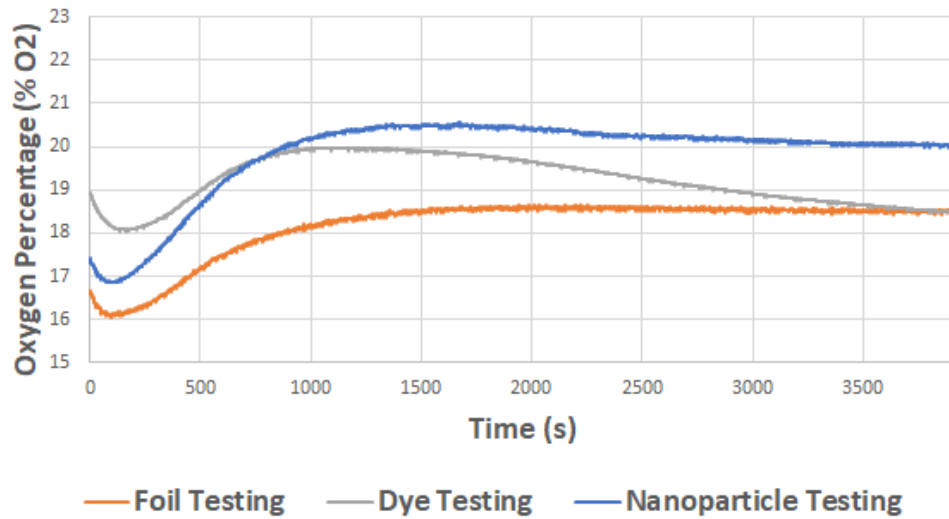
Figure 39: Graph illustrating the results of oxygen percentage data collection over a 4,000 second time interval using the Piccolo$_2$. Each sample was placed in a 21% oxygen DI water solution and the fiber optic was placed a distance of 1 mm away from the sensor format.

For further analysis, an eight-minute segment of data at the end of each test was isolated for each format and statistically analyzed which can be seen in Figures 40, 41, and 42. Each segment was fit with a linear trend line to evaluate how stable the signal was, an average was calculated to assess how close the recorded oxygen percentage matched the expected 21% value, and a range was calculated as a mean of assessing the stability of the signal. All calculated averages and ranges are located in Table 10.

Table 10: A table outlining the averages and ranges of eight-minute segments of oxygen percentage data for each sensing format.

Sensor Format	Average Oxygen Percentage (% O2)	Range (% O2)
Dye	18.6	0.232
Nanoparticles	20.1	0.082
Foil	18.5	0.121

Although the foil was stable which is seen by the small slope of -5 x 10^{-5} %O_2/sec, the foil had an average of 18.5% which was below the expected 21% value. This data can been seen in Figure 40 below.
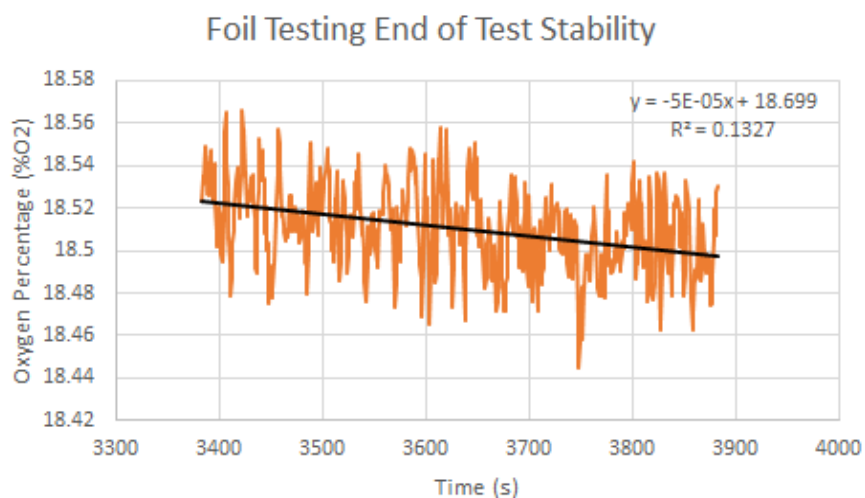
Figure 40: A graph showing an eight-minute segment of the foil oxygen percentage data taken from the end of the graph seen in Figure 39.

Based on the negative slope shown on the graph in Figure 41, the team concluded that the dye format never achieved a completely stable reading after being given an hour to acclimate to standard oxygen levels. This indicates that the dye will not be able to obtain accurate oxygen readings over an extended period of time.
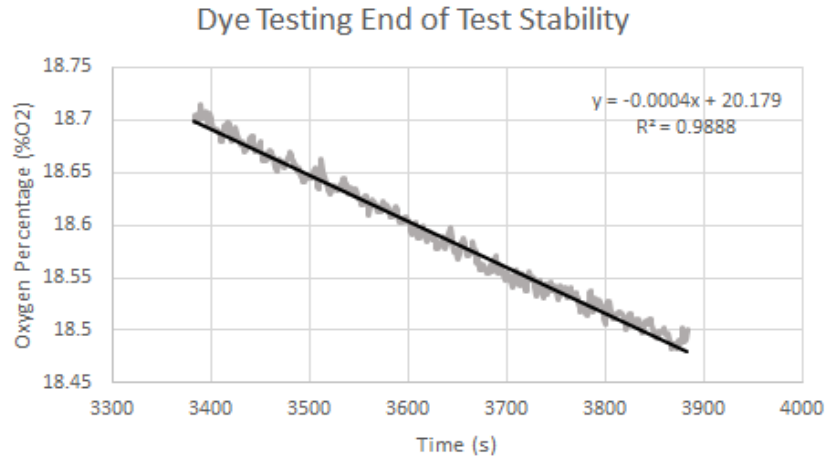
Figure 41: A graph showing an eight-minute segment of the dye oxygen percentage data taken from the end of the graph seen in Figure 39.

As seen in Figure 42, the nanoparticles proved to be the most stable and accurate sensing format with an average oxygen percentage of 20.1%, a range of 0.082 %O_2, and a slope of -6 x 10^{-5} %O_2/sec.
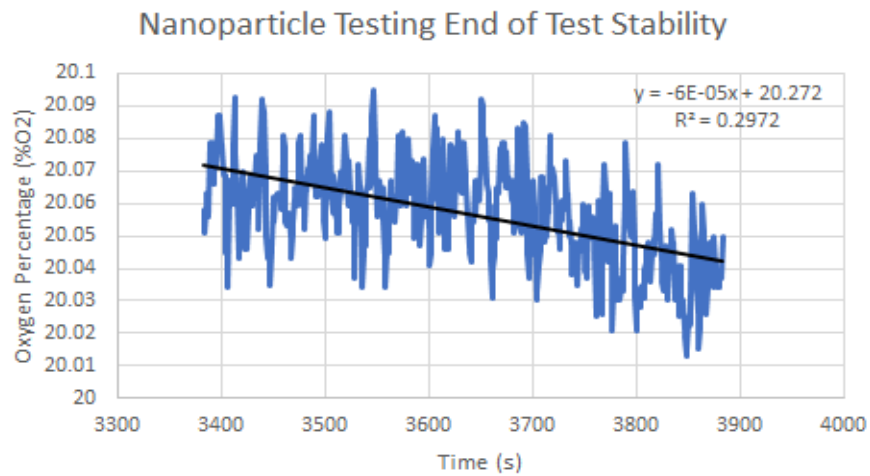
Figure 42: A graph showing an eight-minute segment of the nanoparticle oxygen percentage data taken from the end of the graph seen in Figure 39.

5.7 Final Design Selection

Based on the verification tests discussed above, a Pugh analysis, shown in Table 12, was performed using the pairwise comparison chart of the design constraints, found in below in Table 11.

Table 11: An image of the pairwise comparison chart used to determine the desired characteristic of the final device. The characteristic corresponding to the highest number in the "Total" column is considered to be the most highly prioritized constraint; subsequent constraints were ranked based on the decreasing order of importance associated with decrease in number.

	Biocompatibility	Functionality	Robustness	Patterning	Morphology/ Imaging	Total
Biocompatibility		1	1	1	1	4
Functionality	0		1	1	1	3
Robustness	0	0		1	1	2
Patterning	0	0	0		1	1
Morphology/Imaging	0	0	0	0		0

The Pugh analysis used the weights determined from the pairwise comparison chart to rate each alternative design. The first two columns of the Pugh analysis table contain the design constraints and their respective weight, referred to as 'Importance'. The third column defines the baseline used in Draper's current system for comparing the alternative designs. The baseline design is ranked at zero for each characteristic. In subsequent columns, a value of '1' indicates that the alternative design outperforms the baseline. Additionally, a '0' signifies that the design performs as well as the baseline, with a '-1' indicating the design performs worse than the baseline. These values multiplied by the importance of each constraint sum to determine the final score of each design. These final scores determine the ranking of the design.

Table 12: Table of the Pugh analysis to determine the best design to move forward with during final prototyping and experimentation processes. As shown, the nanoparticles and hydrophilic form of the dye each received equal rankings of preference.

	Importance	Foil	Nanoparticles	Hydrophilic Dye
Biocompatibility	4	0	0	0
Functionality	3	0	1	1
Robustness	2	0	-1	-1
Patterning	1	0	1	1
Morphology/Imaging	0	0	1	0
Total		0	2	2

The nanoparticles and hydrophilic dye ended with the same total score of 2. However, the nanoparticles were noted to exceed the baseline foil in morphology/imaging while the dye met the baseline in this category. Since the weight of this constraint was zero it did not add or subtract from the total score of each design, but acts as a tiebreaker. The nanoparticles had a '1' in this category and the dye had a '0', therefore the nanoparticles were selected as the final design to be subjected to further validation testing.

CHAPTER 6: FINAL DESIGN AND VALIDATION

The team's final design consisted of a concentrated drop of nanoparticles that had been processed using a Carver press onto COC. The design was put through validation tests to determine optimal fabrication parameters. Various conditions were iterated upon to determine how altering Carver press pressure or method time would affect the topography and adherence of the sensor layer to the COC. An automated liquid handler was also used to prove that the final design could be easily incorporated into Draper's final device. Additionally, the verification testing used throughout this project was rationalized against common industry standards. The ethical, health and safety, and manufacturability ramifications of this final product were also analyzed.

6.1 Carver Press Method Condition Testing

The initial conditions used in the preliminary Carver press testing, consisted of applying a pressure of 450 psi, at a platen temperature of 120ºC for a duration of 15 minutes. The team desired to determine the effects of varying both pressure and total time while keeping the 120ºC platen temperature constant. From this, three additional conditions were identified as illustrated in Figure 43 where point one indicates the initial Carver press testing conditions. The new conditions consisted of keeping the same 15 minute time and increasing the applied pressure to 900 psi (point 3), halving the time and keeping the same pressure of 450 psi (point 2), and finally halving the time and increasing the applied pressure to 900 psi (point 4). Specimen for this testing were prepared by depositing a 3 µL drop of solution onto a piece of COC that had been oxygen plasma treated for one minute.
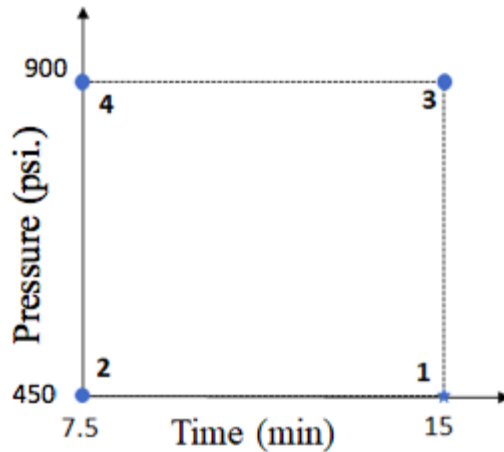
Figure 43: Graph illustrating the four sets of points used to select the optimal Carver press method conditions. The different conditions are shown as points labeled as 1, 2, 3 and 4. This figure shows the variability of time and pressure during the testing with the Carver press.

6.1.1 Condition Testing: Point 1 Results

Figure 44 illustrates the confocal images of the point one condition testing in which 450 psi of force was applied to the sample over a 15 minute timeframe. After applying the heat and pressure cycle, it was noted that the polymer layer appeared to melt under the temperature conditions effectively gluing the dye down to the COC surface. This melting of the polymer layer resulted in an apparent clear film of the dye solution, which had a significantly more uniform distribution after pressing compared to before the pressing procedure. As previously mentioned, a layer of Kapton tape was used in the pressing stack-up. The Kapton tape can operate at extremely high temperatures and acts as a non-adhesive surface on the aluminum blocks used during Carver pressing. During the testing for the sample under condition one, some of the polymer dye residue peeled off onto the Kapton tape. This phenomenon is visible in Figure 44, through the jagged pattern on the boundary between the sensor format and COC.
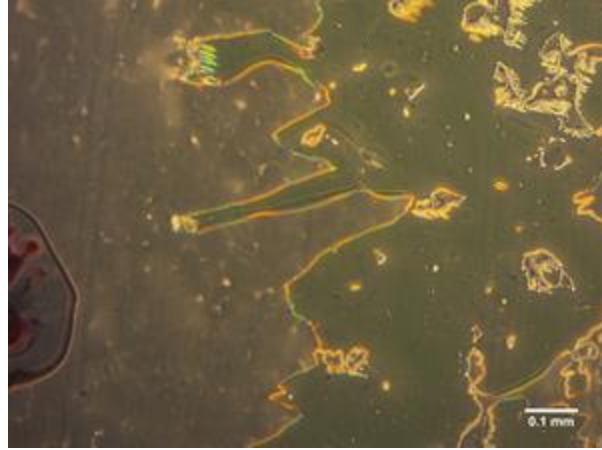
Figure 44: Inverted confocal microscope image of sample N1 at 10X magnification.

6.1.2 Condition Testing: Point 2 Results

Figure 45 illustrates a confocal image under 10X magnification for testing under condition two with 450 psi of applied pressure for 7.5 minutes. Compared to the first condition, the sample did not appear to be pressed for a long enough duration to achieve the clear spread out melted polymer and dye layer, as shown in Figure 45. As shown in Figure 45, this sample showed some melting of the polymer, which was visible under a higher magnification, but it was clear that more time was important to the uniformity and clarity of the sensor polymer layer.
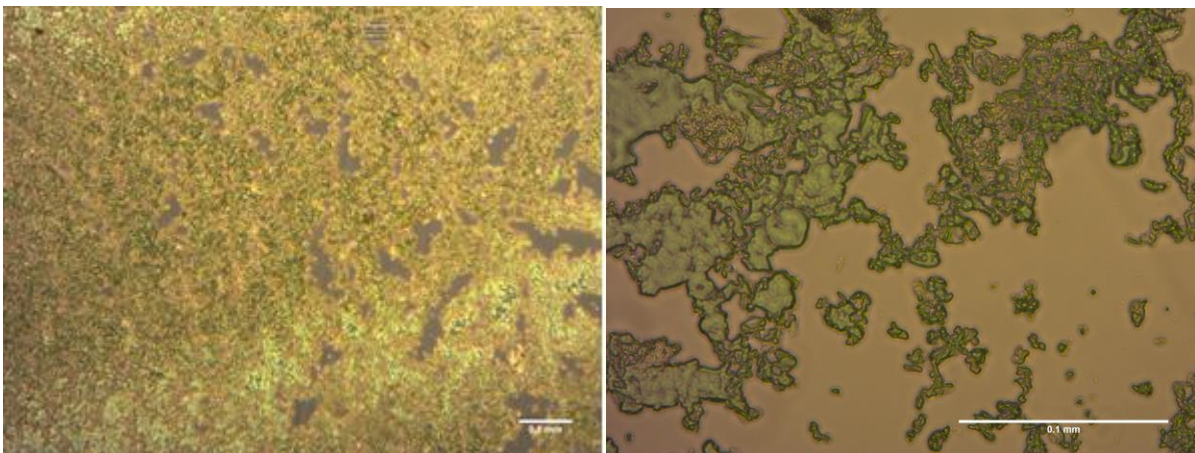
Figure 45: Inverted confocal microscope image of sample N2 at 10X magnification (left) and sample N2 at 40X magnification (right).

6.1.3 Condition Testing: Point 3 Results

Figure 46 illustrates the post press image of the sample for the third testing condition in which 900 psi of pressure was applied to the specimen for 15 minutes. The sample under this iteration yielded a uniform sensor polymer layer that was much more transparent than post press images of the same samples.
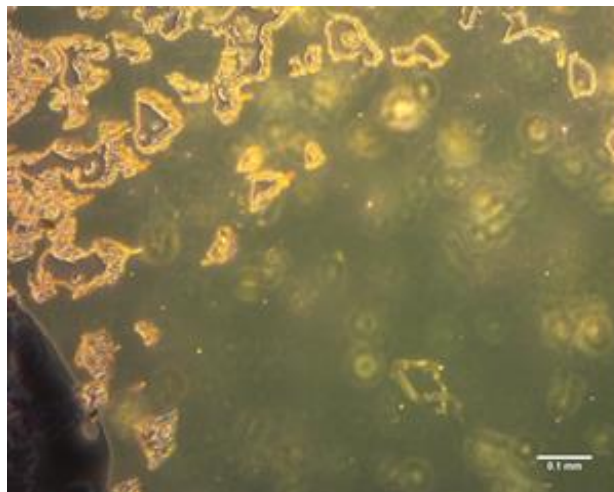
Figure 46: Inverted confocal microscope image of sample N3 at 10X magnification.

6.1.4 Condition Testing: Point 4 Results

Figure 47 illustrates the results of the Carver press condition four testing, in which 450 psi was applied for 7.5 minutes. Similar to the results of the testing from condition one and three, the sample had a clear and seemingly uniform distribution of the sensor polymer layer over the COC surface.
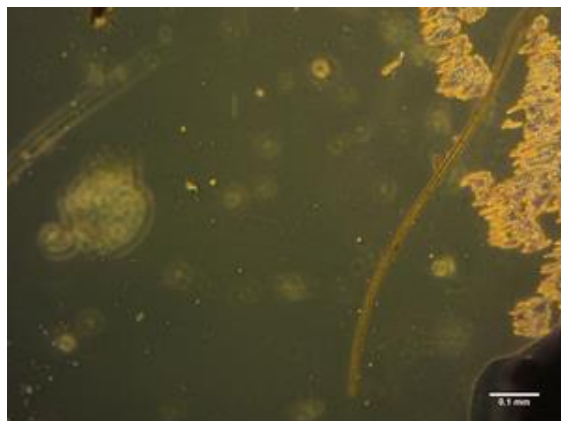
Figure 47: Inverted confocal microscope image of sample N4 at 10X magnification.

6.2 Surface Topography Analysis of Conditions

After pressing, the team utilized an Olympus LEXT OLS4100 3D laser measuring microscope to analyze the surface topography of the samples. This was important to determine if the polymer dye solution was being pressed into the COC after being heated to its glass transition temperature, which is between 80ºC and 180ºC depending on the specific grade of COC used, or if the material was just adhered to the COC surface as a thin film.

6.2.1 Laser Confocal Conditions One Through Four Results

Each sample was imaged using the LEXT microscope with the 50X lens after the Carver press method. Images were taken in the region where the sensor polymer layer tapered off and specialized software was utilized to measure the height of the sensor polymer layer on each sample at various points. Figure 48 illustrates an example of the analysis for a sample under the first set of Carver press conditions. The left hand portion of the image illustrates the region that was analyzed by the microscope, which is differentiated using a green box. The right hand portion of the image illustrates a topographic map of the sample. Similar images for the rest of the samples can be found in Appendix H: Laser Confocal Analysis.
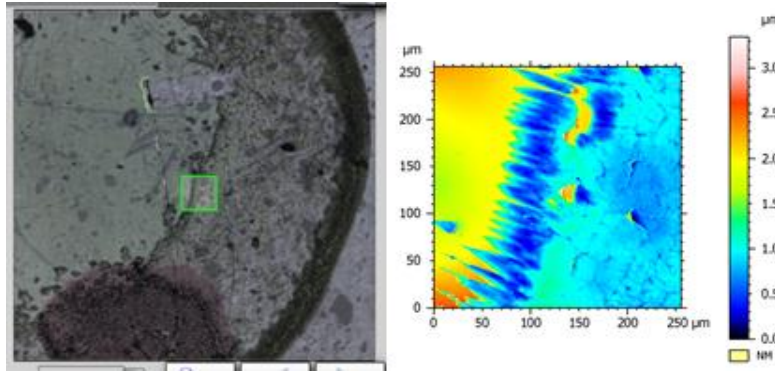
Figure 48: Laser confocal analysis of sample N3 using 50X lens. Area of sample being analyzed by laser confocal (left) and topographic map of area of interest (right)

Each sample was analyzed as illustrated above in Figure 48 and the height of the sensor polymer layer off the COC surface was measured for the region of interest. The height measurements for each sample are illustrated in Table 13. The height of the sensor layer at a point towards the edge of the drop was found to vary from 0.715 μm to 1.62 μm. Definitive conclusions on the height of the sensor layer cannot be drawn from these studies since this method measures the height at one small point from the entire sample. The major conclusion gained from this analysis was that the sensor polymer layer was not fully embedded into the COC surface, but exists as a thin micron-sized layer over the surface of the material.

Table 13: Heights determined and location measurement for each of the samples analyzed using laser confocal imaging. The left column of the table indicates which sample is being studied, the middle column shows the measurement of the sample height, and the right column shows the location at which the height was measured.

Sample ID	Measurement (μm)	Location
N1	0.869	Edge
N3	1.62	Edge
N4	0.715	Edge

A single height measurement was not able to be made for sample N2 due to the lack of a uniform distribution of the sensor polymer layer. The region of interest analyzed and the topographic map for this sample are illustrated in Figure 49. The peaks of the nanoparticle clusters were seen to be up to 10 μm in thickness. The peak heights in this sample were significantly higher than those seen in the samples pressed at a higher pressure or for a longer duration of time. This supports the previous conclusion that the sample under the 450 psi applied force for 7.5 minutes did not sufficiently press the sensor dye compared to previous testing. This was further confirmed by the fact that a sample of a dried drop of nanoparticle solution imaged without undergoing the Carver press method measured peak heights of around 20 μm. Thus, it can be concluded that the N2 sample was pressed to some extent since the peak heights were between the typical pressed samples and the non-pressed samples. However, this set of pressing conditions was deemed ineffective due to a lack of clarity and uniformity in the sensor layer as seen in Figure 49.
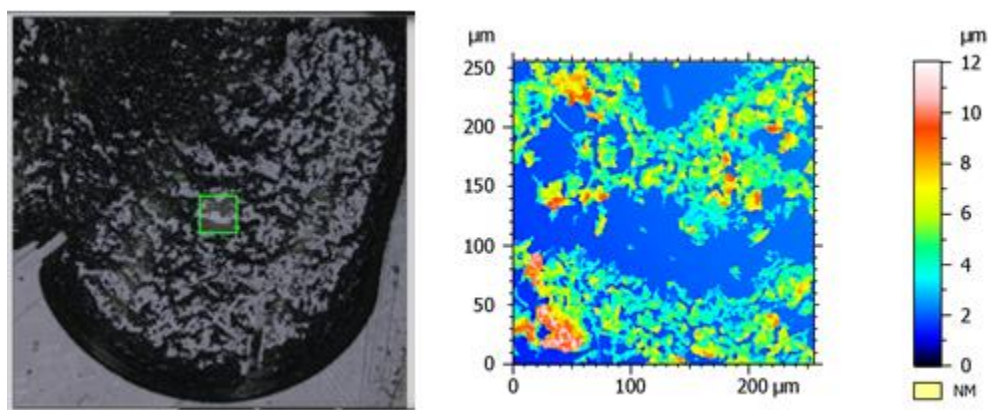
Figure 49: Laser confocal analysis of sample N2 using 50X lens. Area of sample being analyzed by laser confocal (left) and topographic map of area of interest (right). This topographical map shows the height difference across the surface of the sample following processing using the Carver press.

6.3 Automation Validation

An automated liquid handler, a Beckman Coulter Biomek 2000, was used to deposit an array of 3 µL nanoparticle drops on a plasma treated COC surface as illustrated in Figure 50. The purpose of this round of testing was to ensure the feasibility of easily incorporating the nanoparticle format into Draper's device. Due to limitations of the machine used, the smallest drop size able to be attained was roughly 3 mm in diameter, which did not fit within the 300-800 µm diameter size specification necessary for incorporation into Draper's device. To remedy this, the team collaborated with the maker of the chemical indicator to use a machine with higher resolution to drop the hydrophilic dye solution in an array of 96 dots with diameters ranging from 200 to 600 µm as illustrated in the right hand image of Figure 50. The higher resolution device showed success in generating an appropriately scaled array of the indicator dye; the team believes this success is applicable to the nanoparticle solution if the same equipment is used.
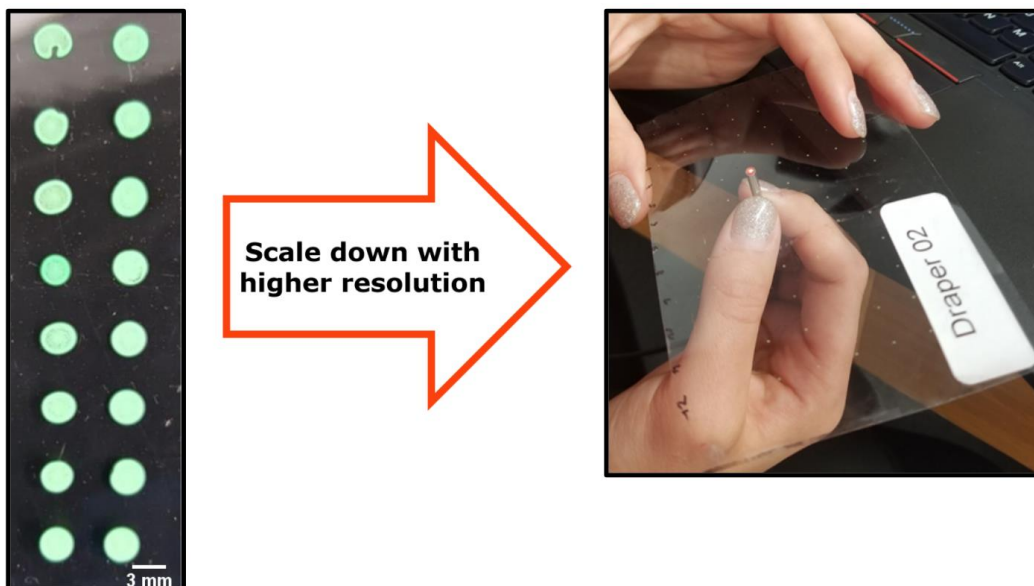
Figure 50: Automation validation of nanoparticle solution. The left hand image illustrates an array of 16 nanoparticle dots dropped on plasma treated COC. This process needs to be scaled down to be applicable in Draper's device. This was achieved through collaboration with the creator of the chemical indicator and the use of the Vermes's Micro Dispensing Valve as illustrated in the right hand image.

The array of dots produced using the Beckman Coulter Biomek 2000 were tested for signal intensity before and after being put through the standard Carver process procedure to ensure functionality of the sensor format. Prior to the Carver press process, the drop signal intensity averaged 176.56 ± 23.09 mV with a maximum drop signal intensity of 210 mV and a minimum of 133 mV. After the Carver press process, the drop signal intensity averaged 94.12 ± 32.39 mV with a maximum drop signal intensity of 129 mV and a minimum of 4 mV. The 4 mV signal intensity was because one of the drops had peeled off the COC when removing the sample from the testing stack-up. This indicates that there is a decrease in signal intensity associated with the pressing process. However, this decrease was not high enough to result in intensities below the 50 mV threshold, meaning the sensor format can still be accurately used with the Piccolo$_2$ sensor. The Carver press procedure also resulted in a more uniform distribution of nanoparticles as well as increased optical clarity as expected and illustrated in Figure 51.
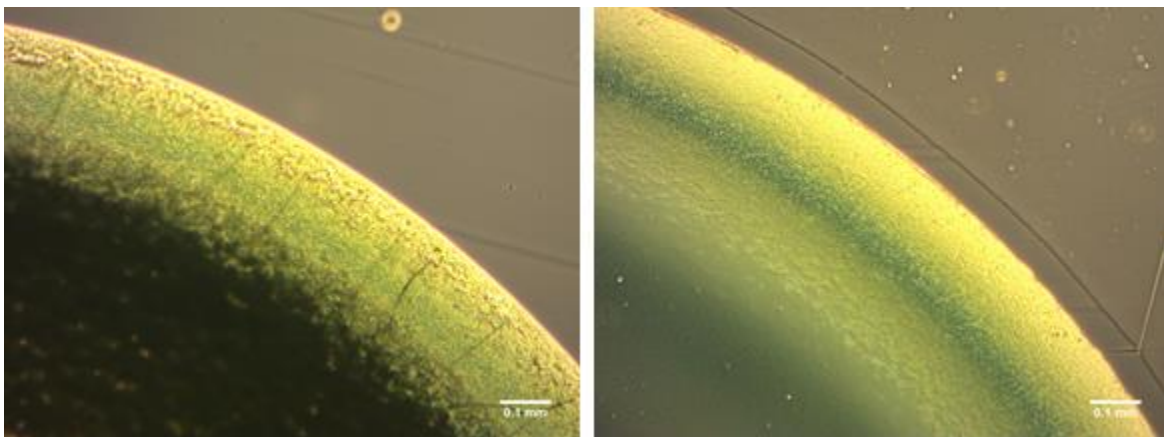
Figure 51: Automation drops pre (left) and post (right) Carver press processing. The uniformity and increase in optical clarity of the sensor layer were seen as expected after processing.

6.4 Standards

All testing was compared against established standards as means of validating that good practice is followed throughout the course of the project.

6.4.1 Scratch Test

The parameters for the scratch test were identified based on the ASTM standard D7027, which provides a standard test method for evaluation of the scratch resistance of polymeric coatings and plastics. The purpose of this standard is to provide a repeatable way to evaluate surface damage of coatings after being exposed to a controlled set of conditions. Test Mode B of this standard was most closely adhered where a constant normal force of 30N at a scratch rate of 0.1 m/s is applied to a 0.1 m length of the sample [43]. These standard parameters could not be replicated exactly due to lack of access to an instrumented scratch machine; however, the team was consistent with who performed each scratch test in hopes of maintaining a constant load and scratch rate from sample to sample. A downside of performing scratch tests in this manner is the presence of user-influenced effects, like scratching the surface of the sensor format with a different force during each test.

6.4.2 Soak Test

When designing the soak test, the team considered the ASTM standard C1247-14 which details a test method for evaluating the durability of sealants that must function in environments subjected to continuous immersion in a liquid. This standard is concerned with how well the sealant is able to maintain adhesion to a substrate after liquid immersion for a set amount of time. The sensor formats being tested are not directly applicable to this standard since they are not sealants, but the method described is still relevant since the sensor format sample must be

durable in continuous immersion in cell culture media. The test method for this standard includes

specimen preparation and immersion of the sample in liquid at 50°C for six weeks. After the

soak test is completed, the sample is subjected to compression and extension loads with testing

parameters specific to the intended use of the specimen [44]. The team followed the idea of this

test method, but changed the soak and post soak testing conditions to match how the sensor

format will be used in Draper's final device. For instance, the temperature of the media was set

to be 37°C and the soak duration used was 14 days per client specifications. Additionally, the

format was determined to maintain integrity after the soak test with signal intensity validation

with the current optical platform.

6.4.3 Thermal Test

The team based the experimental procedure for the thermal test off ASTM standard

D7895/D7895M-14 which details a test method for testing the thermal endurance of coating

powders used for powder coating insulation systems. This standard details a procedure to

determine how resistant coating powders are to exposure to elevated temperatures. Although this

standard is specifically designed for insulating powders used on steel, it was determined that the

general method used in this standard was applicable to the testing of each sensor format on a

COC substrate. The testing parameters of this standard include aging each sample at three

different temperatures above the samples operation temperature. After exposure to elevated

temperatures, the materials are tested using a dielectric proof voltage test to quantify when any

degradations in thermal endurance occur during testing at elevated temperatures [45]. Since only

the ability to withstand thermal cycling at 120°C for one hour was necessary to prove the

functionality of the sensor format on COC from a thermal endurance standpoint, these

parameters were adopted for testing as opposed to three different temperatures. Additionally,

performance was evaluated by comparing the signal intensity output of the Piccolo$_2$ sensor before and after thermal testing. This evaluation metric was chosen based on how the sensor format needs to perform in Draper's final device.

6.4.4 Ethylene Oxide Test

All processing in ethylene oxide sterilization was done per ISO 11135:2014 standards. Specifically, this standard focuses on the regulations regarding the sterilization of health-care products through ethylene oxide. Emphasis within this standard is placed upon the requirements for the development, validation and routine control of a sterilization process for medical devices.

6.5 Ethical Concerns

The organ-on-a-chip system under development at Draper seeks to produce a positive impact on the healthcare and drug development industries by bringing helpful drugs to market faster. Additionally, this organ-on-a-chip device serves as a versatile testing platform for the field of research and development without damaging or degrading the lives of the public or research community. In fact, this organ-on-a-chip device will ideally reduce some of the most prominent ethical concerns related to the healthcare industry, specifically animal testing.

Currently, new procedures and medicines are required to undergo animal studies, which utilize animals such as mice, rabbits, and pigs for validation of the safety and efficacy of the new treatment prior to entering the market. While the FDA has made great strides to prevent suffering or unnecessary damage to the animal test subjects, the act of using animals for these studies still produces an ethical dilemma. The dilemma being, is it right to subject animals to these treatments, which regardless of the success of the test, requires the testing subject to be put down. The development of Draper's organ-on-a-chip technology and associated oxygen sensing

capabilities will help to disrupt the industries dependency on animal studies by providing them with a more accurate and cost effective alternative. Although this technology has yet to be fully validated, it has the potential to alleviate the medical research industry of the ethical dilemma of performing extraneous iterations of animal studies.

6.6 Health and Safety Issues

The broader focus of Project SOAR was to increase the health of individuals that rely on the readings of these organ-on-a-chip devices. By extension, this project provides the pre-existing organ-on-a-chip technology with a means for increasing the accuracy of its results. The addition of oxygen sensing acts as an indicator of cell health which results in an understanding of the effects an experimental drug is having on cells. With this knowledge, researchers have a better likelihood of producing results that are more predictable and translatable to human trials. Effectively, this helps researchers produce fewer results that are categorized as false positive, in which the tests say the drug is safe but in actuality it is not, or false negative, in which the tests say the drug is not safe but in actuality, it is. Either of these scenarios can be potential health risks to the public since patients may be exposed to dangerous drugs or miss out on potentially lifesaving medicines. The addition of the team's oxygen sensing capabilities to the current platform will be able to screen drugs and determine the most promising candidates for rapid advancement through the FDA process.

The manufacturing process poses minor risks to individual's health and safety due to the required heat and pressure associated with the process of producing the oxygen sensing components. The heat required for production of the oxygen sensitive component reaches 120ºC, which can cause serious burns if handled without proper personal protective equipment, PPE. Additionally, the nanoparticles for the oxygen sensing component should not be ingested or

inhaled. The nanoparticles are extremely fine and staticy; therefore they should be handled carefully with PPE, such as gloves, glasses, and a face mask if necessary.

6.7 Manufacturability and Sustainability

One goal of the final design was for it to have the ability to be easily incorporated into large-scale manufacturing processes. Draper is looking for the ability to scale the team's method for producing an oxygen sensing format to their 96 well device for further research. This means that the team's process of producing a working oxygen format does not need to be produced at a high volume; instead, it must be able to be produced in a handful of devices per week as the format is still undergoing research.

The team has defined an implementation process for manufacturing of devices incorporating the new sensor format which can be automated for anywhere from one sensor to 96 sensors. Specifically, the team tested the nanoparticle dropping method in coordination with the thermal bonding process used for creating the full device on the scale of multiple drops. The results of these tests have proved to be successful which acts as a means of validating the feasibility of scaling to the 96 well format. Additionally, the bonding process of the nanoparticles to the base COC follows the same conditions as the final bonding conditions for fabricating the 96 well device. Therefore, it is much easier for Draper to incorporate this additional step into their predefined fabrication methodology. To further validate this option as the best, the team explored other means of implementation such as PDMS stamping. This option consisted of creating PDMS stamps with a specific pattern of circles to match the desired diameter of the sensor format, which was exposed to a surface treatment making the stamp more hydrophilic. Next, the stamps were exposed to a solution of the sensing format, which was subsequently stamped onto the COC to transfer the solution in the desired pattern. Due to the size and

clumping properties of the sensing formats this option did not transfer enough material over to the COC which means further surface treatments would be required to increase adhesion or more solution of the sensing format would have to be used. This process also wasted a sizable volume of the sensing format solution making this process inefficient and costly.

Although the bonding process can be incorporated into Draper's current fabrication techniques, the creation of nanoparticle solutions and the method of depositing them onto the surface requires additional steps. The team determined that a 3 µL drop of 40 mg/mL nanoparticle solution provides a sufficient amount of nanoparticles for the accurate acquisition of oxygen data. The downside to this process is the need for nanoparticle solutions which not only require time to create but also have a high price for purchasing in bulk, $292.00 for 10 mg of raw nanoparticles, therefore making the material a restriction to scaling up to a 96 well format. The nanoparticle sensor format requires an automated mechanism for dispensing the solution over a surface at specific intervals to align with the center of each well. Draper's current method is extremely manual labor intensive by placing each sensor format by hand, which allows on-the-spot modifications to be made. However, this process takes time and personnel to complete, which also exposes the process to human error. One option to improve this process is an automated microplate dispenser, such as BioTek's MultiFlo FX, which is able to dispense drops as small as 1 µL on a surface in a consistent manner with ± 5% accuracy in the form a 96 well format. Additionally, the Thermo Scientific Multidrop Combi nL Reagent Dispenser would be able to dispense drops as small as 50 nL. If a smaller volume is required for fabrication, the Vermes's Micro Dispensing Valve - MDV 3200A is capable of dispensing drops at a volume as low as 1 nL. Once again, this addition requires more time and money to execute which reduces the feasibility of scaling up this process to mass production.

6.8 Economic Impact

A long-term impact of organ-on-a-chip devices, like the one worked with in Project SOAR, is to reduce costs associated with the FDA drug approval process. In recent years, the number of drugs approved through this process have declined which is quantified by an 88% drug development failure rate [46]. In parallel to this trend, research and development costs have climbed dramatically [47]. Both of these trends result in significant price increases for patients that are dependent on drugs developed through this process. To reduce these drug costs for consumers, organ-on-a-chip technology is meant to act as an intervention in the early stages of the process. The earliest stage of the drug approval process costs roughly $9.6 billion USD, which is the highest cost out of the four phases of the process besides clinical trials. An upwards of 10,000 compounds need to be vetted in this phase and organ-on-a-chip technology makes it much easier to test many compounds in bulk [48]. This technology will reduce development costs significantly in comparison to the animal models that are currently used.

6.9 Environmental, Societal, and Political Effects

Microfluidic testing, as a whole, works at an extremely small-scale in an attempt to rid excess waste of materials. By limiting the amount of materials in use in the final device, while ensuring accuracy of all readings and data gathered during testing, researchers are able to limit the volume of chemical and biological waste generated. This lessens the environmental impact that often is of concern with regards to drug testing. Additionally, we considered waste caused by sterilization methods such as exposure to ethylene oxide, which results in the release of this highly toxic chemical into the air or sources of water [49].

The societal and political concerns associated with the final device are centralized around two main scopes: the mitigation of animal testing and the testing of potential medications. The goal of the final device is aimed at limiting the number of preliminary drugs that are tested on animals during the varying phases of preclinical and clinical testing. By better predicting drug success rates using organ-on-a-chip devices, researchers are able to limit the number of drugs progressing towards animal testing. On the same note, through the use of organ-on-a-chip devices, researchers are able to better streamline the drug testing process and improve the rate at which safe and useful drugs are able to reach market. This allows patients across the globe better accessibility to potentially life-saving medications.

CHAPTER 7: DISCUSSION

7.1 Project Goals

At the beginning of the project, the team defined goals to guide the direction of the testing and analysis of the sensor format. The major goals were defined as creating a means of sensing oxygen in Draper's organ-on-a-chip device and creating a method of implementation for said format into the current system. The sensor format must be biocompatible, optically clear for imaging cells, accurate, adaptable for future iterations, compatible with automation efforts, and able to function in a cellular environment for the duration of up to 14 days continuously. Based off iterative testing exploring various options and techniques, the team was able to produce a result that fits Draper's desired outcomes. Additionally, the goals defined above remained constant as the project progressed allowing the team to keep focused while sifting through the dynamic amount of possible solutions presented through research and testing.

7.2 Discussion of Results

The results from testing primarily included, oxygen percentage and signal intensity readings from the Piccolo$_2$, optical confocal microscope images, and laser confocal images and measurements. Each of these results helped the team determine the next steps in testing and eventually, which of the solutions proved to be the best.

7.2.1 Piccolo$_2$ Testing

Testing the various formats with the Piccolo$_2$ provided quantitative data in the form of live oxygen measurements and signal intensity. The live feed of the oxygen measurements allowed for an understanding of the consistency and accuracy of the oxygen sensing format

being tested. The signal intensity was important in the process of selecting an effective concentration of nanoparticles required to produce a sensing format with accurate results. As defined in the methodology, a signal intensity of greater than 50 mV is recommended for reliable data acquisition. With this in mind, the team was able to iterate through various concentrations while having a means of validating their progress. The difficulty of this iterative process was finding a balance between the concentration and the strength of the signal. The ideal was a low concentration, to obtain the maximum level of optical clarity, with a high signal intensity, to obtain the maximum reading accuracy. Compared to Draper's previous format, the foil material, the team was able to produce a more versatile format, nanoparticles, which can be fine-tuned to the desired signal strength.

7.2.2 Optical Clarity

Another means for validating the team's progress was the use an optical confocal microscope, which was a quick way to observe the effects of surface modifications, dilutions, and optical clarity. A majority of the results from this method were qualitative, allowing the team to visualize the power of surface modifications such as plasma treatment. Additionally, this also impacted the team's decisions for dilutions since it allowed for a close up analysis of the packing of the nanoparticles which directly relates to the optical clarity of the sensor format. This visualization of the optical clarity was the defining factor in deciding which preliminary design was the best method to satisfy the design objectives and project goals. For example, qualitative optical clarity tests allowed the team to make the conclusion that the nanoparticles would be a better format to proceed with compared to the dye, which was too dense for optical clarity even after multiple dilutions and Carver press treatment.

Similar to the optical confocal microscope, the laser confocal images provided the team with qualitative data of the topology of the various sensor formats. However, the laser confocal can attain higher resolution images at higher magnifications allowing for quantitative analysis of the topology on a micron scale. This analysis technique was critical for the team's development of a method for utilizing the Carver press, since it showed how the nanoparticles were pressed onto the surface of the COC. The resulting product of the iterative process of tuning the Carver press's pressure and processing time was a sensor spot of a much thinner thickness compared to Draper's previous format. With a smaller thickness, the sensing obstruction of flow in Draper's microfluidic channels caused by the sensing material decreases; in contrast, a larger thickness, such as the foil material, could cause turbulence in the channel.

7.2.3 Soak Test

The data collected from the 14 day soak test provided insight into each format's ability to function in a cell culture environment required for the final device. The dye and foil both seemed to withstand the environment of the media, while the nanoparticles ended the testing with an insufficient signal intensity. However, the dip below the 50 mV threshold for the nanoparticles was not determined to be noteworthy because the signal intensity prior to the soak test was already close to the 50 mV threshold. The foils also showed a similar magnitude of signal intensity degradation compared to the nanoparticles after the 14 day soak test; however, since the foil started with a higher signal intensity, this degradation did not push the value below the 50 mV threshold. With this in mind, the concentration of nanoparticle solution used could be optimized to ensure that the small degradation in signal intensity after 14 days in media would not result in an insufficient intensity reading.

7.2.4 Thermal Test

The thermal test was meant to ensure that the chosen sensor format would be able to withstand Draper's device fabrication parameters without degrading. All sensor formats were determined to not be sufficiently affected after one hour thermal cycle. The variations in signal intensity from the before to after testing were -5 mV, -8 mV, and 5 mV for the dye, foil, and nanoparticle samples respectively. None of the signal intensities dipped below the 50 mV threshold and the 5 mV and 8 mV degradation were not considered to be direct results of the exposure to the elevated temperature. The slight variation in signal intensity before and after testing was attributed to holding the fiber optic cable in slightly different positions below the drop between the readings. Since the concentration of the sensor format, for the dye and nanoparticles, is not completely uniform throughout the drop, it is logical that slight positioning variations of the fiber optic could result in signal discrepancies. Overall, all sensor formats exhibited sufficient thermal endurance to maintain integrity as a result of the thermal parameters of the current fabrication process.

7.2.5 Ethylene Oxide Test

To ensure that the sensor format was able to withstand all sterilization parameters that are utilized with the current organ-on-a-chip device. Based on the current standards for sterilization used at Draper, the sensor formats were subjected to ethylene oxide sterilization treatments. The different sensor formats did not show significant variability prior to and following sterilization with ethylene oxide. The dye showed a decrease of 12 mV in signal intensity, while the nanoparticles and foils showed decreases of 15 mV and 11 mV, respectively. Experience has shown that such variability can be correlated with slight movements in the fiber optic during the testing procedure.

7.2.6 Duration Test

The purpose of the duration testing with the Piccolo$_2$ was to provide an accurate depiction of the consistency of each format's oxygen percentage readings over the span of an hour. Results from this test seen in Figure 39 showed an initial curve, which can be attributed to the change in temperature as a result of opening the incubator when setting up the test. As the temperature in the incubator reheated to 37°C the oxygen percentage of each format increased until a stable temperature was met. At this point, both the foil and nanoparticles leveled out at 18.6% and 20.4% respectively while the dye seemed to decrease in percentage. This decrease could have been a result of residual 0% sodium sulfite calibration solution in the testing well or the tested dye had a fabrication defect. Overall, the nanoparticles was the closest to meeting the expected 21% value over the span of an hour, however it did show a slight decrease over time. The foil, despite its consistency, leveled out below the expected 21%, which could have been due to human error during calibration.

7.3 Limitations and Issues

Despite the success of meeting the project's goals, the project was not without issues that complicated the team's results. A major point noticed repeatedly in preliminary testing was clumping of the nanoparticles. Based on this, finding a way to evenly distribute the nanoparticles on the surface was essential. The nanoparticles were very staticy and seemed to be attracted to each other, causing them to clump up when drying due to the surface tension between the particles and the COC. This problem was addressed via the use of the Carver press to even out the clumpiness, however this did not remedy the entire issue. Some regions of the pressed dots showed a gradient of nanoparticle concentration across the surface or even a void in the sensor layer as illustrated in Figure 52.

Figure 52: Specimen illustrating voids commonly seen in pressed samples as a result of nanoparticle clumping during drying of the solution. To improve the current fabrication technique, the process should be reevaluated and replicated with the goal of lessening and removing these voids.

Other attempts of resolving this issue included dispersing the nanoparticles in various detergents and organic solvents, but these attempts proved to be insufficient in breaking the clumps. Regardless of this issue, the pressed nanoparticles were still able to produce accurate $Piccolo_2$ results and dots with sufficient optical clarity.

A constant limitation to the collected data was the $Piccolo_2$'s inability to account for an environment with a dynamic range of temperatures. The importance of controlling the temperature was determined through initial studies and is illustrated in Figure 53. At two points during testing, as illustrated by the arrows, a member of the team breathed on the sample to increase the temperature. This resulted in a nearly instantaneous decrease of about 3% in the oxygen percentage reading, which leveled back off when the temperature was allowed to stabilize. Thus, it was very important to be cognizant of the temperature fluctuations in the environment during testing with this optical platform as even the air conditioning in a room caused excessive noise in the form of oxygen percentage fluctuations.
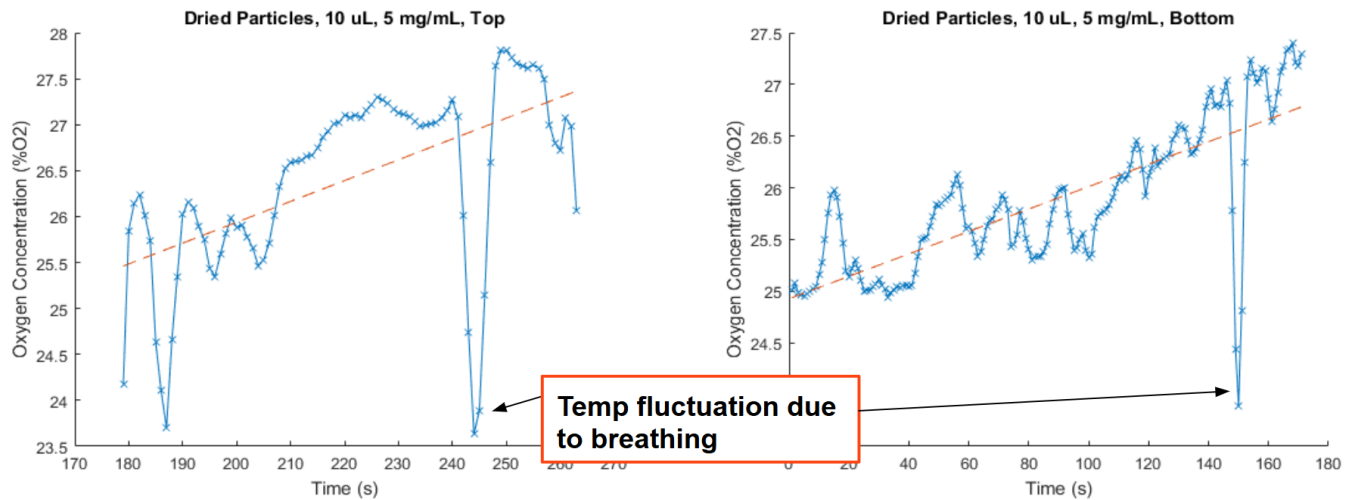
Figure 53: Oxygen percentage versus time for testing of dried nanoparticle films on a glass slide. Arrows indicate temperature sensitivity of the sensor due to breathing on the specimen to create a temperature increase during testing.

To reduce the Piccolo$_2$'s exposure to the environment a custom containment chamber was constructed out of a cardboard box. This creation significantly reduced the noise from the environment, however even the slight temperature variations in the box still manifested as drift in the oxygen percentage over time in some tests. A long-term fix for this issue would be the use of the FireStingO$_2$, or another optical platform, which has the ability to actively normalize the temperature variations in real time. Despite this limitation, the team was able to acquire relevant data for validation of the tested formats.

Another issue that was encountered when utilizing the Piccolo$_2$ was the duration of time required for the team to perform the two point calibration before each test. Two-point calibration was performed using a 21% oxygen DI water solution and a 0% oxygen sodium sulfite solution. While the sensor readings stabilized quickly when using the 0% oxygen solution, the 21% oxygen DI water often required extensive amounts of time – from a half an hour to three hours – to reach a stable oxygen reading. The team hypothesized the solution took a long time to stabilize because the equilibrium oxygen percentage of the solution was disrupted during transfer

into the testing environment. One limitation encountered during Piccolo$_2$ testing was the inability to confirm that the 21% oxygen DI water truly was 21%.

The implementation of the team's oxygen sensor format using the Carver press method also provided a variety of challenges. The major issue that arose from the Carver press appeared after a failure of the hydraulic unit that was required to apply pressure to the sample. This failure resulted in the need to dismantle and reconstruct the hydraulic unit component of the Carver press. Before the reconstruction, the sensor dots were being flattened evenly, but after the reconstruction, the sensor dots started showing some abnormalities. These abnormalities included uneven flattening and the inability to be removed from the Carver press stack-up without sticking to the Kapton tape and tearing off the COC. An example of this tearing phenomenon is seen in the confocal image in Figure 54 producing cliff like features on the sensor dot.
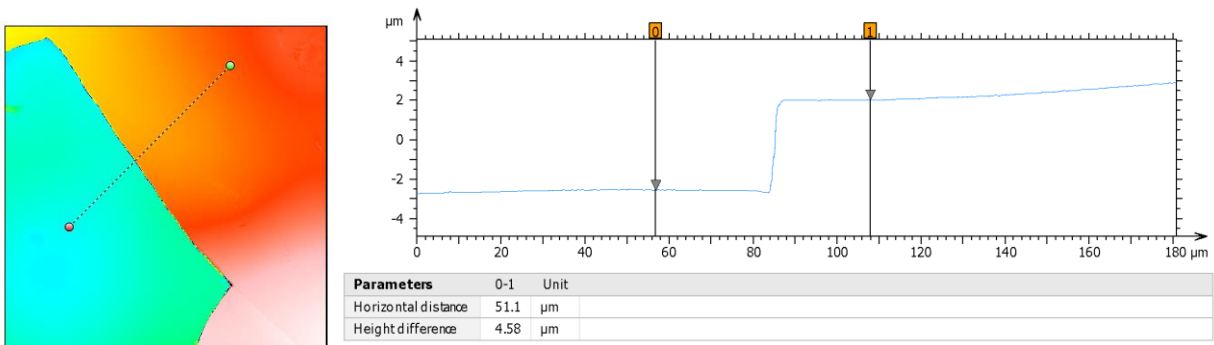
Figure 54: Laser confocal topographical image (left), measurement of of height difference between the pressed nanoparticle material and the COC base layer (right). The height difference between the nanoparticle materials and the COC base layer is determined using software designed to work specifically with the laser confocal microscope used throughout the imaging process.

This issue was assumed to be a result of the repaired hydraulic unit applying force off-center which in turn prevented a uniform distribution of force across the sample. A longer cool

down time of the sample post press was experimented with to alleviate the tearing effect; however, this did not solve the issue. While this proved to impede the team's progress, it was not a large-scale issue as Draper can fine-tune the Carver press method to meet their needs in the future. Even with all of the limitations and issues mentioned above, none proved to be severe enough to devalue the results reached by the team. Most of the issues described previously were resolved throughout the testing process or will not affect Draper since the issues are local to the limitations of the equipment used at WPI, such as the faulty Carver press or the lack of a temperature compensating testing platform.

7.4 Cost Analysis

Being that the team recommends a concentration of 40 mg/mL, a single vial of the nanoparticles would result 0.25 mL of solution, since there are 10 mg of nanoparticles within each vial. Each vial costs $292; therefore, the total cost at this concentration would be $1168/mL. Based on the worst-case scenario, meaning that the process cannot be scaled down to any extent, the project would continue working with individual dots of 3 µL in volume; this would result in a total volume of 288 µL. At this scale, the total cost of nanoparticle solution within a single microfluidic device would be $336.39. Assuming the ideal range of 300-800 µm diameter dots, the dot volumes would span between 0.0007 and 0.0050 µL, assuming a cylindrical approximation of dot volume. This means that the total volume divided across an array of 96 dots would span between 0.0678 and 0.4825 µL. Assuming these volumes, the price per device would span between $0.08 and $0.57. All cost values are reported in USD.

CHAPTER 8: CONCLUSIONS AND RECOMMENDATIONS

8.1 Final Results and Impact

Thorough testing led the team to produce a result that satisfied nearly all of the objectives set by Draper. The final design consisted of 3 µL drops of 40 mg/mL nanoparticle solution pressed into the COC via a Carver press at the conditions of 120°C at 450 psi for 15 minutes. The sensing format was required to be biocompatible, optically clear for imaging cells, accurate, adaptable for future iterations, and is compatible with automation efforts, but further testing is required to determine if the nanoparticles are able to function in a cellular environment for the duration of up to 14 days continuously.

Assessments of optical clarity via the use of the inverted confocal microscope were conducted on all iterations of the format, and the final sensing format proved to be the best combination of clarity, signal intensity, and concentration. The optical clarity was primarily modified through the use of the Carver press which helped the team determine that 120°C at 450 psi for 15 minutes were the best conditions for producing optically clear sensing formats. Even though the nanoparticles leave a green tinge on the surface of the COC, it does not hinder the process of imaging cells.

The final sensing format proved to be accurate through $Piccolo_2$ testing since the format produced a signal intensity greater than 50 mV as well as the expected oxygen readings. While this phase of testing could benefit from further validation with a larger sample size, it still meets the goals set by the project allowing Draper to utilize it in their 96 well format.

The team's method was designed to be flexible such that the sensor format could be applied in multiple ways, with various geometries, from manual deposition to automated

processes. Additionally, the sensing format is able to function in a variety of temperatures and lighting conditions while being unreactive in common biological environments.

Overall, the team's final sensing format will enable Draper to add another analytical method to their existing organ-on-a-chip system. With oxygen data, Draper will be able to assess the health of cells being tested within the organ-on-a-chip system, which is essential for understanding the effects of various drugs or other conditions, such as temperature, on the cells. Additionally, the oxygen sensing capabilities will provide Draper's system with an advantage over the rest of the market since many systems are unable to produce both accurate oxygen percentage data and large-scale replicates for testing. In the short term, the new sensing format will propel Draper's development of the 96 well format by allowing Draper to acquire live and accurate data from their iterative design correlated to cell health. In the long term, the developed sensing format could become a staple in Draper's organ-on-a-chip systems, as oxygen sensing is a valuable analyte for understanding the health of cells with respect to the experimental variable.

8.2 Recommendations and Future Work

Throughout the development of the new sensing format, many options for optimization were explored; however, some were determined to be out of the time range or scope of the project. While not all of these options were worthy of pursuing, the ones that were, have become recommendations and possibilities for future work. Recommendations for Draper are based off observations the team has made over the duration of the project and help outline the conditions that can produce the best results. Future work is explained as action items, which may be advantageous for Draper to act on to improve the oxygen sensing system or its means of data acquisition.

Based off the team's testing, it is recommended that Draper adopts the oxygen sensing format utilizing PyroScience nanoparticles which have been pressed at 120^oC and 450 psi for 15 minutes via the use of a Carver press. This combination of factors results in a format that meets Draper's goals and acts as a foundation for future testing and iterations to build off for further optimization. With this recommendation, the team also recommends that Draper build a relationship with PyroScience such that purchasing nanoparticles in bulk will reduce the overall cost. With a deal like this in place the promise of utilizing nanoparticles in the long term becomes much more feasible and cost effective.

One of the most notable issues with the current oxygen sensing data is its high variability due to the $Piccolo_2$'s sensitivity and inability to adjust to temperature fluctuations. To remove this limitation, the team recommends that Draper employ the use of the $FireStingO_2$ or similar technology developed in house which has the ability to normalize the incoming oxygen percentage data with respect to temperature. This would allow for more meaningful and accurate oxygen percentage data to be acquired without the threat of temperature variation interfering with data collection. In addition to this, Draper's LED based optical sensing system, which has been developed in conjunction with this project, requires characterization with the team's recommended sensing format. Basic tests such as two-point calibration with known standards and duration testing over a span of 14 days would provide Draper with important information on the accuracy of their custom sensing system. In addition, the team recommends that all future work involves multiple iterations of testing to prevent any complications or deviations due to the small testing sample size of the studies outlined in this report. Performing multiple iterations of testing would remove the heightened effect that outliers play in the analysis of results.

For more possible tests in the future, the team recommends that Draper explore the use of toluene as a co-solvent for both the COC they are using as well as the structural polymer of the nanoparticles based on observations during testing. By dissolving these two together and letting them solidify it may be possible to produce a layer of the nanoparticle solution that is embedded on to the surface of the COC, thus removing the need for bonding using a Carver press. Tests to achieve this vision include dropping toluene onto a dried drop of nanoparticles on the COC. Ideally, the drop would melt the COC and nanoparticles such that only the top about 20 μm are affected. This would allow the nanoparticles to embed themselves into the COC such that they are still exposed to the environment and do not cause serious surface deformations, which could promote turbulence when testing with flow.

The removal of the reliance on a Carver press will also improve the prospect of scaling the sensing system up to the full 96 well platform, which leads into another avenue for future work. While the team was able to develop a sensor format that is highly adaptable, the team was unable to extensively test means of scaling the format up. Since the final system has 96 wells, the first tests should be centered on automating the process of dispensing 3 μL drops of the 10 mg/mL nanoparticle solution on a piece of COC in the patter of a 96 well plate. This can be accomplished by using BioTek's MultiFlo FX, Thermo Scientific's Multidrop Combi nL Reagent Dispenser, or Vermes's Micro Dispensing Valve - MDV 3200A to automate the ejection of drops as mentioned in Section 6.7 Manufacturability and Sustainability. The means of automation should then be confirmed to work at a smaller scale and higher resolution to achieve the desired 300-800 μm droplets with a placement tolerance of 100 μm. Assuming a cylindrical approximation of the flattened droplets and a desired height of 10 μm, the droplets must span

between 0.7 nL and 5 nL in volume to achieve diameters between 300 μm and 800 μm. Thus, the selected device must be able to operate on the nanoliter scale.

Another recommendation would be exploring the use of the hydrophobic dye, which has a different composition and fabrication process compared to its hydrophilic counterpart. During the span of this project, the creator of these dyes provided the team with predeposited drops of the hydrophobic dye, which proved to have exceptional optical clarity and signal intensity when the Piccolo$_2$ was directly in contact with the drop. Figure 55 below shows the potential for the hydrophobic dye's clarity as it barely hinders the image quality of the histological slide. Further testing using the dye could result in a better alternative to the nanoparticles.

Figure 55: Hydrophobic dye in the optical path of a histological slide containing human skin. The hydrophobic dye droplet is located off to the right of the image.

The team also recommends a fabrication process for Draper to incorporate the final design into their current organ-on-a-chip device. This process is illustrated in Appendix I: Processing Protocol. First, a piece of COC, cut to size, must be oxygen plasma treated for one hour. Directly after this process, a desired volume of prepared nanoparticle solution at a concentration of 40 mg/mL should be deposited on the COC surface in the pattern of the 96 well

97

device. Using the Carver press stack up previously described, the sensor format should be bonded to the COC under a pressure of 450 psi and a temperature of 120°C for 15 minutes. After this step, the prepared sheet can then be incorporated into the final thermal bond of Draper's device. A step-by-step protocol for this process is illustrated in Appendix I: Processing Protocol.

APPENDIX A: GANTT CHART
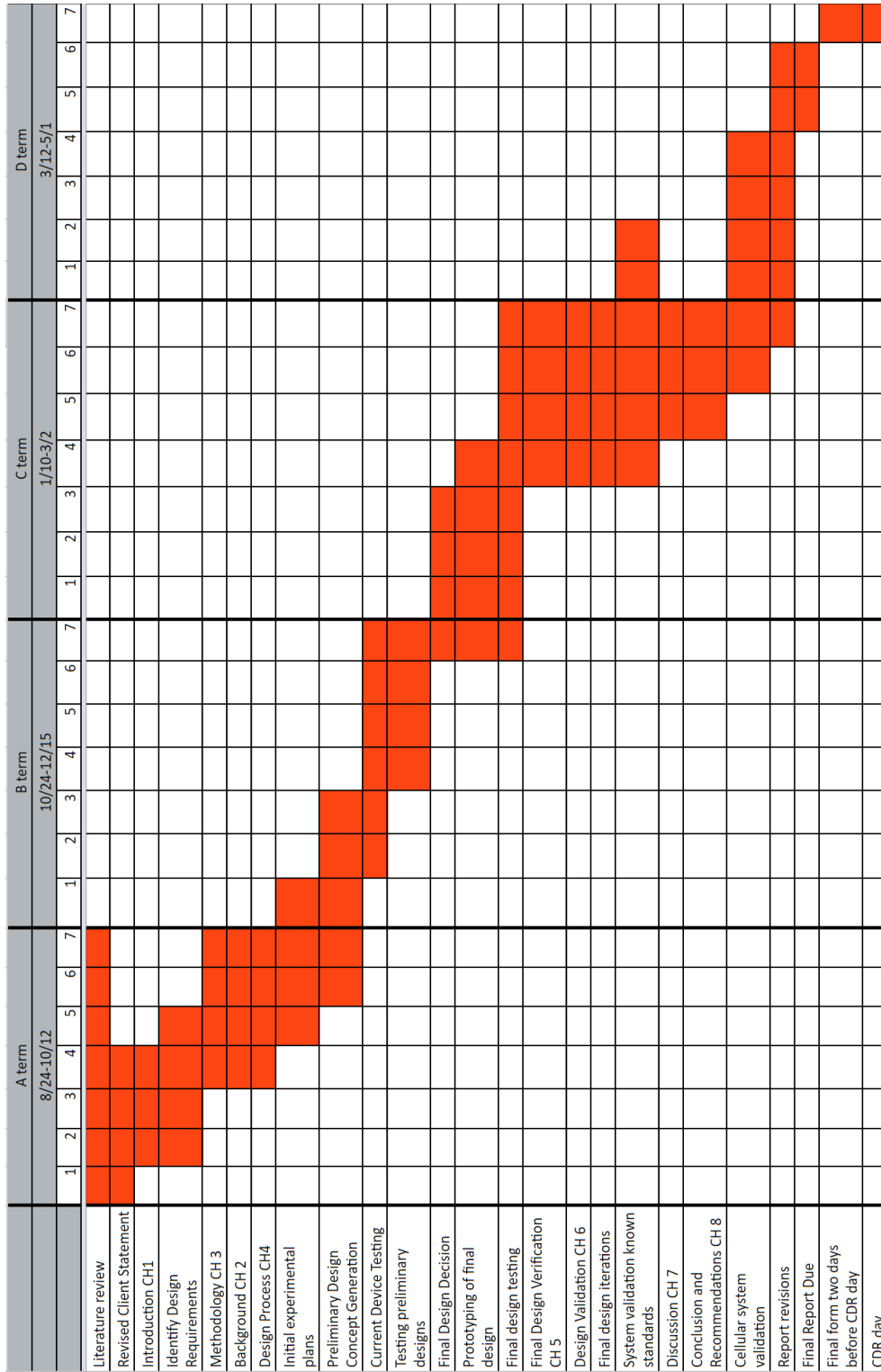
Figure 56: The team's Gantt chart.

APPENDIX B: WORK BREAKDOWN CHART
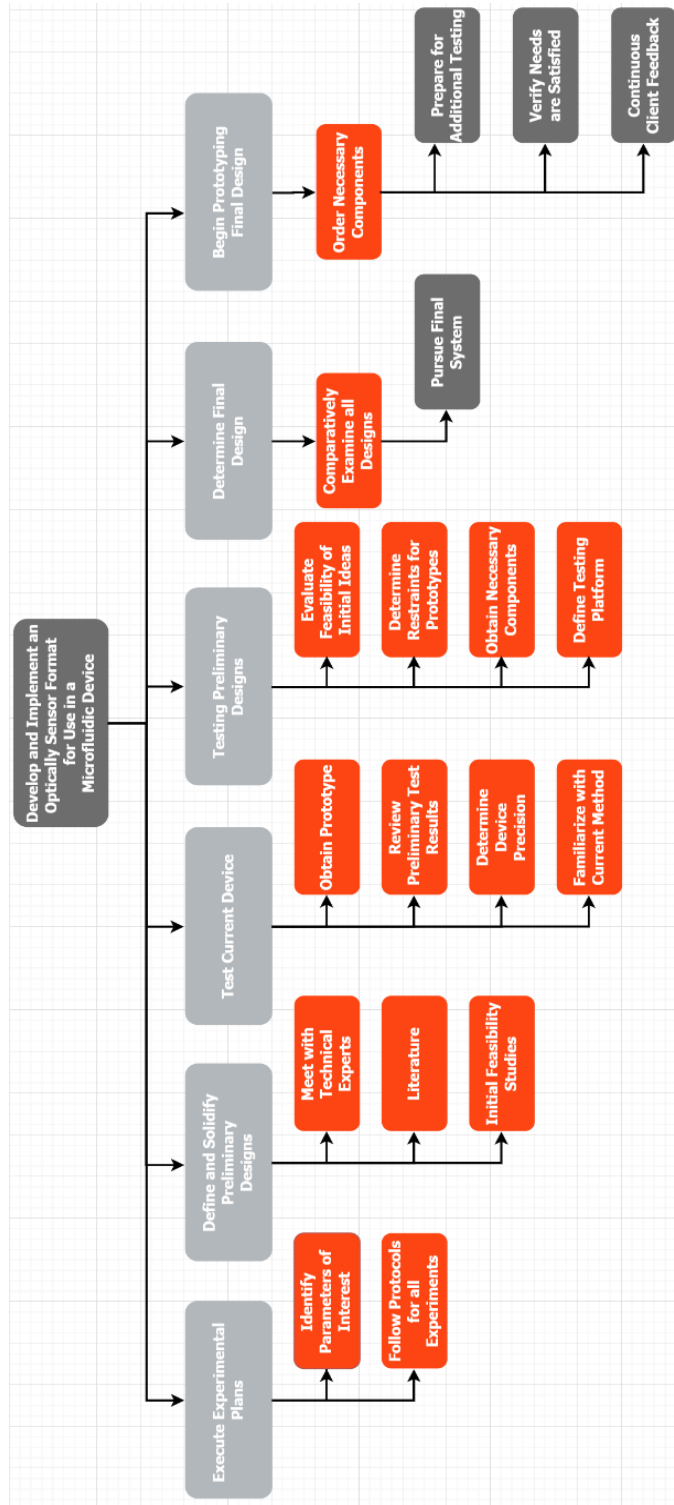
Figure 57: The team's work breakdown chart.

APPENDIX C: DYE

To use the hydrophilic form of the indicator dye, the two components must be combined with a mixture of ethanol and DI water in a 9:1 ratio. To use the hydrophobic form, the dye component must be combined with a mixture of tetrahydrofuran, referred to as THF, and toluene in a 7:3 ratio. The hydrophilic form of the dye results in a homogeneous suspension while the hydrophobic form results in a clear solution. The hydrophilic form of the dye is shown in Figure 58 below.

Figure 58: The hydrophilic form of the dye-based indicator. This dye was prepared using a combination of 200 proof ethanol and DI water in a 9:1 ratio.

The prominent green color shown in the suspension in Figure 58 indicates that there was a high concentration of the indicator present in the sample. Being that the hydrophilic and hydrophobic forms of the dye-based indicator solutions require the use of different chemicals to

generate the liquid form of the dye, the team explored the effects that these chemicals have

individually on the COC material used to construct the final device. As mentioned, the

hydrophilic form of the dye requires the use of ethanol and DI water. Being that DI water has

been used extensively in previous tests and has shown no significant effects on the COC, the

team focused on studying the effects of ethanol. Preliminary tests showed no significant effects

on the integrity of the COC material, although a cloudy film was left behind after the ethanol

evaporated as seen in Figure 59 below.
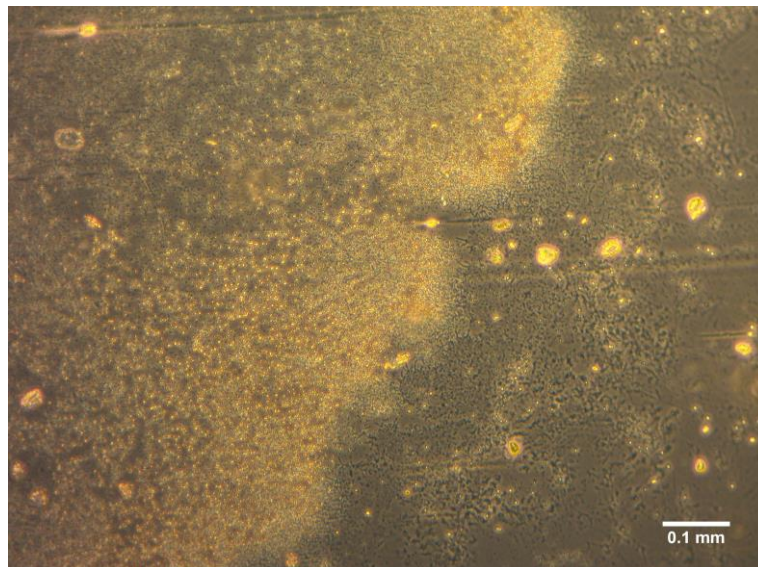
Figure 59: The surface of COC following the evaporation of 5 µL of ethanol at 10X. There is obvious opacity that is
generated as the ethanol evaporates quickly from the surface of the COC.

The hydrophobic form of the dye requires a mixture of toluene and tetrahydrofuran, THF.

To ensure that the use of the hydrophobic form of the dye will not compromise the final device,

the team studied the effects of both of the aforementioned chemicals on COC. After applying

toluene to the surface of the COC, a tacky layer began to form creating an extremely sticky

surface. Additionally, there was a significant amount of degradation of the COC visible when the

sample was analyzed under 10X magnification microscopy, which can be Figure 60.
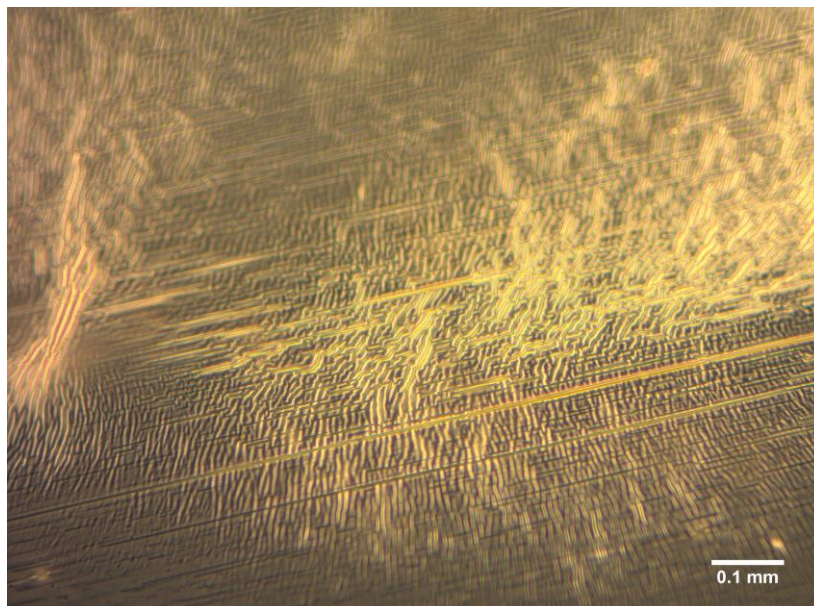
Figure 60: The surface of the COC following the evaporation of 5 µL of toluene at 10X. The toluene generates a rough topography across the surface of the COC.

APPENDIX D: MATLAB CODE FOR PICCOLO$_2$ DATA ANALYSIS

```matlab
%% MQP PiccolO2 Data Analysis

% Emma MacIntyre

% November 22, 2017


clear; clc; close all;


%read raw PiccolO2 data from a .txt file

%fileName = input('Enter filename in quotes: ');

fileName = 'pdmsencap121317.txt'

data = readtable(fileName); %reads data as a table

time = str2double(data.Var3(2:end)); %create column vector of time data

%time =data.Time(2:end); %create column vector of time data

o2Conc = str2double(data.Oxygen(2:end)); %column vector of oxygen conc

%dphi = str2double(data.dphi(2:end)); %column vector of dphi values

intensity = str2double(data.Intensity(2:end)); %column vector of intensity

%intensity = data.intensity(2:end); %column vector of intensity

reps = input('Enter replicates:');

count = 1;


while count < reps + 1

    %identify data section to analyze

    startTime = input('Enter start time: ');

    endTime = input('Enter end time: ');

    stringTitle = input('Enter Title: ');

    %startTime = startTime +1; %correct index since vector starts at zero

    %endTime = endTime +1; %correct index since vector starts at zero
```

```matlab
%extract oxygen and time data to plot

timePlot = time(startTime:endTime);

o2ConcPlot = o2Conc(startTime:endTime);

intensityPlot = intensity(startTime:endTime);


%plot oxygen conc versus time

figure

hold on

plot(timePlot,o2ConcPlot,'-x');

xlabel('Time (s)');

ylabel('Oxygen Concentration (%O2)');

title(stringTitle);


%linear fit

linearFit = polyfit(timePlot,o2ConcPlot,1);

yfit = polyval(linearFit, timePlot);

plot(timePlot,yfit,'--');

yresid = o2ConcPlot - yfit;

SSresid = sum(yresid.^2);

SStotal = (length(o2ConcPlot)-1) * var(o2ConcPlot);

rsq = 1 - SSresid/SStotal


averageO2(count) = sum(o2ConcPlot)/length(o2ConcPlot);

rangeO2(count) = max(o2ConcPlot) - min(o2ConcPlot);

averageSigIn(count) = sum(intensityPlot)/length(intensityPlot);

slope(count)= linearFit(1);


count = count +1;
```

```matlab
end


%calculate parameters

averageConc= sum(averageO2)/reps;

fprintf('Average O2: %f %%\n',averageConc);

averageRange= sum(rangeO2)/reps;

fprintf('Range O2: %f %%\n',averageRange);

averageIn= sum(averageSigIn)/reps;

fprintf('Average Singal Intensity: %f mV\n',averageIn);

averageSlope = sum(slope)/reps;

fprintf('Average Slope: %f %%O2/s\n',averageSlope);
```

APPENDIX E: DILUTION TESTING OF NANOPARTICLES

The team obtained oxygen measurements for each sample by placing the plate in a controlled temperature environment, which varied between 21.1°C and 21.8°C, based on inaccuracies in initial benchtop testing due to temperature fluctuation. In this environment, the plate rested on a metal shelf as seen in Figure 61. Team members fixed the fiber optic between the grids of the metal shelf and placed the well plate on the top of the cable. The fiber was held flush against the bottom of the plate and readings were taken for both settled and mixed samples at nanoparticle amounts ranging from 0.5 mg to 0.025 mg for 120 seconds. Between each reading, the box was opened from the top, as seen in Figure 61A, and the well plate was manually moved to align the next testing well with the fiber optic cable. For the mixed samples, the solution was agitated between each replicate of testing using a micropipette.

Figure 61: The fiber optic cable fixed in place under a metal grate and the well plate was moved to the cable for each trial. The fiber optic cable is attached to the grates of the stand using a custom prototyped holder and adhesive tape. The temperature is monitored within the enclosure using a standard thermoprobe.

The change in percent oxygen versus time for the temperature controlled dilution test can be seen in Figure 62A. The team concluded that the mixed replicates had an oxygen percent drop

off much quicker than the settled replicates, which can be correlated to a decrease in signal

intensity. In both cases, the drop-off in percent oxygen occurred after the signal intensity fell

below 50 mV, which is the minimum signal intensity required for accurate reading per the

Piccolo$_2$'s specifications. All values obtained using the Piccolo$_2$ involved taking measurements at

the area with the approximate highest density of nanoparticles. In terms of signal intensity, the

mixed samples consistently showed a lower signal intensity than the settled particles. On the

other hand, only two samples in the settled study had too low of a signal intensity for accurate

readings. This is illustrated in Figure 62B, below.
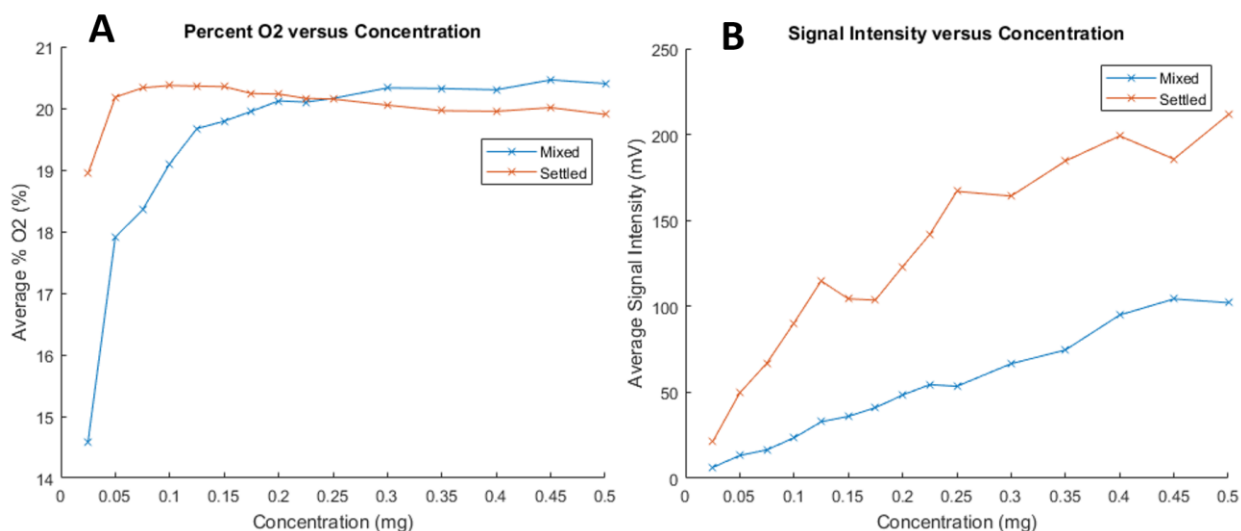
Figure 62: Percent of oxygen versus concentration (A) and signal intensity versus concentration (B) graphs for both mixed and settled dilution trials. There are obvious trends indicating that the settled mixtures provide much higher signal intensity readings, which is expected since the particles will be closer to the source of excitation. The oxygen percentage readings, when stabilized, are relatively constant among the two.

In terms of characterization, the temperature controlled testing illustrated that the

Piccolo$_2$ shows a decay in percent oxygen readings for each replicate with time when signal

intensity is adequate, as seen in Figure 63A. As the signal intensity decreases below 50 mV, the

oxygen readings tend to increase steadily as illustrated in Figure 63B.
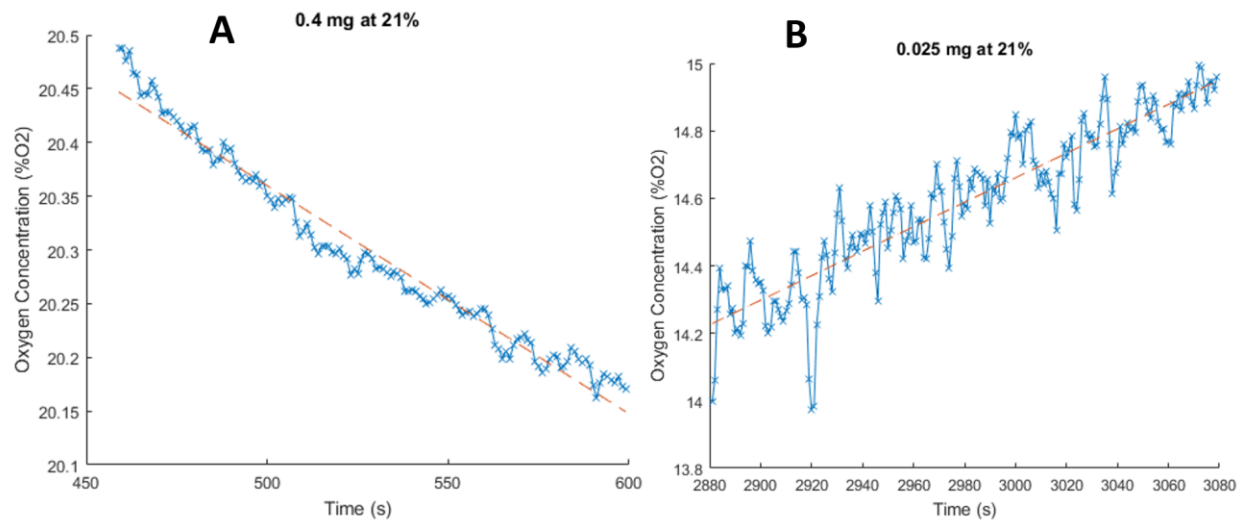
Figure 63: Oxygen percentage versus time for 0.4 mg (left) and 0.025 mg (right) concentration trials for mixed testing. Graph A illustrates a constant decrease in oxygen percentage with adequate signal intensity, while the graph B illustrates an increase in oxygen percentage with a poor signal intensity

A major goal of the dilution testing was to determine the minimum amount of nanoparticles required to attain the appropriate signal intensity. The concentration tests illustrated the anticipated relationship of a decrease in signal intensity in a relatively linear fashion as a function of nanoparticle concentration. During testing, a signal intensity lower than 50 mV was found when there were less than 0.075 mg of nanoparticles in the solution. Thus, it was concluded that 0.075 mg of nanoparticles was the minimum amount required to obtain accurate readings in this testing format. This amount of nanoparticles was deposited in a polystyrene 96-well plate, which has a well diameter of 9 mm and a corresponding area of 63.62 mm^2. This results in a minimum particle density of 0.0012 mg/mm^2.

APPENDIX F: NANOPARTICLES IN PDMS

After allowing a drop of PDMS to cure over a dried droplet of nanoparticles, a blade was used to peel the cured PDMS droplets off the glass slide. The PDMS droplets were then bonded in a 24 well plate with the nanoparticles open to the air using an additional drop of PDMS as illustrated in Figure 64.
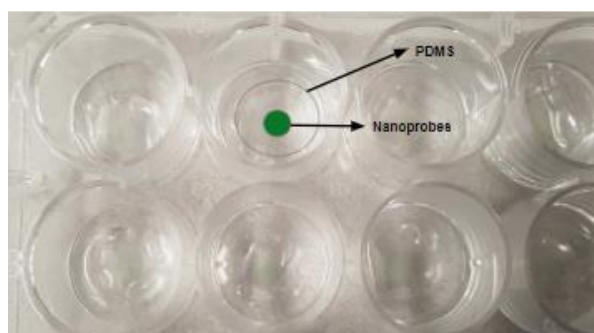
Figure 64: PDMS was peeled off the glass slide and bonded to the bottom of a polystyrene well plate using PDMS. The green dot in the center of the top well represents the nanoparticle solution. This dot is surrounded by a layer of PDMS, which is outlined in the light gray color for emphasis.

When peeling the PDMS stamps off the glass slide it was noted that not all of the nanoparticles transferred from the glass slide to the PDMS, leaving a noticeable residue behind, as illustrated in Figure 65. Figure 65A shows the residue transferred to the PDMS after stamping, while Figure 65B shows the residue left behind on the glass slide, although it appeared that more nanoparticles were transferred to the PDMS stamp than not. The Piccolo$_2$ was then used to measure the signal intensity of this sensor format. The signal intensity values for all concentrations in this PDMS peel method were found to be below the required 50 mV threshold, rendering this method ineffective.
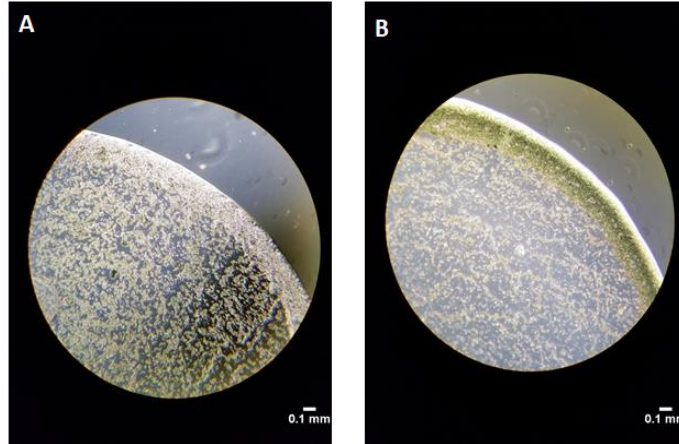
Figure 65: PDMS peel testing all imaged at 10X magnification of an inverted microscope. A) 3 µL, 5 mg/mL nanoparticle droplet remaining on PDMS surface after being peeled off. B) Residual 3 µL, 5 mg/mL drop remaining on glass slide after PDMS was peeled off the surface

Three other fabrication methods using nanoparticles and PDMS were tested as illustrated in Figure 66. The first method, seen in Figure 66A, involved dropping PDMS on a glass slide and mixing a drop of nanoparticles into the PDMS. It was found that it was not possible to obtain a uniform nanoparticle distribution using this method, as illustrated by the nanoparticle clumps visible in Figure 66A. Figure 66B illustrates the encapsulation of nanoparticles between PDMS. A drop of PDMS was placed on a glass slide, a drop of nanoparticle solution was placed on top of the PDMS, and then more PDMS was placed on top of the nanoparticle solution. Finally, in Figure 66C, a drop of nanoparticle solution was placed on the surface of a PDMS droplet and the PDMS was allowed to cure.
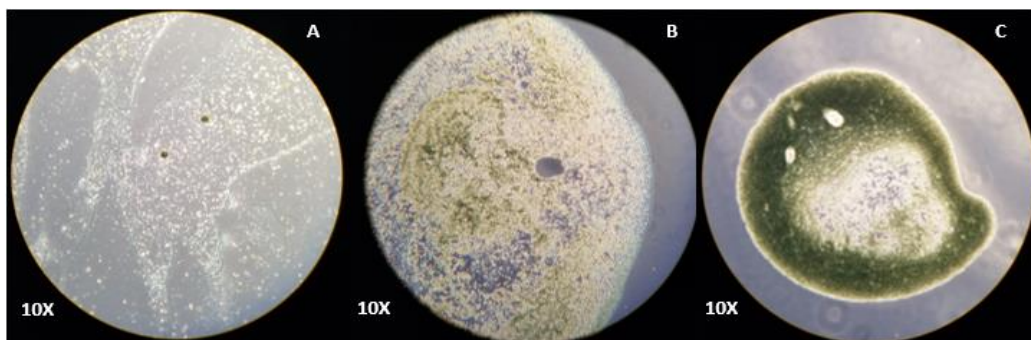
Figure 66: PDMS testing concepts all imaged at 10X magnification of an inverted microscope. A) 3 µL of 5mg/mL nanoparticle solution mixed into PMDS. B) 3 µL of 5 mg/mL nanoparticle droplet encapsulated in PDMS. C) Drop of 5 mg/mL nanoparticle solution on surface of PDMS droplet

For the study illustrated in Figure 66A, the signal intensity was not readable and oxygen percentage readings were unable to be collected. The average signal intensity for the encapsulated study illustrated in Figure 66B was 112.06 mV. Finally, the highest signal intensity of the three PDMS tests as illustrated in Figure 66C was determined to be 199.73 mV. The area of the droplet in Figure 66B was 0.681 mm^2 and the area of the droplet in Figure 66C is 1.602 mm^2. This corresponds to nanoparticle concentrations of 0.022 mg/mm^2 and 0.0094 mg/mm^2 for Figure 66B and Figure 66C respectively. Both of these determined particle densities were much higher than the minimum particle density of 0.0012 mg/mm^2 determined from the settled dilution testing. This makes sense since these trials had almost double the signal intensity compared to the corresponding dilution trial.

APPENDIX G: NANOPARTICLE DRIED FILM

To test the effects of detergent and salt on the dispersion of the nanoparticles, the team created two separate mixtures: one of the nanoparticles in DI water and table salt and another of the nanoparticles in DI water and dish detergent. After thorough mixing of each of these solutions, the team placed a 3 µL droplet of each solution on pieces of COC. These droplets were allowed to dry completely and were then imaged under 10X magnification. As shown in Figure 67, the nanoparticle solution was much more evenly dispersed when mixed using detergent and salt, as compared to a control of DI water.
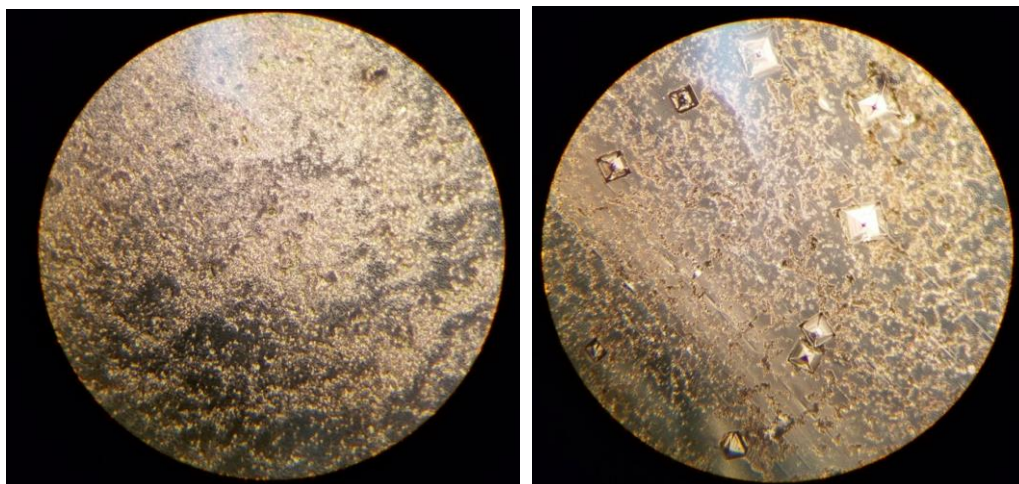
Figure 67: Dried nanoparticle solution with and dish detergent at 10X (left) and dried nanoparticle solution with salt at 10X (right). As shown, both the detergent mixture and the salt mixture fostered the distribution of the nanoparticles within the solution and lessened the amount of clumping.

The nanoparticles, when mixed using a dish detergent base, spread evenly across the surface of the COC. However, because this indicator must be utilized in a cellular environment, the team did not want to further pursue a method in which the chemistry of the indicator solution was heavily altered. Furthermore, there was an obvious presence of salt crystals located

surrounding the nanoparticles in the dried droplet of the DI water, salt, and nanoparticle mixture. Being that this indicator will be used in a cellular environment, the team decided that the salinity of the solution should not be greatly modified and the presence of salt crystals must be avoided. Due to this, the team chose to not pursue the use of salt as means of dispersing the nanoparticle solution.

APPENDIX H: LASER CONFOCAL ANALYSIS
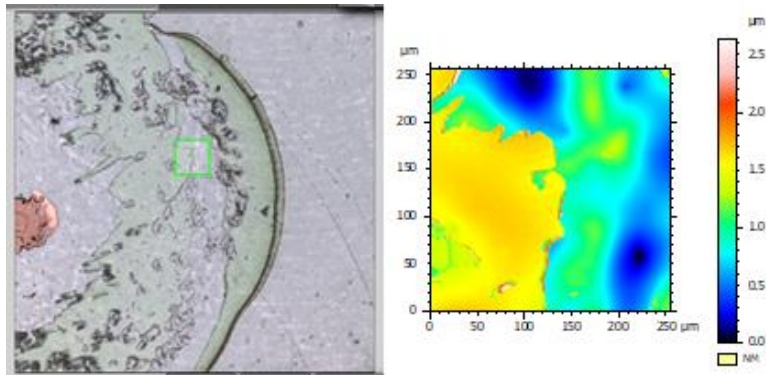
Figure 68: Laser confocal analysis of sample N1 using 50X lens. Area of sample being analyzed by laser confocal (left) and topographic map of area of interest (right).
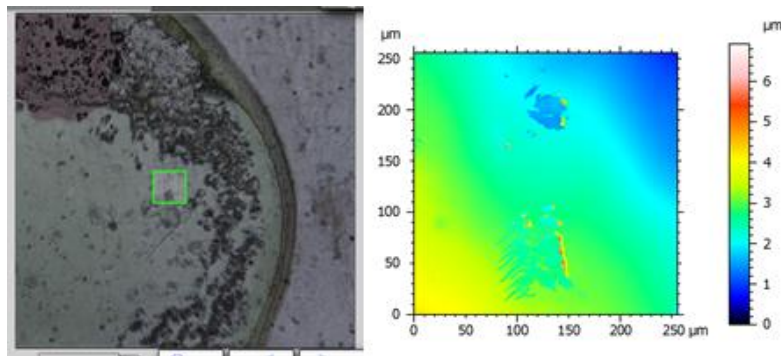
Figure 69: Laser confocal analysis of sample N4 using 50X lens. Area of sample being analyzed by laser confocal (left) and topographic map of area of interest (right).

APPENDIX I: PROCESSING PROTOCOL
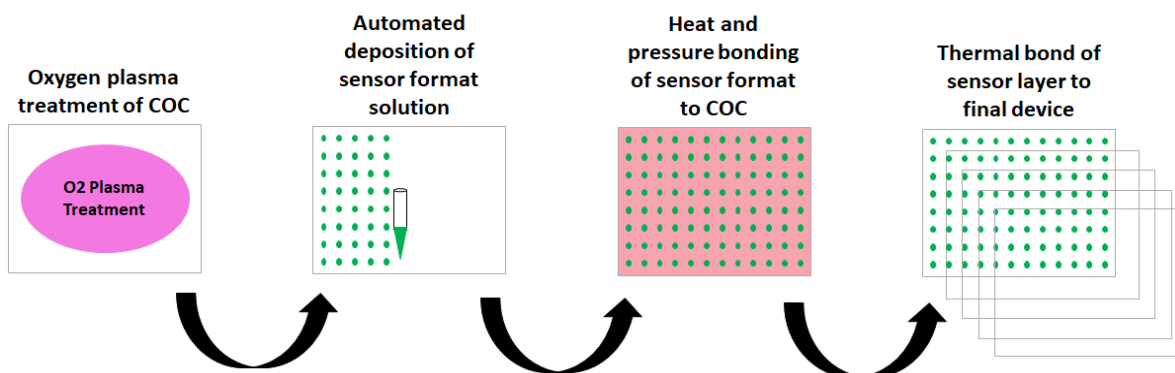
Figure 70: Recommended process for the incorporation of the nanoparticle design into Draper's organ-on-a-chip device.

Detailed Protocol

1. Obtain raw PyroScience nanoparticles.*

    a. Add 0.25 mL of DI water to a 10 mg vial of raw nanoparticles.

    b. Sonicate the vial for 10 minutes or until the solution is mixed such that no nanoparticles are visible to the naked eye.

*Store nanoparticles shielded from light in a chilled environment when not using.

2. Prepare the COC for the deposition of the sensor format.

    a. Cut a piece of raw material to the dimensions of a standard 96 well plate.

    b. Remove the protective covers from both sides of the COC.

    c. Place COC in an oxygen plasma chamber for 1 minute of exposure.

3. Set-up the desired automated system for deposition of the sensor format.

    a. Transfer solution containing the sensor format into a 96 well plate.

    b. Program the automated machine to drop the desired volume and positioning of each drop in the 96 well format.

c. Allow the solution to dry.

4. Bond the deposited sensor format to the COC using Carver press method.

   a. Cut two ⅛'' pieces of aluminum to dimensions slightly bigger than the sheet of COC.

   b. Cut two compliance layers (rubber would suffice) to a size slightly bigger than the aluminum sheets.

   c. Coat aluminum pieces in Kapton ensuring to minimize any air bubbles or particulates under the surface.

   d. Transfer COC sheet with deposited sensor format onto one of the Kapton covered pieces of aluminum.

   e. Place other aluminum piece on top and tape sides with Kapton tape to prevent sliding of the aluminum layers.

   f. Place the rubber pieces on either side of the aluminum.

   g. Carefully transfer testing stack-up to a Carver press machine with heated platens.

   h. Place the sample between the platens in the center and apply a small amount of pressure such that the stack up is in contact with both platens and heat the press to 120°C.

   i. Once the Carver press is heated to 120°C, apply a force of 1000 lbs on the Carver press which should equal a 450 psi pressure on the sample.

   j. After 15 minutes, remove pressure and turn the Carver press off.

   k. Let the sample cool for 12 hours and carefully peel the COC sheet from the stack-up.

APPENDIX J: COPYRIGHT APPROVAL

ELSEVIER LICENSE
TERMS AND CONDITIONS

Mar 26, 2018

This Agreement between Worcester Polytechnic Institute -- Emma MacIntyre ("You") and Elsevier ("Elsevier") consists of your license details and the terms and conditions provided by Elsevier and Copyright Clearance Center.

License Number	4306500900318
License date	Mar 12, 2018
Licensed Content Publisher	Elsevier
Licensed Content Publication	Analytica Chimica Acta
Licensed Content Title	Microfluidic device coupled with a microfabricated oxygen electrode for the measurement of bactericidal activity of neutrophil-like cells
Licensed Content Author	Anna Yamagishi,Koji Tanabe,Masatoshi Yokokawa,Yuji Morimoto,Manabu Kinoshita,Hiroaki Suzuki
Licensed Content Date	Sep 8, 2017
Licensed Content Volume	985
Licensed Content Issue	n/a
Licensed Content Pages	6
Start Page	1
End Page	6
Type of Use	reuse in a thesis/dissertation
Portion	figures/tables/illustrations
Number of figures/tables/illustrations	1
Format	electronic
Are you the author of this Elsevier article?	No
Will you be translating?	No
Original figure numbers	Figure 1, A
Title of your thesis/dissertation	Sensing Oxygen Autonomously In Real-Time
Expected completion date	May 2018
Estimated size (number of pages)	130
Requestor Location	Worcester Polytechnic Institute 100 Institute Road

WORCESTER, MA 01609 United States Attn: Worcester Polytechnic Institute |
Publisher Tax ID	98-0397604
Total	0.00 USD
Terms and Conditions	

INTRODUCTION

1. The publisher for this copyrighted material is Elsevier. By clicking "accept" in connection with completing this licensing transaction, you agree that the following terms and conditions apply to this transaction (along with the Billing and Payment terms and conditions established by Copyright Clearance Center, Inc. ("CCC"), at the time that you opened your Rightslink account and that are available at any time at http://myaccount.copyright.com).

GENERAL TERMS

2. Elsevier hereby grants you permission to reproduce the aforementioned material subject to the terms and conditions indicated.

3. Acknowledgement: If any part of the material to be used (for example, figures) has appeared in our publication with credit or acknowledgement to another source, permission must also be sought from that source. If such permission is not obtained then that material may not be included in your publication/copies. Suitable acknowledgement to the source must be made, either as a footnote or in a reference list at the end of your publication, as follows:

"Reprinted from Publication title, Vol /edition number, Author(s), Title of article / title of chapter, Pages No., Copyright (Year), with permission from Elsevier [OR APPLICABLE SOCIETY COPYRIGHT OWNER]." Also Lancet special credit - "Reprinted from The Lancet, Vol. number, Author(s), Title of article, Pages No., Copyright (Year), with permission from Elsevier."

4. Reproduction of this material is confined to the purpose and/or media for which permission is hereby given.

5. Altering/Modifying Material: Not Permitted. However figures and illustrations may be altered/adapted minimally to serve your work. Any other abbreviations, additions, deletions and/or any other alterations shall be made only with prior written authorization of Elsevier Ltd. (Please contact Elsevier at permissions@elsevier.com). No modifications can be made to any Lancet figures/tables and they must be reproduced in full.

6. If the permission fee for the requested use of our material is waived in this instance, please be advised that your future requests for Elsevier materials may attract a fee.

7. Reservation of Rights: Publisher reserves all rights not specifically granted in the combination of (i) the license details provided by you and accepted in the course of this licensing transaction, (ii) these terms and conditions and (iii) CCC's Billing and Payment terms and conditions.

8. License Contingent Upon Payment: While you may exercise the rights licensed immediately upon issuance of the license at the end of the licensing process for the transaction, provided that you have disclosed complete and accurate details of your proposed use, no license is finally effective unless and until full payment is received from you (either by publisher or by CCC) as provided in CCC's Billing and Payment terms and conditions. If full payment is not received on a timely basis, then any license preliminarily granted shall be deemed automatically revoked and shall be void as if never granted. Further, in the event that you breach any of these terms and conditions or any of CCC's Billing and Payment terms and conditions, the license is automatically revoked and shall be void as if never granted. Use of materials as described in a revoked license, as well as any use of the materials beyond the scope of an unrevoked license, may constitute copyright infringement and publisher reserves the right to take any and all action to protect its copyright in the materials.

9. Warranties: Publisher makes no representations or warranties with respect to the licensed material.

10. Indemnity: You hereby indemnify and agree to hold harmless publisher and CCC, and their respective officers, directors, employees and agents, from and against any and all claims arising out of your use of the licensed material other than as specifically authorized pursuant to this license.

11. No Transfer of License: This license is personal to you and may not be sublicensed, assigned, or transferred by you to any other person without publisher's written permission.

119

12. No Amendment Except in Writing: This license may not be amended except in a writing signed by both parties (or, in the case of publisher, by CCC on publisher's behalf).

13. Objection to Contrary Terms: Publisher hereby objects to any terms contained in any purchase order, acknowledgment, check endorsement or other writing prepared by you, which terms are inconsistent with these terms and conditions or CCC's Billing and Payment terms and conditions. These terms and conditions, together with CCC's Billing and Payment terms and conditions (which are incorporated herein), comprise the entire agreement between you and publisher (and CCC) concerning this licensing transaction. In the event of any conflict between your obligations established by these terms and conditions and those established by CCC's Billing and Payment terms and conditions, these terms and conditions shall control.

14. Revocation: Elsevier or Copyright Clearance Center may deny the permissions described in this License at their sole discretion, for any reason or no reason, with a full refund payable to you. Notice of such denial will be made using the contact information provided by you. Failure to receive such notice will not alter or invalidate the denial. In no event will Elsevier or Copyright Clearance Center be responsible or liable for any costs, expenses or damage incurred by you as a result of a denial of your permission request, other than a refund of the amount(s) paid by you to Elsevier and/or Copyright Clearance Center for denied permissions.

<div align="center">LIMITED LICENSE</div>

The following terms and conditions apply only to specific license types:

15. **Translation**: This permission is granted for non-exclusive world **English** rights only unless your license was granted for translation rights. If you licensed translation rights you may only translate this content into the languages you requested. A professional translator must perform all translations and reproduce the content word for word preserving the integrity of the article.

16. **Posting licensed content on any Website**: The following terms and conditions apply as follows: Licensing material from an Elsevier journal: All content posted to the web site must maintain the copyright information line on the bottom of each image; A hyper-text must be included to the Homepage of the journal from which you are licensing at http://www.sciencedirect.com/science/journal/xxxxx or the Elsevier homepage for books at http://www.elsevier.com; Central Storage: This license does not include permission for a scanned version of the material to be stored in a central repository such as that provided by Heron/XanEdu.

Licensing material from an Elsevier book: A hyper-text link must be included to the Elsevier homepage at http://www.elsevier.com . All content posted to the web site must maintain the copyright information line on the bottom of each image.

Posting licensed content on Electronic reserve: In addition to the above the following clauses are applicable: The web site must be password-protected and made available only to bona fide students registered on a relevant course. This permission is granted for 1 year only. You may obtain a new license for future website posting.

17. **For journal authors:** the following clauses are applicable in addition to the above:
Preprints:
A preprint is an author's own write-up of research results and analysis, it has not been peer-reviewed, nor has it had any other value added to it by a publisher (such as formatting, copyright, technical enhancement etc.).

Authors can share their preprints anywhere at any time. Preprints should not be added to or enhanced in any way in order to appear more like, or to substitute for, the final versions of articles however authors can update their preprints on arXiv or RePEc with their Accepted Author Manuscript (see below).

If accepted for publication, we encourage authors to link from the preprint to their formal publication via its DOI. Millions of researchers have access to the formal publications on ScienceDirect, and so links will help users to find, access, cite and use the best available

version. Please note that Cell Press, The Lancet and some society-owned have different preprint policies. Information on these policies is available on the journal homepage.

Accepted Author Manuscripts: An accepted author manuscript is the manuscript of an article that has been accepted for publication and which typically includes author-incorporated changes suggested during submission, peer review and editor-author communications.

Authors can share their accepted author manuscript:

- immediately
  - via their non-commercial person homepage or blog
  - by updating a preprint in arXiv or RePEc with the accepted manuscript
  - via their research institute or institutional repository for internal institutional uses or as part of an invitation-only research collaboration work-group
  - directly by providing copies to their students or to research collaborators for their personal use
  - for private scholarly sharing as part of an invitation-only work group on commercial sites with which Elsevier has an agreement
- After the embargo period
  - via non-commercial hosting platforms such as their institutional repository
  - via commercial sites with which Elsevier has an agreement

In all cases accepted manuscripts should:

- link to the formal publication via its DOI
- bear a CC-BY-NC-ND license - this is easy to do
- if aggregated with other manuscripts, for example in a repository or other site, be shared in alignment with our hosting policy not be added to or enhanced in any way to appear more like, or to substitute for, the published journal article.

Published journal article (JPA): A published journal article (PJA) is the definitive final record of published research that appears or will appear in the journal and embodies all value-adding publishing activities including peer review co-ordination, copy-editing, formatting, (if relevant) pagination and online enrichment.

Policies for sharing publishing journal articles differ for subscription and gold open access articles:

Subscription Articles: If you are an author, please share a link to your article rather than the full-text. Millions of researchers have access to the formal publications on ScienceDirect, and so links will help your users to find, access, cite, and use the best available version. Theses and dissertations which contain embedded PJAs as part of the formal submission can be posted publicly by the awarding institution with DOI links back to the formal publications on ScienceDirect.

If you are affiliated with a library that subscribes to ScienceDirect you have additional private sharing rights for others' research accessed under that agreement. This includes use for classroom teaching and internal training at the institution (including use in course packs and courseware programs), and inclusion of the article for grant funding purposes.

Gold Open Access Articles: May be shared according to the author-selected end-user license and should contain a CrossMark logo, the end user license, and a DOI link to the formal publication on ScienceDirect.

Please refer to Elsevier's posting policy for further information.

18. **For book authors** the following clauses are applicable in addition to the above: Authors are permitted to place a brief summary of their work online only. You are not allowed to download and post the published electronic version of your chapter, nor may you scan the printed edition to create an electronic version. **Posting to a repository:** Authors are permitted to post a summary of their chapter only in their institution's repository.

121

19. **Thesis/Dissertation**: If your license is for use in a thesis/dissertation your thesis may be submitted to your institution in either print or electronic form. Should your thesis be published commercially, please reapply for permission. These requirements include permission for the Library and Archives of Canada to supply single copies, on demand, of the complete thesis and include permission for Proquest/UMI to supply single copies, on demand, of the complete thesis. Should your thesis be published commercially, please reapply for permission. Theses and dissertations which contain embedded PJAs as part of the formal submission can be posted publicly by the awarding institution with DOI links back to the formal publications on ScienceDirect.

Elsevier Open Access Terms and Conditions

You can publish open access with Elsevier in hundreds of open access journals or in nearly 2000 established subscription journals that support open access publishing. Permitted third party re-use of these open access articles is defined by the author's choice of Creative Commons user license. See our open access license policy for more information.

Terms & Conditions applicable to all Open Access articles published with Elsevier:
Any reuse of the article must not represent the author as endorsing the adaptation of the article nor should the article be modified in such a way as to damage the author's honour or reputation. If any changes have been made, such changes must be clearly indicated.
The author(s) must be appropriately credited and we ask that you include the end user license and a DOI link to the formal publication on ScienceDirect.
If any part of the material to be used (for example, figures) has appeared in our publication with credit or acknowledgement to another source it is the responsibility of the user to ensure their reuse complies with the terms and conditions determined by the rights holder.
Additional Terms & Conditions applicable to each Creative Commons user license:
CC BY: The CC-BY license allows users to copy, to create extracts, abstracts and new works from the Article, to alter and revise the Article and to make commercial use of the Article (including reuse and/or resale of the Article by commercial entities), provided the user gives appropriate credit (with a link to the formal publication through the relevant DOI), provides a link to the license, indicates if changes were made and the licensor is not represented as endorsing the use made of the work. The full details of the license are available at http://creativecommons.org/licenses/by/4.0.
CC BY NC SA: The CC BY-NC-SA license allows users to copy, to create extracts, abstracts and new works from the Article, to alter and revise the Article, provided this is not done for commercial purposes, and that the user gives appropriate credit (with a link to the formal publication through the relevant DOI), provides a link to the license, indicates if changes were made and the licensor is not represented as endorsing the use made of the work. Further, any new works must be made available on the same conditions. The full details of the license are available at http://creativecommons.org/licenses/by-nc-sa/4.0.
CC BY NC ND: The CC BY-NC-ND license allows users to copy and distribute the Article, provided this is not done for commercial purposes and further does not permit distribution of the Article if it is changed or edited in any way, and provided the user gives appropriate credit (with a link to the formal publication through the relevant DOI), provides a link to the license, and that the licensor is not represented as endorsing the use made of the work. The full details of the license are available at http://creativecommons.org/licenses/by-nc-nd/4.0.
Any commercial reuse of Open Access articles published with a CC BY NC SA or CC BY NC ND license requires permission from Elsevier and will be subject to a fee.
Commercial reuse includes:

- Associating advertising with the full text of the Article
- Charging fees for document delivery or access
- Article aggregation
- Systematic distribution via e-mail lists or share buttons

122

Posting or linking by commercial companies for use by customers of those companies.

20. **Other Conditions**:

v1.9

123

March 20, 2018

Via email to: efmacintyre@wpi.edu; draper@wpi.edu

Emma MacIntyre
Worcester Polytechnic Institute
100 Institute Road
Box #3442
Worcester, MA 01609

      Re: Permission to Copy and Republish Agilent Image

Dear Ms. MacIntyre:

This is in response to your email requests seeking consent to copy and republish an image in which Agilent Technologies, Inc. ("Agilent") owns the copyright. I have attached for clarity a copy of the emails that set out your requests in Attachment A. Specifically, you have requested permission to copy and republish a photograph of an Agilent Seahorse XFe96 Analyzer (the "Agilent Image") in your Worcester Polytechnic Institute undergraduate senior project titled "Sensing Oxygen Autonomously in Real-time" (the "Work"). A high-resolution copy of the Agilent Image is enclosed with this letter.

I am pleased to advise that you and Worcester Polytechnic Institute have Agilent's permission to copy and republish the Agilent Image in the Work in any and all media of expression now known or later developed, worldwide, and in all languages. This consent is conditioned upon there being included with the Agilent Image an appropriate acknowledgement and copyright notice in a form similar to the following:

<div align="center">

© Agilent Technologies, Inc.
Reproduced with Permission, Courtesy of Agilent Technologies, Inc.

</div>

By reproducing these materials, you and Worcester Polytechnic Institute acknowledge and agree: (1) that the Agilent Image and the information contained therein are accepted "AS IS"; (2) that Agilent does not make any representations or warranties of any kind with respect to the Agilent Image and disclaims any responsibility for the content as reproduced by you and Worcester Polytechnic Institute; (3) that Agilent reserves the right to review any use of the Agilent Image and to terminate this consent and require its immediate removal if altered, modified, or portrayed in any way that, in Agilent's opinion, is in poor taste or diminishes the reputation of Agilent or its products; (4) that Agilent will not be liable for any damages, whether special, incidental, consequential, direct, indirect or punitive, resulting from or in connection with the use, copying or disclosure of the Agilent Image, and (5) to indemnify Agilent for all claims, actions, damages, and expenses (including attorneys' fees) incurred by Agilent as a result of the Agilent Image being reproduced, modified, or distributed pursuant to this consent.

124

Agilent

This limited consent does not grant a license to use any Agilent trademark. Except for the limited consent to use the Agilent Image referenced herein, this limited consent does not grant a license to use any other Agilent copyrighted work.

Thank you for your interest in Agilent Technologies, Inc. and its products and services.

Sincerely,

Janet Shih Hajek
Corporate Counsel
Agilent Technologies, Inc.

Exhibit A (E-mail requests)

From: MacIntyre, Emma Frances [mailto:efmacintyre@wpi.edu]
Sent: Monday, March 19, 2018 6:31 PM
To: HAJEK,JANET (A-USA,ex1) <janet.hajek@agilent.com>; draper@WPI.EDU
Subject: Re: IM168385462 - Request - Web Operations – Web Support Form / Worcester Polytechnic Insitute / Emma MacIntyre / copyright / ya

Janet,

Thank you for the quick response. The information required is provided below:

1. **Mailing Address:** Emma MacIntyre, 100 Institute Road, Box #3442, Worcester, MA 01609
2. **Project Title:** Sensing Oxygen Autonomously in Real-time
3. **Aglient URL & Exact Image:** https://www.agilent.com/en/products/cell-analysis-(seahorse)/seahorse-analyzers/seahorse-xfe96-analyzer

Seahorse XFe96 Analyzer | Agilent

www.agilent.com

Seahorse XFe96 Analyzer measures OCR and ECAR of live cells in a 96-well plate format.

4.
5. **High resolution:** this is not necessary, but would be used and appreciated if provided

Please let me know if there is any other information that you need.

Best,

Emma MacIntyre

Emma F. MacIntyre
Worcester Polytechnic Institute 2018
Mechanical and Biomedical Engineering
Alpha Eta Mu Beta- President
Tau Beta Pi- Recording Secretary

Women's Cross Country and Track & Field
efmacintyre@wpi.edu

Dear Ms. MacIntyre,

We received your copyright consent request below. Can you please provide the following information:

1. Your mailing address;
2. The official name (or proposed name) of your undergraduate senior project/paper in which you are proposing to use the image of Agilent's Seahorse XFe96 Analyzer;
3. The specific Agilent URL and exact image that you are requesting permission to use; and
4. Whether you will need a high resolution image.

Please let me know if you would like to discuss and if you have any questions.

Best regards,
Janet

Janet Shih Hajek
Corporate Counsel
Intellectual Property Group
Agilent Technologies, Inc.
T: +1 303 588 7502 | www.agilent.com

Agilent

Subject: Request - Web Operations – Web Support Form

Your form "Agilent.com Website Support and Feedback" has received the following response:

Submitted on: 3/19/2018 4:26:46 PM
Completion time: 2 min. 15 sec.

Q. Given Name:
R. Emma

Q. Family Name :
R. MacIntyre

Q. Country
R. United States

Emails:

Q. Email Address:
R. draper@wpi.edu

Q. Confirm Email Address:
R. draper@wpi.edu

Q.
R.

Q. Questions/Comments:
R. Hello,

I am a student at Worcester Polytechnic Insitute currently working on my undergraduate senior project on oxygen sensing in a microfluidic device. My team and I were interested in using an image of the Seahorse XFe96 Analyzer obtained from your website. This image would be used in the background section of our paper which will be published by our institution in an online format. I am writing to ask for premission to reproduce this image in our paper understanding that we will cite the image appropriately.

Best,

Emma MacIntyre

Campaign Code:
Form Url: https://www.agilent.com/en-us/contact-us/agilent-website-support-feedback

Re: Pyroscience Image Use Inquiry

Info Pyro Science <info@pyro-science.com>

Tue 3/20/2018 6:39 AM

To: MacIntyre, Emma Frances <efmacintyre@wpi.edu>;

Hello Emma,

thanks for your email and you can include both images if cited appropriately. Could you please send us a link/copy of this publication?

Thanks and kind regards,

Andrea

Am 19/03/2018 um 23:15 schrieb MacIntyre, Emma Frances:

> Hello,
>
> I am a student at Worcester Polytechnic Insitute currently working on my undergraduate senior project on oxygen sensing in a microfluidic device. My team and I were interested in using the following pictures which were retrieved from your website. These images would be used in the background section of our paper which will be published by our institution in an online format. I am writing to ask for premission to reproduce these images in our paper understanding that we will cite the images appropriately.

> All the best,
>
> Emma MacIntyre
>
> **Emma F. MacIntyre**
> Worcester Polytechnic Institute 2018
> Mechanical and Biomedical Engineering
> Alpha Eta Mu Beta- President
> Tau Beta Pi- Recording Secretary
> Women's Cross Country and Track & Field
> efmacintyre@wpi.edu

--

--

Pyro Science GmbH
Hubertusstr. 35
D-52064 Aachen
GERMANY
fon: +49 (0)241 518322-10
fax: +49 (0)241 518322-99

mailto:info@pyro-science.com
http://www.pyro-science.com

CEO / Geschaeftsfuehrer: Dr. Roland Thar

Registered / Amtsgericht: Aachen HRB 17329 Germany

Re: AW: Email from PreSens

MacIntyre, Emma Frances

Wed 3/21/2018 7:49 AM

To: draper@wpi.edu <draper@WPI.EDU>; Artinger, Christina <christina.artinger@presens.de>;

Cc: John, Gernot Thomas <g.john@presens.de>;

Hi Tina,

Awesome, thank you for your help!

Best,

Emma MacIntyre

From: Artinger, Christina <Christina.Artinger@presens.de>
Sent: Wednesday, March 21, 2018 3:01:28 AM
To: MacIntyre, Emma Frances; draper@wpi.edu
Cc: John, Gernot Thomas
Subject: AW: Email from PreSens

Hi Emma,

Thank you. Yes, of course this would be no problem if you reference the source accordingly to www.presens.de

Let us know if you have any further questions.

Best regards,
Tina

Von: MacIntyre, Emma Frances <efmacintyre@wpi.edu>
Gesendet: Mittwoch, 21. März 2018 02:58
An: Artinger, Christina <Christina.Artinger@presens.de>; draper@wpi.edu
Cc: John, Gernot Thomas <G.John@presens.de>
Betreff: Re: Email from PreSens

Hi Tina,

I have reproduced the photo I was referring to below. The photo was found at the following link, https://www.presens.de/products/imaging.html.

Imaging Products - PreSens

www.presens.de

PreSens VisiSens™ imaging systems combine fluorescent sensor foils with 2D read-out technology allowing visualization of O2, pH or CO2 distributions

Best,

Emma MacIntyre

Emma F. MacIntyre
Worcester Polytechnic Institute 2018
Mechanical and Biomedical Engineering
Alpha Eta Mu Beta- President
Tau Beta Pi- Recording Secretary
Women's Cross Country and Track & Field
efmacintyre@wpi.edu

From: Artinger, Christina <Christina.Artinger@presens.de>
Sent: Tuesday, March 20, 2018 5:01:52 AM
To: draper@wpi.edu
Cc: John, Gernot Thomas
Subject: AW: Email from PreSens

Hi Emma,

Thanks for reaching out.
Just to double-check, is this the photo you are referring to?

https://www.presens.de/fileadmin/user_upload/products/meters/DU01_new.jpg

Best regards,
Tina

Tina Artinger
Marketing & Sales

Am BioPark 11 - 93053 Regensburg - Germany
Phone +49 941 942 72 132, Fax +49 941 942 72 111
christina.artinger@presens.de, **www.PreSens.de**

○○

Please meet us at:

Analytica 2018

April 10 - 13, 2018, Munich, Germany, Analytica2018, Messe München, Hall A2, Booth 324

3D Cell Culture

June 05 - 07, 2018 Freiburg, Germany, 3DCellCulture, Konzerthaus Freiburg

Lab-on-a-Chip & Microfluidics EUROPE 2018

June 05 - 06, 2018 Rotterdam, The Netherlands, Lab-on-a-Chip, De Delen

○○

Registergericht: Amtsgericht Ingolstadt, Handelsregister: HRB 101505, Geschäftsführer: Achim Stangelmayer

Von: MacIntyre [mailto:draper@wpi.edu]
Gesendet: Montag, 19. März 2018 23:34
An: PreSens <info@presens.de>
Betreff: Email from PreSens

Your personal information

Salutation:	Ms/Mrs
Family Name:	MacIntyre
Given name(s):	Emma
Company/Organization:	Worcester Polytechnic Institute
Email:	draper@wpi.edu
Telephone:	716-604-7893
How did you get to know us:	Search engine (e.g. Google)

Your message

Subject: PreSense Image Use Inquiry

Message: Hello, I am a student at Worcester Polytechnic Insitute currently working on my undergraduate senior project on oxygen sensing in a microfluidic device. My team and I were interested in using an image of your Detector Unit DUO1 which was retrieved from your website. This image would be used in the background section of our paper which will be published by our institution in an online format. I am writing to ask for premission to reproduce this images in our paper understanding that we will cite the image appropriately. Best, Emma MacIntyre

Other data

Privacy notice accepted: yes

Newsletter:

Special: https://www.presens.de/products/imaging.html

xmindProductId:

JOHN WILEY AND SONS LICENSE
TERMS AND CONDITIONS

Mar 26, 2018

This Agreement between Worcester Polytechnic Institute -- Emma MacIntyre ("You") and John Wiley and Sons ("John Wiley and Sons") consists of your license details and the terms and conditions provided by John Wiley and Sons and Copyright Clearance Center.

License Number	4307891005556
License date	Mar 14, 2018
Licensed Content Publisher	John Wiley and Sons
Licensed Content Publication	Journal of Applied Toxicology
Licensed Content Title	Cardiotoxicity testing using pluripotent stem cell-derived human cardiomyocytes and state-of-the-art bioanalytics: a review
Licensed Content Author	Carl-Fredrik Mandenius,Daniella Steel,Fozia Noor,Thomas Meyer,Elmar Heinzle,Julia Asp,Sarina Arain,Udo Kraushaar,Susanne Bremer,Reiner Class,Peter Sartipy
Licensed Content Date	Feb 16, 2011
Licensed Content Pages	15
Type of use	Dissertation/Thesis
Requestor type	University/Academic
Format	Electronic
Portion	Figure/table
Number of figures/tables	1
Original Wiley figure/table number(s)	Figure 5
Will you be translating?	No
Title of your thesis / dissertation	Sensing Oxygen Autonomously In Real-Time
Expected completion date	May 2018
Expected size (number of pages)	130
Requestor Location	Worcester Polytechnic Institute 100 Institute Road

WORCESTER, MA 01609 United States Attn: Worcester Polytechnic Institute |
Publisher Tax ID	EU826007151
Total	0.00 USD
Terms and Conditions	

TERMS AND CONDITIONS

This copyrighted material is owned by or exclusively licensed to John Wiley & Sons, Inc. or one of its group companies (each a"Wiley Company") or handled on behalf of a society with which a Wiley Company has exclusive publishing rights in relation to a particular work

(collectively "WILEY"). By clicking "accept" in connection with completing this licensing transaction, you agree that the following terms and conditions apply to this transaction (along with the billing and payment terms and conditions established by the Copyright Clearance Center Inc., ("CCC's Billing and Payment terms and conditions"), at the time that you opened your RightsLink account (these are available at any time at http://myaccount.copyright.com).

Terms and Conditions

- The materials you have requested permission to reproduce or reuse (the "Wiley Materials") are protected by copyright.

- You are hereby granted a personal, non-exclusive, non-sub licensable (on a stand-alone basis), non-transferable, worldwide, limited license to reproduce the Wiley Materials for the purpose specified in the licensing process. This license, **and any CONTENT (PDF or image file) purchased as part of your order,** is for a one-time use only and limited to any maximum distribution number specified in the license. The first instance of republication or reuse granted by this license must be completed within two years of the date of the grant of this license (although copies prepared before the end date may be distributed thereafter). The Wiley Materials shall not be used in any other manner or for any other purpose, beyond what is granted in the license. Permission is granted subject to an appropriate acknowledgement given to the author, title of the material/book/journal and the publisher. You shall also duplicate the copyright notice that appears in the Wiley publication in your use of the Wiley Material. Permission is also granted on the understanding that nowhere in the text is a previously published source acknowledged for all or part of this Wiley Material. Any third party content is expressly excluded from this permission.

- With respect to the Wiley Materials, all rights are reserved. Except as expressly granted by the terms of the license, no part of the Wiley Materials may be copied, modified, adapted (except for minor reformatting required by the new Publication), translated, reproduced, transferred or distributed, in any form or by any means, and no derivative works may be made based on the Wiley Materials without the prior permission of the respective copyright owner.**For STM Signatory Publishers clearing permission under the terms of the STM Permissions Guidelines only, the terms of the license are extended to include subsequent editions and for editions in other languages, provided such editions are for the work as a whole in situ and does not involve the separate exploitation of the permitted figures or extracts,** You may not alter, remove or suppress in any manner any copyright, trademark or other notices displayed by the Wiley Materials. You may not license, rent, sell, loan, lease, pledge, offer as security, transfer or assign the Wiley Materials on a stand-alone basis, or any of the rights granted to you hereunder to any other person.

- The Wiley Materials and all of the intellectual property rights therein shall at all times remain the exclusive property of John Wiley & Sons Inc, the Wiley Companies, or their respective licensors, and your interest therein is only that of having possession of and the right to reproduce the Wiley Materials pursuant to Section 2 herein during the continuance of this Agreement. You agree that you own no right, title or interest in or to the Wiley Materials or any of the intellectual property rights therein. You shall have no rights hereunder other than the license as provided for above in Section 2. No right, license or interest to any trademark, trade name, service mark or other branding ("Marks") of WILEY or its licensors is granted hereunder, and you agree that you shall not assert any such right, license or interest with respect thereto

137

- NEITHER WILEY NOR ITS LICENSORS MAKES ANY WARRANTY OR REPRESENTATION OF ANY KIND TO YOU OR ANY THIRD PARTY, EXPRESS, IMPLIED OR STATUTORY, WITH RESPECT TO THE MATERIALS OR THE ACCURACY OF ANY INFORMATION CONTAINED IN THE MATERIALS, INCLUDING, WITHOUT LIMITATION, ANY IMPLIED WARRANTY OF MERCHANTABILITY, ACCURACY, SATISFACTORY QUALITY, FITNESS FOR A PARTICULAR PURPOSE, USABILITY, INTEGRATION OR NON-INFRINGEMENT AND ALL SUCH WARRANTIES ARE HEREBY EXCLUDED BY WILEY AND ITS LICENSORS AND WAIVED BY YOU.

- WILEY shall have the right to terminate this Agreement immediately upon breach of this Agreement by you.

- You shall indemnify, defend and hold harmless WILEY, its Licensors and their respective directors, officers, agents and employees, from and against any actual or threatened claims, demands, causes of action or proceedings arising from any breach of this Agreement by you.

- IN NO EVENT SHALL WILEY OR ITS LICENSORS BE LIABLE TO YOU OR ANY OTHER PARTY OR ANY OTHER PERSON OR ENTITY FOR ANY SPECIAL, CONSEQUENTIAL, INCIDENTAL, INDIRECT, EXEMPLARY OR PUNITIVE DAMAGES, HOWEVER CAUSED, ARISING OUT OF OR IN CONNECTION WITH THE DOWNLOADING, PROVISIONING, VIEWING OR USE OF THE MATERIALS REGARDLESS OF THE FORM OF ACTION, WHETHER FOR BREACH OF CONTRACT, BREACH OF WARRANTY, TORT, NEGLIGENCE, INFRINGEMENT OR OTHERWISE (INCLUDING, WITHOUT LIMITATION, DAMAGES BASED ON LOSS OF PROFITS, DATA, FILES, USE, BUSINESS OPPORTUNITY OR CLAIMS OF THIRD PARTIES), AND WHETHER OR NOT THE PARTY HAS BEEN ADVISED OF THE POSSIBILITY OF SUCH DAMAGES. THIS LIMITATION SHALL APPLY NOTWITHSTANDING ANY FAILURE OF ESSENTIAL PURPOSE OF ANY LIMITED REMEDY PROVIDED HEREIN.

- Should any provision of this Agreement be held by a court of competent jurisdiction to be illegal, invalid, or unenforceable, that provision shall be deemed amended to achieve as nearly as possible the same economic effect as the original provision, and the legality, validity and enforceability of the remaining provisions of this Agreement shall not be affected or impaired thereby.

- The failure of either party to enforce any term or condition of this Agreement shall not constitute a waiver of either party's right to enforce each and every term and condition of this Agreement. No breach under this agreement shall be deemed waived or excused by either party unless such waiver or consent is in writing signed by the party granting such waiver or consent. The waiver by or consent of a party to a breach of any provision of this Agreement shall not operate or be construed as a waiver of or consent to any other or subsequent breach by such other party.

- This Agreement may not be assigned (including by operation of law or otherwise) by you without WILEY's prior written consent.

- Any fee required for this permission shall be non-refundable after thirty (30) days from receipt by the CCC.

138

- These terms and conditions together with CCC's Billing and Payment terms and conditions (which are incorporated herein) form the entire agreement between you and WILEY concerning this licensing transaction and (in the absence of fraud) supersedes all prior agreements and representations of the parties, oral or written. This Agreement may not be amended except in writing signed by both parties. This Agreement shall be binding upon and inure to the benefit of the parties' successors, legal representatives, and authorized assigns.

- In the event of any conflict between your obligations established by these terms and conditions and those established by CCC's Billing and Payment terms and conditions, these terms and conditions shall prevail.

- WILEY expressly reserves all rights not specifically granted in the combination of (i) the license details provided by you and accepted in the course of this licensing transaction, (ii) these terms and conditions and (iii) CCC's Billing and Payment terms and conditions.

- This Agreement will be void if the Type of Use, Format, Circulation, or Requestor Type was misrepresented during the licensing process.

- This Agreement shall be governed by and construed in accordance with the laws of the State of New York, USA, without regards to such state's conflict of law rules. Any legal action, suit or proceeding arising out of or relating to these Terms and Conditions or the breach thereof shall be instituted in a court of competent jurisdiction in New York County in the State of New York in the United States of America and each party hereby consents and submits to the personal jurisdiction of such court, waives any objection to venue in such court and consents to service of process by registered or certified mail, return receipt requested, at the last known address of such party.

WILEY OPEN ACCESS TERMS AND CONDITIONS
Wiley Publishes Open Access Articles in fully Open Access Journals and in Subscription journals offering Online Open. Although most of the fully Open Access journals publish open access articles under the terms of the Creative Commons Attribution (CC BY) License only, the subscription journals and a few of the Open Access Journals offer a choice of Creative Commons Licenses. The license type is clearly identified on the article.
The Creative Commons Attribution License
The Creative Commons Attribution License (CC-BY) allows users to copy, distribute and transmit an article, adapt the article and make commercial use of the article. The CC-BY license permits commercial and non-
Creative Commons Attribution Non-Commercial License
The Creative Commons Attribution Non-Commercial (CC-BY-NC)License permits use, distribution and reproduction in any medium, provided the original work is properly cited and is not used for commercial purposes.(see below)

Creative Commons Attribution-Non-Commercial-NoDerivs License
The Creative Commons Attribution Non-Commercial-NoDerivs License (CC-BY-NC-ND) permits use, distribution and reproduction in any medium, provided the original work is properly cited, is not used for commercial purposes and no modifications or adaptations are made. (see below)
Use by commercial "for-profit" organizations
Use of Wiley Open Access articles for commercial, promotional, or marketing purposes requires further explicit permission from Wiley and will be subject to a fee.

139

Further details can be found on Wiley Online Library
http://olabout.wiley.com/WileyCDA/Section/id-410895.html

Other Terms and Conditions:

v1.10 Last updated September 2015

Questions? customercare@copyright.com or +1-855-239-3415 (toll free in the US) or +1-978-646-2777.

REFERENCES

[1] Zhang, B. Milica R. "Organ-on-a-Chip Devices Advance to Market." *Lab on a Chip*, vol. 17, no. 14, 2017, pp. 2395–2420.

[2] Anonymous. "Draper to Build Preclinical Microphysiological Systems with Pfizer to Help Predict Clinical Outcomes," vol. 2017. Retrieved September 17, 2017, from http://www.draper.com/news/draper-build-preclinical-microphysiological-systems-pfizer-help-predict-clinical-outcomes.

[3] Whitesides, G. M. (2006). The origins and the future of microfluidics. *Nature*, *442*(7101), 368.

[4] Research and Markets. (2016, December 21). Global $6.13 Billion Organ-On-Chip Market Analysis & Trends 2016-2025 - Latest Growth Opportunities/Investment Opportunities. Retrieved September 24, 2017, from https://globenewswire.com/news-release/2016/12/21/899548/0/en/Global-6-13-Billion-Organ-On-Chip-Market-Analysis-Trends-2016-2025-Latest-Growth-Opportunities-Investment-Opportunities.html

[5] Matos Pires, N.M., Dong, T., Hanke, U., and Hoivik, N. "Recent Developemnts in Optical Detection Technologies in Lab-on-a-Chip Devices for Biosensing Applications," pp.15458–15479, 2014. Retrieved August 29, 2017 from http://www.mdpi.com/1424-8220/14/8/15458.

[6] Gruber, Pia, et al. "Integration and Application of Optical Chemical Sensors in Microbioreactors." *Lab on a Chip*, vol. 17, no. 16, 2017, pp. 2693–2712.

[7] Grist, S. M., Chrostowski, L., & Cheung, K. C. (2010). Optical Oxygen Sensors for Applications in Microfluidic Cell Culture. *Sensors (Basel, Switzerland)*, *10*(10), 9286–9316.

[8] PyroScience. (n.d.). Piccolo2. Retrieved from http://www.pyro-science.com/media/files/Piccolo2-Brochure.pdf

[9] Paguirigan, A. L., & Beebe, D. J. (2008). Microfluidics meet cell biology: bridging the gap by validation and application of microscale techniques for cell biological assays. BioEssays : News and Reviews in Molecular, Cellular and Developmental Biology, 30(9), 811.

[10] Temiz, Y., Lovchik, R. D., Kaigala, G. V., & Delamarche, E. (2015). Lab-on-a-chip devices: How to close and plug the lab?. Microelectronic Engineering, 132, 156-175.

[11] van den Berg, A. (2010, October). Labs on a chip for health care applications. In The 14th International Conference on Miniaturized Systems for Chemistry and Life Sciences. http://www.rsc.org/binaries/loc/2010/pdfs/papers/002_9002.pdf

[12] Whitesides, G. M. (2006). The origins and the future of microfluidics. Nature, 442 (7101), 368. http://fennetic.fairlystable.org/pub/the_origin_and_future_of_microfluidics.pdf

[13] Ong, S. E., Zhang, S., Du, H., & Fu, Y. (2008). Fundamental principles and applications of microfluidic systems. Frontiers in Bioscience, 13(7), 2757-2773. http://www3.ntu.edu.sg/ThinFilms/mae-thinfilms/Thinfilms/pdfpapers/microfluidicsystems.pdf

[14] "The Drug Development and Approval Process." FDA Review, Independent Institute, 2016, www.fdareview.org/03_drug_development.php.

[15] Human Organs-on-Chips. (2017, June 14). Retrieved October 01, 2017, from https://wyss.harvard.edu/technology/human-organs-on-chips/

[16] Kyung-Jin Jang, Ali Poyan Mehr, Geraldine A Hamilton, Lori A McPartlin, Seyoon Chung, Kahp-Yang Suh, et al. (2013). Human kidney proximal tubule-on-a-chip for drug transport and nephrotoxicity assessment. Integrative Biology: Quantitative Biosciences from Nano to Macro, 5(9), 1119-1129.

[17] Bridging the gap between in vitro and in vivo research. (2015). https://www.nortisbio.com/

[18] Grist, S. M., Chrostowski, L., & Cheung, K. C. (2010). Optical Oxygen Sensors for Applications in Microfluidic Cell Culture. Sensors (Basel, Switzerland), 10(10), 9286–9316. https://www.ncbi.nlm.nih.gov/pmc/articles/PMC3230974/

[19] Wang et al, *Chem. Soc. Rev* (2014) **43** 3666-3761

[20] Fundamentals of Environmental Measurements. (2016). Measuring Dissolved Oxygen. Retrieved October 04, 2017, from http://www.fondriest.com/environmental-measurements/equipment/measuring-water-quality/dissolved-oxygen-sensors-and-methods/#DOE1

[21] Harvey, D. (2013, July 31). Clark Electrode for Dissolved Oxygen. Retrieved October 04, 2017, from http://community.asdlib.org/imageandvideoexchangeforum/2013/07/31/clark-electrode-for-dissolved-oxygen/

[22] Yamagishi et al, *Analytica Chimica Acta* (2017) **985** 1-6

[23] Harvey, D. (2013). Clark electrode for dissolved oxygen.http://community.asdlib.org/imageandvideoexchangeforum/2013/07/31/clark-electrode-for-dissolved-oxygen/

[24] Grist, S. M., Chrostowski, L., & Cheung, K. C. (2010). Optical oxygen sensors for applications in microfluidic cell culture. Sensors (Basel, Switzerland), 10(10), 9286-9316.

[25] Sharma, A., & Wolfbeis, O. S. (1988). Fiberoptic oxygen sensor based on fluorescence quenching and energy transfer. Applied Spectroscopy, 42(6), 1009-1011.

[26] Mueller, J. (2006). Quenching and FRET. Retrieved from http://fitzkee.chemistry.msstate.edu/sites/default/files/ch8990/Fluoro6.pdf

[27] Fluorescence Quenching. (2016). Retrieved September 15, 2017, from

https://www.chem.uzh.ch/dam/jcr:571775eb-8b0e-4930-8aa4-

ad0da5c11aec/FluorescenceQuenching_HS16.pdf

[28] Quaranta, M., Borisov, S., & Klimant, I. (2012). Indicators for optical oxygen sensors.

Bioanalytical Reviews, 4(2), 115-157.

[29] Butler, J. M. (2011). Advanced topics in forensic DNA typing: methodology. Academic

Press.

[30] Quaranta, M., Borisov, S., & Klimant, I. (2012). Indicators for optical oxygen sensors.

Bioanalytical Reviews, 4(2), 115-157.

[31] Technologie Seahorse XF. (n.d.). Retrieved September 07, 2017, from

http://hpst.cz/molekularni-biologie/bunecna-analyza-seahorse-xf/technologie-seahorse-xf

[32] Agilent. (2018). Seahorse XFe96 analyzer. Retrieved September 05, 2017, from

https://www.agilent.com/en/products/cell-analysis/seahorse-analyzers/seahorse-xfe96-analyzer

[33] PyroScience. (n.d.). Fiber-optic Oxygen Meter User Manual. Retrieved August 05 2017,

from http://www.pyro-science.com/media/files/Manual%20Piccolo2.pdf

[34] PyroScience. (n.d.). FireSting O2 . Retrieved September 05, 2017, from http://www.pyro-

science.com/media/files/Firesting-O2-Flyer.pdf

[35] PreSens. (n.d.). O2 Sensor. Retrieved August 29, 2017, from

https://www.presens.de/products/imaging.html

[36] Mandenius, CF., Steel, D., Noor, F., Meyer, T., Heinzle, E., Asp, J., Arain, S., Kraushaar,

U., Bremer, S., Class, R., and Sartipy, P. (2011). Cardiotoxicity testing using pluripotent stem

cell-derived human cardiomyocytes and state-of-the-art bioanalytics: A review. Journal of

applied toxicology: JAT. 31. 191-205.

[37] Corey, P. L. (2017, April 19). NIST-on-a-Chip: Microfluidics. Retrieved October 02, 2017, from https://www.nist.gov/pml/nist-chip-microfluidics

[38] Klapperich, C. M. (2009). Microfluidic diagnostics: Time for industry standards. Expert Review of Medical Devices, 6(3), 211-213. doi:10.1586/erd.09.11

[39] Crockett, M. (2017). Microfluidics—Why Your Next IC Packaging Project May Require More Than Your Known Electronics/Materials Methods and Practices. *Semiconductor Equipment and Materials International*. Retrieved September 29, 2017 http://www.semi.org/en/mems-microfluidics-standards

[40] ISO - International Organization for Standardization. (2014, June 30). Retrieved October 02, 2017, from https://www.iso.org/standard/59515.html

[41] ISO. (2016, August 24). IWA 23:2016. Retrieved October 02, 2017, from https://www.iso.org/standard/70603.html

[42] Office of the Commissioner. (n.d.). The Drug Development Process - Step 2: Preclinical Research. Retrieved September 24, 2017, from https://www.fda.gov/ForPatients/Approvals/Drugs/ucm405658.htm

[43] ASTM D7027-13, Standard Test Method for Evaluation of Scratch Resistance of Polymeric Coatings and Plastics Using an Instrumented Scratch Machine, ASTM International, West Conshohocken, PA, 2013, www.astm.org

[44] ASTM C1247-14, Standard Test Method for Durability of Sealants Exposed to Continuous Immersion in Liquids, ASTM International, West Conshohocken, PA, 2014, www.astm.org

[45] ASTM D7895 / D7895M-14, Standard Test Method for Thermal Endurance of Coating Powders Used for Powder Coating Insulation Systems, ASTM International, West Conshohocken, PA, 2014, www.astm.org

[46] Draper. (2018). How do you improve success of drug development earlier?. Retrieved from

http://www.draper.com/solution/human-organ-systems

[47] Autoimmunity Research Foundation. (2017). Incidence and prevalence of chronic disease.

Retrieved from https://mpkb.org/home/pathogenesis/epidemiology

[48] Singh, H. (2018). Drug Development Challenges. Retrieved from

https://www.pharmafocusasia.com/strategy/drug-development-challenges

[49] Ethylene oxide treatment technologies. (2004). Retrieved from

https://www.env.go.jp/policy/etv/en/pdf/proto_ethylene_s.pdf